UNIVERSIDADE ESTADUAL DE CAMPINAS
Faculdade de Engenharia Química

SILVIA MARINA ARAUJO DAZA

NUSSELT NUMBER CORRELATION FOR A JACKETED STIRRED TANK USING COMPUTATIONAL FLUID DYNAMICS

OBTENÇÃO DE CORRELAÇÃO DE NUMERO DE NUSSELT PARA UM TANQUE DE MISTURA JAQUETADO UTILIZANDO FLUIDODINÂMICA COMPUTACIONAL

Campinas
2017

Silvia Marina Araujo Daza

NUSSELT NUMBER CORRELATION FOR A JACKETED STIRRED TANK USING COMPUTATIONAL FLUID DYNAMICS

Dissertation presented to the Faculty of Chemical Engineering of the University of Campinas in partial fulfillment of the requirements for the degree of Master in Chemical Engineering.

Dissertação apresentada à Faculdade de Engenharia Química da Universidade Estadual de Campinas como parte dos requisitos exigidos para a obtenção do título de Mestra em Engenharia Química.

Supervisor: Guilherme José de Castilho
Co-supervisor: Ronald Jaimes Prada

Este exemplar corresponde à versão final da dissertação defendida pela aluna Silvia Marina Araujo Daza, e orientada pelo Prof. Dr. Guilherme José de Castilho

Campinas
2017

Agência(s) de fomento e nº(s) de processo(s): CNPq

Ficha catalográfica
Universidade Estadual de Campinas
Biblioteca da Área de Engenharia e Arquitetura
Luciana Pietrosanto Milla - CRB 8/8129

D338n

Daza, Silvia Marina Araujo, 1988-
Nusselt number correlation for a jacketed stirred tank using computational fluid dynamics (CFD) / Silvia Marina Araujo Daza. – Campinas, SP : [s.n.], 2017.

Orientador: Guilherme José de Castilho.
Dissertação (mestrado) – Universidade Estadual de Campinas, Faculdade de Engenharia Química.

1. Calor - Transferência. 2. Tanques. 3. Fluidodinâmica computacional. 4. Escoamento turbulento. I. Castilho, Guilherme José, 1983-. II. Universidade Estadual de Campinas. Faculdade de Engenharia Química. III. Título.

Informações para Biblioteca Digital

Título em outro idioma: Obtenção de correlação de número de Nusselt para un tanque de mistura jaquetado ataravés da fluidodinâmica computacional
Palavras-chave em inglês:
Heat - Transfer
Tank
Computational fluid dynamics
Turbulent flow
Área de concentração: Engenharia Química
Titulação: Mestra em Engenharia Química
Banca examinadora:
Guilherme José de Castilho [Orientador]
Dirceu Noriler
Celso Fernandes Joaquim Junior
Data de defesa: 05-10-2017
Programa de Pós-Graduação: Engenharia Química

Dissertação de mestrado defendida pela aluna Silvia Marina Araujo Daza e aprovada em 05 de setembro 2017 pela banca examinadora constituída pelos professores:

Prof. Dr. Guilherme José de Castilho

Prof. Dr. Celso Fernandes Joaquim Junior

Prof. Dr. Dirceu Noriler

A ata de defesa, assinada pelos membros da Comissão Examinadora, consta no processo de vida acadêmica da aluna.

Para Varo, Mary, Robe, Andrea, Elena, Nicolás y Rubén:
Gracias por esperar

Agradecimentos

Agradeço,

A Deus, pela vida e as grandes capacidades que deu para nós.
A meus pais, meus irmãos e meus sobrinhos porque são minha inspiração, minha motivação e minha força.
A quem caminha do meu lado por ser meu apoio incondicional e minha fortaleza ainda à distância.
Ao meu orientador Prof. Dr. Guilherme de Castilho pelos conhecimentos compartilhados, sua grande ajuda, confiança e disposição durante o desenvolvimento deste projeto.
Aos meus coorientadores Prof. Dr. Roberto Nunhez e Dr. Ronald Jaimes por sua colaboração e suas importantes contribuições.
Aos meus amigos brasileiros por ter me acolhido e me fazer sentir em casa e a toda minha família brasileira pelos inesquecíveis momentos vividos do seu lado.
Aos meus colegas e amigos do laboratório L-CFD pelos agradáveis momentos compartilhados dia a dia.
A CNPq pelo apoio financeiro e a UNICAMP pela oportunidade e a formação.

A todos aqueles que contribuíram para concluir com sucesso este projeto: Gratidão.

Resumo

Um dos maiores desafios relacionados aos tanques de mistura é a troca de calor. Diversos estudos têm sido desenvolvidos para obter correlações do número de Nusselt que represente o coeficiente de transferência de calor por convecção nestes equipamentos. Esta correlação é geralmente obtida por métodos experimentais e é válida apenas para um conjunto de condições específicas. Os estudos experimentais permitem a análise de diferentes aspectos e parâmetros gerando um cenário exato e de fácil compreensão do fenômeno. No entanto, são demorados, caros e demandam uma grande variedade de equipamentos para obter os resultados. A fluidodinâmica computacional (CFD) é uma alternativa que proporciona resultados mais rápidos, mais claros e de baixo custo e, também, permite obter um amplo conhecimento de todos os fenômenos que ocorrem dentro do tanque como os padrões de fluxo e de transferência de calor. Nesta pesquisa, a fluidodinâmica computacional (CFD) foi aplicada para a determinação de uma correlação de número de Nusselt em um tanque de mistura jaquetado equipado com um impelidor tipo Rushton. Para a simulação dos fenômenos envolvidos no processo de agitação, a geometria do tanque foi construída utilizando malha hexaédrica e abordagem *Multiple Reference Frame* (MRF). O modelo de turbulência *Shear Stress Trasport* (SST) e o esquema de discretização Upwind foram empregados para solucionar as equações de conservação e obter resultados precisos. Como a validação é essencial para a modelagem CFD, os resultados simulados foram comparados com medidas experimentais reportadas por Strek (1963). A correlação do número de Nusselt obtida a partir do modelo simulado concorda com os dados experimentais fornecendo uma representação precisa da transferência de calor no tanque.

Palavras-chave: Transferência de Calor; Tanques de Mistura; Fluidodinâmica Computacional; Escoamento Turbulento; Número de Nusselt.

Abstract

One of the biggest challenges related to mixing tanks is the heat exchange. Several studies have been developed to obtain Nusselt number correlations that represent the heat transfer coefficient by convection. This correlation is usually obtained by experimental methods and is valid only for a set of specific conditions. The experimental studies allow the analysis of different aspects and parameters giving an accurate scenario and easy understanding of the phenomenon. However, it is time consuming, expensive and demands a wide variety of equipment to get the results. Computational Fluid Dynamics (CFD) is an alternative that delivers faster, clearer, lower-cost results, and provides a broad understanding of all phenomena occurring inside the tank such as flow and heat transfer patterns. In this research, Computational Fluid Dynamics (CFD) was applied for the determination a Nusselt number correlation in a jacketed stirred tank equipped with Rushton turbine impeller. For the simulation of the phenomena involved in the stirring process, the tank geometry was constructed using hexahedral mesh and Multiple Reference Frame approach (MRF). The Shear Stress Transport k-ω turbulence model and the Upwind discretization scheme were employed to solve conservation equations and to obtain accurate results. Since a model validation is essential for CFD modeling, the simulated results were compared with experimental measures reported by Strek (1963). The Nusselt number correlation obtained from the simulated model satisfactorily agrees with the experimental data providing an accurate representation of the heat transfer in the tank.

Keywords: Heat Transfer, Stirred Tanks; Computational Fluid Dynamics; Turbulent Flow; Nusselt number.

Figures list

Tables list

Nomenclature

Latin letters

$\vec{g}$	Gravitational acceleration vector	m/s^2
$\overline{v_i' v_j'}$	Reynolds stresses	
a	Thickness of the impeller blade	m
B	Baffle width	m
C	Impeller height	m
$CD_{k\omega}$	The positive portion of the cross-diffusion term	
C_p	Specific heat capacity	J/kg K
C_μ	Empiric constant the k-ε turbulence model	
$C_{\varepsilon 1}$	Empiric constant of the k-ε turbulence model	
$C_{\varepsilon 2}$	Empiric constant of the k-ε turbulence model	
D	Impeller diameter	m
D_o	Disk diameter	m
e	Shaft diameter	m
E	Energy	J
f	Disk thickness	m
F_1, F_2	Blending function	
h_o	Heat transfer coefficient	W/m^2 K
h	Static enthalpy	m or J
$h_{j'}$	Enthalpy for the species j’	J
k	Turbulence kinetic energy	J/kg
k_{eff}	Effective conductivity	W/m K
L	Width of the impeller blade	
N	Impeller speed	rpm
p	Fluid pressure	Pa
$\bar{p}$	Modified pressure	Pa

P	Impeller power	W
P_k	Turbulence production due to viscous forces	
q	Heat transfer rate	W/m^2
S	Source term	
T	Tank diameter	m
T_w	Wall temperature	K
T_f	Local fluid temperature	K
U_i	Velocity in the direction i	m/s
U	Velocity vector	m/s
u_τ	Friction velocity	m/s
W	Height of the impeller blade	m
y	Distance to the wall	m
Z	Liquid height	m

Greek letters

α	Thermal diffusivity or	m^2/s
	Empiric constant of the SST turbulence model	
β	Empiric constant of the k- ω and SST turbulence models	
β^*	Empiric constant of the SST turbulence model	
β'	Empiric constant of the k- ω turbulence model	
ε	Turbulent energy dissipation rate	m^2/s^3
κ	Thermal conductivity	W/m K
μ	Fluid dynamic viscosity	Pa s
μ_t	Turbulent or eddy viscosity	Pa s
μ_{ef}	Effective viscosity	Pa s
v	Kinematic viscosity	m^2/s
v_t	Turbulent momentum diffusivity	m^2/s
ϱ	Fluid density	kg/m^3
σ_k	Empiric constant of the k- ω and k- ε turbulence models	
σ_ω	Empiric constant of the k- ω turbulence model	
σ_ε	Empiric constant of the k-ε turbulence model	
τ	Viscous shear stress tensor	N/m^2

τ_w	Shear stress at the wall	N/m^2
δ_{ij}	Strain rate tensor	1/s
ω	Turbulence frequency	1/s

Dimensionless

Nu	Nusselt number
Np	Power number
Pr	Prandtl number
Re	Reynolds number
Vi	Viscosity ratio
u^+	Dimensionless velocity
y^+	Dimensionless distance

Abbreviations

CFD	Computational Fluid Dynamics
IBM	Impeller Boundary Conditions approach
IO	Inner and Outer Iterative Procedure
LDV	Laser-Doppler Velocimetry
LES	Large Eddy Simulations
MFR	Multiple Frames of Reference
PIV	Particle Image Velocimetry
QUICK	Quadratic Upstream Interpolation
RANS	Reynolds averaged Navier-Stokes equations
RMS	Root Mean Square
RNG	Renormalization Group RSM Reynolds Stress Model
SG	Sliding Grid
SM	Sliding Mesh
STR	Stirred Tank Reactor

Contents

Chapter 1

Introduction

Agitation and mixing play a vital role in chemical engineering and have considerable industrial relevance. These complex operations are extensively used in industrial processes that involve hydrodynamics, thermal, chemical, and mechanical phenomena. The demand for high-quality products increases day by day in the market. Therefore, it is greatly required improving the mixing efficiency.

Stirred tanks are the most popular equipment used to perform these operations. Usually, jackets or coils submerged in the fluid are implemented to provide heat exchange. Several challenging problems still exist to improve the quality of the mixture and to design the stirred tank configuration correctly. Thermal energy transfer is one of the biggest challenges related to stirred tanks design. Heat exchange is mainly due to overall movements supplied to the fluid by the impeller and the fluid molecules randomness as well, having significant effects on the heat transfer coefficient.

Lately, there is great interest in local properties throughout the stirred tanks because the localized hydrodynamics and phase distributions within the stirred tank are more informative in order to perform the tank designs. Experimental techniques as Laser Doppler Anemometry (LDV) and Particle Image Velocimetry (PIV) have been widely used to study this type of equipment because they provide an exact scenario and real understanding of the phenomenon happening. This information is subsequently used to design and scale-up the stirred tanks.

However, there are numerous restrictions in the equipment design due to the variations on the geometric relationships of the tank depending on the desired application and the fluids involved. Thus, it is necessary to construct new models and carry out several tests to evaluate each particular application, using later scaling models with geometric correlations or volume units. Most of these experiments are based on single-impeller measurements, whereas multiple impeller systems are common in production tanks. The location of the impellers is another problem since it can be different in the laboratory and in industrial systems. Due to these and other factors, there are significant inaccuracies in the mixing time predictions, which is a critical parameter in determining the efficiency of a stirred system.

Additionally, the experimental techniques have several limitations, as high time consumption, high capital investment, and require a broad range of equipment to obtain the results. All these problems are intensified when heat exchange is involved.

Experimental studies have been focused on evaluating the influence of the tank configuration and the type of impeller on the heat transfer coefficient by means of a Nusselt number correlation (CHILTON *et al*., 1944; ASKEW AND BECKMANN, 1965; MAN *et al*., 1984; STREK, 1963). This correlation depends, as well, on the fluid properties and type of heating device, being valid only for the parameters used in the calculus and very similar configurations.

Nowadays, the computational fluid dynamics (CFD) has become a great tool for the process engineering because of the low cost, high speed in obtaining results, and easy understanding of physical phenomena. Computational fluid dynamics involves the solution of the governing equations -continuity, momentum, and energy- and chemical reactions. The calculation is done dividing the computational flow domain into tiny fluid elements or volumes. On each control volume, the governing equations are enforced and solved (VERSTEEG AND MALALASEKERA, 2007).

The use of CFD allows engineers to obtain numerical solutions to problems with complex geometries for a wide range of operating conditions, without the physical equipment being fabricated. A CFD analysis can provide values of temperature, concentration, velocity or pressure throughout the solution domain and offers comprehensive knowledge of the fluid dynamic behavior produced inside of a tank as turbulent flow patterns and/or energy transfer.

Many of the published studies of CFD modeling in stirred tanks have evaluated different configurations that have been validated with experimental works. Special attention is given to the impeller-baffles approaches, the turbulence models, and the discretization schemes to obtain accurate numerical results (AUBIN *et al*., 2004; BRUCATO *et al*., 1998; DEGLON AND MEYER, 2006; MURTHY AND JOSHI, 2008; RAJ *et al*., 2014). Several authors claim that CFD offers satisfactory predictions of the parameters analyzed.

The aim of this work is to use computational fluid dynamics to determine a Nusselt number correlation of a jacketed stirred tank with a flat bottom and four baffles, equipped with a Rushton turbine impeller and obtain an accurate heat transfer coefficient. The capability of the CFD modeling is evaluated comparing the simulations results with the experimental data. The validated model would contribute to the optimization of integrated mixing and heat transfer processes in stirred tanks, providing a tool to test different tank configurations and heat sources, which result in better chemical operations regarding lower design cost, high product quality, and cost reductions in power and heat generation.

1.1 Objectives

1.1.1 Overall objective

The present work aims to obtain a Nusselt number correlation that allows calculating the heat transfer coefficient in a jacketed stirred tank. This correlation will be achieved using a computational fluid dynamics modeling. The simulation results will be compared with experimental data reported in the literature.

1.1.2 Specific objectives

This research is proposed to:

- Develop a three-dimensional computational model for a jacketed stirred tank based on the experimental configuration used in the study of Strek (1963).

- Determine through numerical experimentation the correlation of the Nusselt number of the proposed configuration and validate the model with experimental data.
- Evaluate the influence of the impeller diameter (D/T) and impeller height (C/T) on the heat transfer coefficient with the simulations results.

1.2 Thesis overview

This thesis consists of five main chapters. The opening chapter describes an overall context, the motivation and the problem statement for the research proposed in this work. Chapter 2 presents the theory and fundamentals behind the mathematical methods used in this thesis and an overview of the literature of previous experimental and CFD works in jacketed stirred tanks. Chapter 3 describes the computational methodology employed in CFD simulations, which is divided in pre-processing, solver and post-processing; it includes the description of the geometry and mesh creation, physical and numerical models, and the boundary conditions. Chapter 4 details the numerical results, the analysis of the CFD simulations and the model validation. Finally, Chapter 5 contains the major conclusions of the present research work, emphasizing the novel findings and including topics for future work.

Chapter 2

Theoretical foundation and literature review

This chapter covers the theoretical basis studied to develop the current investigation. Additionally, a literature review of the most significant experimental and CFD works in jacketed agitated tanks is presented.

2.1 Mechanically stirred tanks

In the chemical industry, several processes are performed in stirred tanks. The operations, in batch or continuous flow, include chemical reactions and mixing of liquids or liquid-solids systems. The configuration of the tank depends on the intended operation. Once the operation is decided, the form of the tank is determined. This selection includes the bottom shape (flat, dished or round), the type of the impeller, the use of baffles, and the source of heat transfer which is usually provided by a wall jacket or immersed coils (ASKEW AND BECKMANN, 1965). Figure 2.1 shows a stirred tank in the most basic configuration.

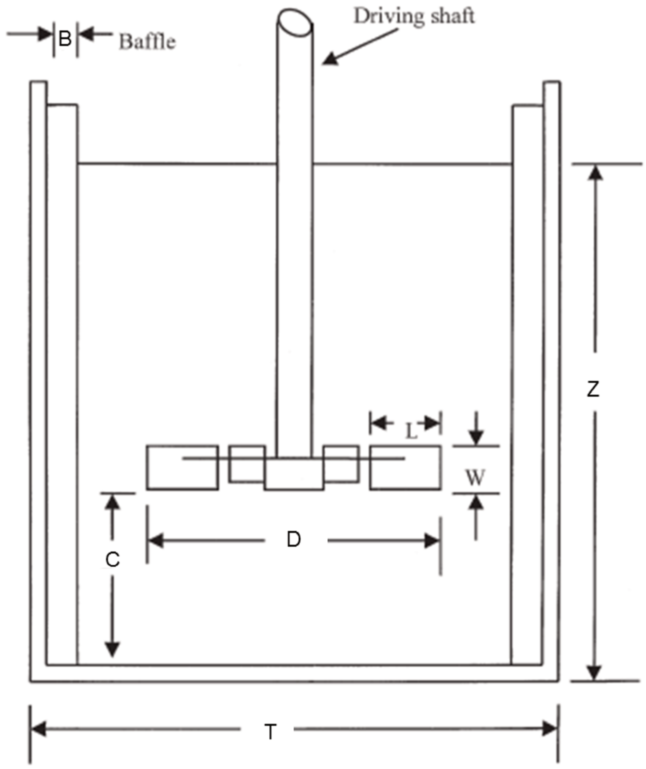

Figure 2.1 Standard stirred tank configuration (Adapted from COKER, 2001)

The selection of the tank internals and the size and type of the impeller is critical because these factors can significantly affect the quality of the agitation and mixing and the mass or heat transfer process. Stirred tanks used for liquid systems commonly have a flat bottom, conventional impellers such as the Rushton turbine (Figure 2.1) and baffles or draft tubes to avoid dead zones at the wall joints (YANG AND MAO, 2014; OCHIENG *et al*., 2009).

These characteristics, related geometrically to the dimensions of the tank, also determine an efficient flow pattern. Table 2.1 provides the standard geometric relationships for stirred tanks, where "D" is the impeller diameter, "Z" the liquid height, "T" the tank diameter, "C" the height of the impeller from the bottom of the tank, "B" the baffle width, and "L" and "W" the length and width of the impeller blade, respectively.

These relative proportions vary depending on the application and characteristics of the mixing fluid; each process requires a particular dimension to achieve the best efficiency (JOAQUIM JUNIOR *et al*., 2007).

Table 2.1 Geometric proportions in standard stirred tanks

Geometrical relationship	***Value***
D/T	1/4 – 1/2
Z/T	1
B/T	1/10 – 1/12
C/T	1/6 – 1/2
L/D	1/4
W/D	1/4 – 1/6

Data: *Agitação e Mistura na Industria* (JOAQUIM JUNIOR *et al.*, 2007)

2.1.1 Impeller types

A rotating impeller has the function of imparting flow and shear in the fluid. Impellers are classified depending on the laminar or turbulent operation. For laminar flow, the impellers have large blades (approximated to the tank diameter) and a low speed of rotation. Anchors, paddles and helical screws are typical impellers for laminar flow (JOAQUIM JUNIOR *et al.*, 2007).

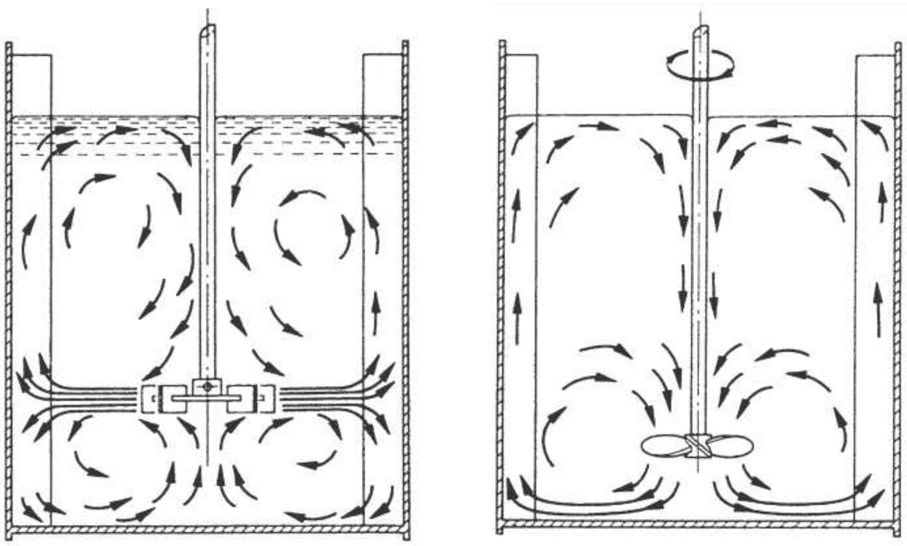

Figure 2.2. a. Radial flow pattern. b. Axial flow pattern (HOLLAND AND BRAGG, 1995, as cited in COKER, 2001)

For turbulent flow, the impeller features are high speed and small blade area. These devices are cataloged depending on the axial or radial flow. The radial flow impellers impose high shear stress to the fluid and produce a two-stage flow pattern; they are used for mixing low to medium viscosity fluids or gas-liquids mixtures (Figure 2.2a). The axial flow impellers create one-stage flow pattern and often are used for homogenization processes and solid suspensions (Figure 2.2b) (HEMRAJANI AND TATTERSON, 2004; JOAQUIM JUNIOR *et al.*, 2007).

Each type of impeller has two specific characteristics: the pumping and power numbers (N_Q, N_p). These features depend on the Reynolds number of the impeller and become constant in turbulent flow (Re > 10000). In the literature are found the values of N_Q and N_p for commonly used impellers, this information is considered as a reference to choose a suitable impeller for the desired operation. Figure 2.3 illustrates typical impellers types, where letter c shows the Rushton impeller used in this work.

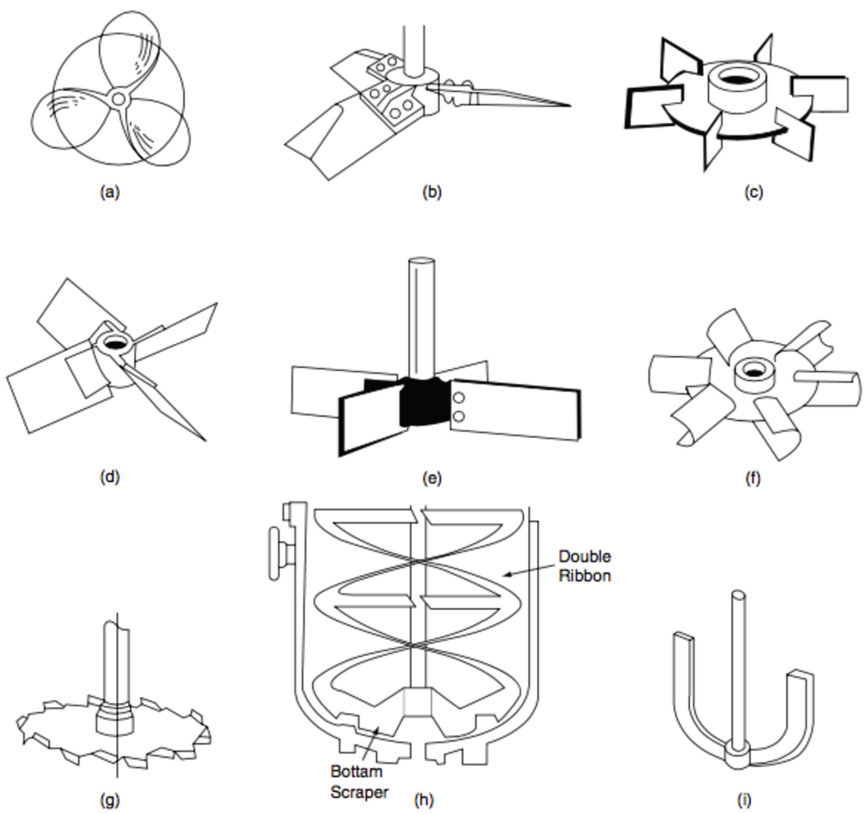

Figure 2.3 Impeller types commonly used in mechanically stirred tanks. a) Three-bladed Marine Propeller (MP) b) Chemineer HE-3 hydrofoil c) Rushton turbine d) Four-blade 45° pitched

blade (4BP) e) Four-blade flat blade (4BF) f) Six-blade disk-style concave blade (CBI) g) Sawtooth (or Cowles type) h) Helical ribbon i) Anchor (COUPER et al., 2004)

2.1.2 Baffles

The baffles are vertical strips installed perpendicular to the tank walls. Adequate baffling promotes the mixing and is essential to prevent swirls and the rotation of the liquid bulk as a whole, which is the behavior on unbaffled tanks (Figure 2.4). The baffles, also contribute to an increase in heat transfer and chemical reaction rates. The flow patterns change when using baffles, transforming radial and circumferential velocity component into axial velocity component.

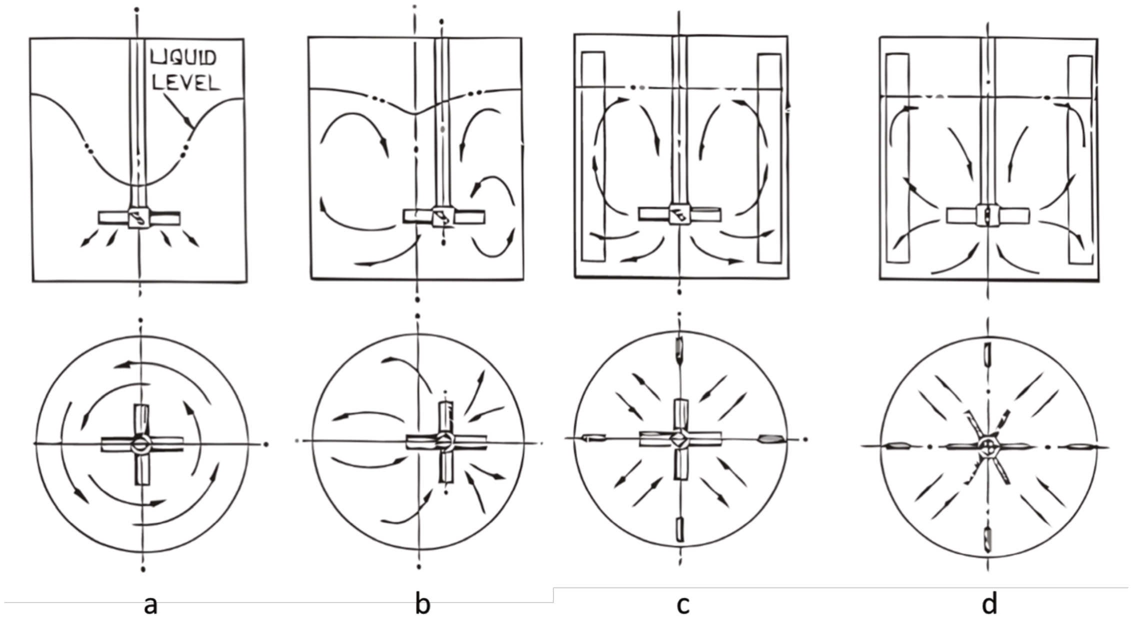

Figure 2.4. Different types of flow pattern in a stirred tank a. Vortex created with axial or radial impellers without baffles. b. Impeller positioned off the center decreasing the vortex. c. Impeller of axial flow with baffles. d. Impeller of radial flow with baffles (COUPER et al., 2004)

2.1.3 Heat transfer in stirred tanks

The heat transfer surfaces most commonly used in stirred tanks are jackets, internal helical coils, and internal baffle coils (Figure 2.5). The conventional jackets consist of a casing surrounding the cylindrical part or the entire tank; these surfaces are the most used in small tanks and high-pressure applications.

Jacketing is usually chosen due to several advantages, such as larger heat transfer surface, low-cost construction materials, easier maintenance and fewer problems in a viscous fluid flow. Additionally, the jackets can be used independently of the agitator size and type, contrary to the coils that restrict the dimensions of the impeller. The coils have the benefit of a higher overall film coefficient. However, internal coils have the tendency to affect the flow inside stirred tanks because they restrict the fluid circulation (COKER, 2001; PEDROSA AND NUNHEZ, 2002).

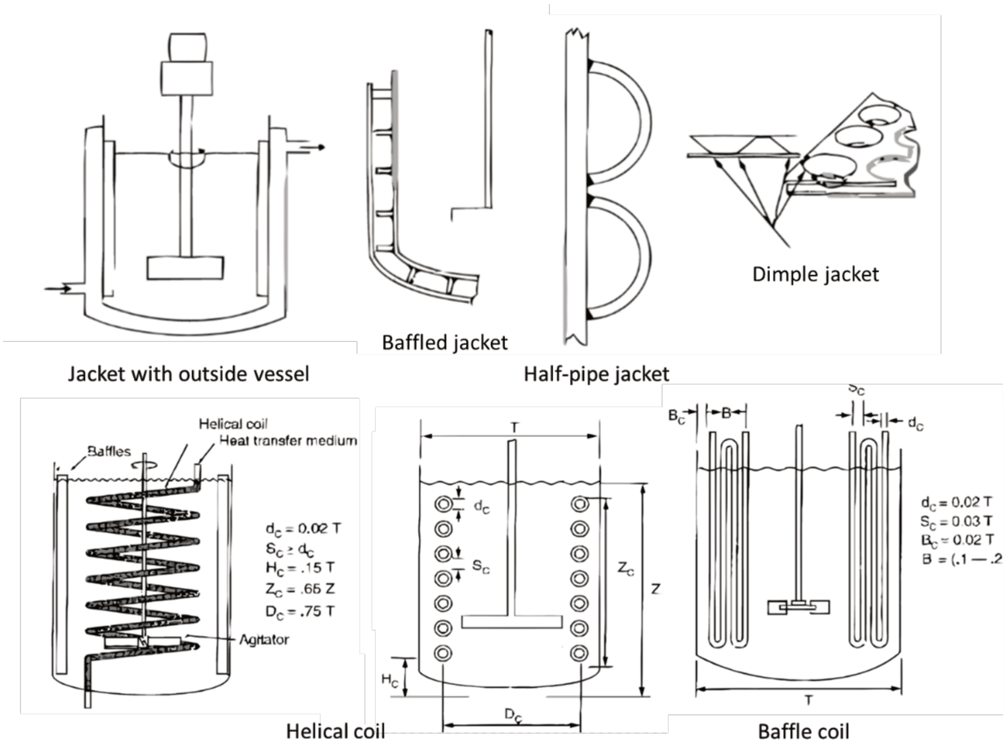

Figure 2.5. Most commonly heat transfer surfaces for stirred tanks (HEMRAJANI AND TATTERSON, 2004)

In stirred tanks, the transfer of thermal energy is mainly due to the overall movements supplied for the impeller to the fluid that has significant effects on the overall heat transfer coefficient. In a jacketed stirred tank, the heat transfer mechanism occurs by conduction and forced convection. The rate of heat transfer (Q) is governed by the general heat transfer equation and is proportional to the temperature difference between a solid surface and the process fluid. The overall heat transfer equation can be expressed as follow (OLDSHUE, 1983):

$$Q = UA\Delta T \tag{2.1}$$

where A is the heat transfer area and U is the overall heat transfer coefficient, the main parameter affected by the activity of the impeller.

The overall coefficient (U) is the sum of various heat transfer resistances as shown in Figure 2.6 and can be written as:

$$\frac{1}{U_o} = \frac{1}{h_o} + \frac{l}{k} + \frac{1}{h_i}\frac{A_o}{A_i} + ff \tag{2.2}$$

In Equation 2.2, the fluid process side is represented by the subscript *o,* and the heat transfer fluid side is represented by the subscript i. The term $(1/U_o)$ is the overall heat transfer resistance, $(1/ho)$ is the coefficient on the process fluid side, l and k are the thickness and the thermal conductivity of the material, respectively. $(1/hi)$ is the coefficient on inside surface of jacket adjusted to the heat transfer area basis (Ao/Ai), and *ff* is the fouling factor considering corrosion or dirtiness on both sides (OLDSHUE, 1983; COKER, 2001).

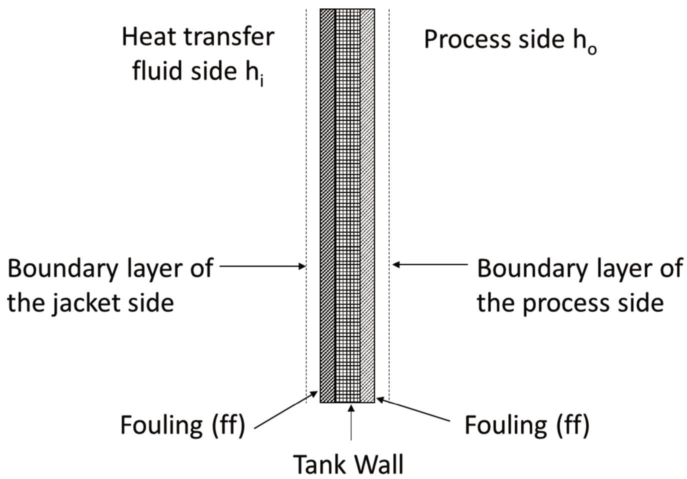

Figure 2.6. Resistances of the jacketed wall of the stirred tank

The heat transfer coefficient (h_o) is dependent on materials and fluid properties, such as density, viscosity, thermal conductivity and specific heat. It is a function of the surface geometry and the flow conditions, which may be laminar or turbulent. This dependence is a result of the boundary layer influence on the convection heat transfer.

There are several possibilities for calculating convective heat transfer coefficients from empirical correlations, but due to the specific conditions for which these correlations were determined, its application in heat transfer problems is restricted. Dimensionless quantities as the Nusselt, Reynolds and Prandtl numbers involving the fluid and system characteristics are used to predict the heat transfer coefficient in a stirred tank, as shown below:

$$Nu = f(Re, Pr) \tag{2.3}$$

Equation 2.3 has been expanded in many experimental studies (as presented in the following section) using an expression similar to the correlation of SIEDER AND TATE (1936). In order to increase the range of validity to different geometries, the expressions include the geometry parameters of the tank and the impeller, the physical properties of the fluids and the agitation grade. Then equation 2.3 can be written as:

$$Nu = \frac{h_o T}{\kappa} = f\left(\frac{D^2 N}{\mu}, \frac{C_p \mu}{\kappa}, \frac{\mu}{\mu_s}, \frac{D}{T}, \frac{C}{T}\right) \tag{2.4}$$

Reordering the equation 2.4, it can take the form

$$\frac{h_o T}{\kappa} = K\left(\frac{D^2 N}{\mu}\right)^a \left(\frac{C_p \mu}{\kappa}\right)^b \left(\frac{\mu}{\mu_s}\right)^c \left(\frac{D}{T}\right)^d \left(\frac{C}{T}\right)^e \tag{2.5}$$

The terms K, a, b, c, d, and e are evaluated experimentally. The constant K depends on the impeller geometry and the heat transfer coefficient and varies between 0.3 and 1.5. The exponents of dimensionless numbers rely on the particular system; a correlation obtained experimentally can only be used for another system when there is a similarity between the geometries and the process (MOHAN *et al*., 1992).

2.1.4 Experimental studies of heat transfer in jacketed stirred tanks

Jacketed stirred tanks have been widely researched due to the popular use of the jackets as heat transfer surface. The first study in heat transfer in stirred tanks investigated the film heat transfer coefficient in an unbaffled stirred jacketed vessel using paddle impellers. This study established the methods and techniques to determine heat transfer coefficients using a general correlation (CHILTON *et al.,* 1944) as Equation 2.5. The values of the constants in the Nusselt number correlation were calculated using a graphical method and the results found were, a=2/3, b=1/3, c=0.14, and K equal to 0.36.

The general procedure proposed by Chilton *et al*. (1944) has been a basis for subsequent works. The authors proposed a graphical method for a conventional stirred tank with jacket and coils immersed in the liquid. This method has been used for different types of impellers and viscous fluids (UHL, 1955) and also for different configurations; for a larger tank totally jacketed with internal coils, higher heat transfer coefficients (about 16% for coils and about 11% for jackets) have been found (CUMMINGS AND WEST, 1950). Further studies have incorporated the computer analysis to replace graphic analysis and obtain more accurate results (CHAPMAN *et al*., 1964).

The study of the effect of tank configuration on the heat transfer coefficient includes the effects of the impeller geometry (i.e. diameter D/T and height C/T). For radial impellers, an increment in the diameter increases the heat transfer coefficient due to the higher turbulence caused by the increased Reynolds number (STREK, 1963; SURYANARAYANAN *et al*., 1976). In the case of axial impellers, the heat transfer coefficient increases when small axial flow impellers are used (ASKEW AND BECKMANN, 1965).

The impeller position has also been investigated by changing the distance between the center of the impeller and the bottom of the tank. A decrease in the heat transfer coefficient has been reported when the impeller is close to the bottom. Several studies have confirmed that as the distance between the bottom and the impeller is increased, the coefficient increases because of the reduction of the vortices and the better mixing conditions (STREK, 1963; AKSE *et al.,* 1967; SURYANARAYANAN *et al.*, 1976; RAI *et al.*, 2000).

However, some authors have reported a decrease in the coefficient when the impeller distance from the bottom of the tank is considerable. The optimum lengths reported in the literature are about $C/T = 0.55$ (RAI *et al.*, 2000) and $C/T \leq 0.7$ (STREK, 1963), approximately at the center of the tank. When it comes to the local heat transfer coefficient this depends on the vertical distance that exists from the plane of rotation of the impeller to the measurement point (AKSE *et al.,* 1967).

The addition of baffles on the tanks has notable effects on the heat transfer coefficients. Under turbulent conditions (Re > 10.000), increases of about 37% have been found in the coefficient value (BROOKS AND SU, 1959; STREK, 1963). This increment occurs because of the turbulence inside of the tank increases in the presence of the baffles and by consequence the thickness of the liquid layer decrease at the tank wall. Also, in stirred jacketed tanks equipped with disc turbine, non-standard baffles can increase in approximately 20% the heat transfer coefficient compared with tanks with standard geometries (KARCZ AND STREK 1995).

More recently, Debab *et al.* (2011) with an experimental design methodology, established the effects of the impeller geometry and the baffles on the overall heat transfer coefficient using a mechanically jacketed stirred tank equipped with a turbine impeller for non-Newtonian liquids. It was demonstrated that the heat transfer coefficient increases with the increment of the diameter of the impeller and it is subject to the speed of it. The authors found correlations of the heat transfer coefficient, for each impeller, based on the power number. Also, was proposed an agitated tank with flat blade disc turbine and baffles as the most favorable for heat transfer processes with non-Newtonian fluids.

Another important feature is the liquid height, which has appreciably influence on the heat transfer coefficient and has been introduced in the Nusselt number correlations with exponents between -0.47 and -0.56 (CHAPMAN *et al.,* 1964; RAI *et al.*, 2000).

The electrochemical technique has been applied to measure local variations of the mass transfer coefficient at the tank wall. The results of mass transfer were turned into heat transfer data using an analogy. With this technique, significant variations were observed in the heat transfer coefficients in the axial direction and were presented two correlations: one for the region above the impeller and another for the zone below the impeller (MAN *et al.,* 1984).

The boundary layer at the wall controls the heat transfer rate towards or from the wall in jacketed agitated vessels (NAGATA *et al.,* 1972). Studies have been shown that it is crucial to include the heat transfer due to the boundary layer mixed with the bulk in the heat balance of the tank. Overall correlations that consider the boundary layer and combines it with the heat transfer coefficient for the regions above and below the impeller have been developed. (BALAKRISHNA AND MURTHY, 1979).

The transient method is a more recent technique that uses experimentally measured temperatures of the wall and the liquid. This approach has been proposed to calculate the convective heat transfer coefficient by solving the transient enthalpy balance. The results have shown values of the heat transfer coefficient and Nusselt number slightly higher than those of similar correlations reported in the literature (PETERA *et al*., 2008).

Table 2.2 summarizes the main experimental studies made in jacketed stirred tanks to determine Nusselt number correlations. In the following section, more current studies that include CFD models are presented.

Table 2.2. Summary of previous works in jacketed stirred tanks

Author	***Type of impeller***	***Tank interns***	***Correlation***
Chilton et al., 1944	Flat paddle	Coil, unbaffled	$Nu = 0.36Re^{2/3}Pr^{1/3}Vi^{0,14}$
Cumming and West, 1950	Turbine 6 flat blades	Coil, unbaffled	$Nu = 0.4Re^{2/3}Pr^{1/3}Vi^{0,14}$
Brooks and Su, 1959	Turbine, 6 flat blades	Unbaffled and baffled	$Nu = kRe^{2/3}Pr^{1/3}Vi^{0,14}$ k=0.54 [1] k=0.74 [2]
Chapman, 1964	Turbine, 6 flat blades	Baffled	$Nu = 0.76\ Re^{2/3}Pr^{1/3}Vi^{0,24}$ [3] $Nu = 1.15\ Re^{2/3}Pr^{1/3}Vi^{0,24}\left(\frac{H_i}{D_T}\right)^{0.4}\left(\frac{H_L}{D_T}\right)^{-0.56}$ [4]
Strek, 1963	Rushton turbine	Baffled	$Nu = 0.76\ Re^{2/3}Pr^{1/3}Vi^{0,14}$ [3] $Nu = 1.01Re^{2/3}Pr^{\frac{1}{3}}Vi^{0,14}(\frac{d}{D})^{0,13}(\frac{h}{D})^{0,12}$ [4]
Nagata, 1972	Flat blade paddle, Rushton turbine	Baffled	$Nu = 0.42\ Re^{2/3}Pr^{1/3}Vi^{0,14}$
Suryanarayanan et al., 1976	Four flat-bladed turbine	Baffled	$Nu = 0.22Re^{0.63}Pr^{0.33}\left(\frac{D_a}{D}\right)^{0,14}\left(\frac{H_a}{D}\right)^{0,09}\left(\frac{D_c}{D}\right)^{-0,21}\left(\frac{d_o}{D}\right)^{0,14}$
Akse et al., 1967	Six-blade, disc-type turbine	Baffled	$Nu = 0.81\ Re^{0,68}Pr^{\frac{1}{3}}Vi^{0,14}\left\{\left(\frac{h}{D}\right)^{2/3} + \left(1-\frac{h}{D}\right)^{2/3}\right\}$
Man et al., 1984	Rushton turbine Propeller	Baffled Coil	$Nu = 0.4\ Re^{0,68}Pr^{1/3}(X/D)^{-0,33}$ [5] $Nu = 0.76\ Re^{2/3}Pr^{1/3}(X/D)^{-0,06}$ [6]
Balakrishna and Murthy, 1980	Rushton turbine	Baffled	$\left(\frac{h_1L_1}{K}\right) = 0.664\ (UL_1\rho/\mu)^{0,5}\left(C_p\mu/k\right)^{1/3}(Vi)^{0,14}$ [5] $\left(\frac{h_2L_2}{K}\right) = 0.664\ (UL_2\rho/\mu)^{0,5}\left(C_p\mu/k\right)^{1/3}(Vi)^{0,14}$ [6]
Karcz and Strek, 1995	Disc turbine	Baffled	$Nu = 0.88\ Re^{2/3}Pr^{1/3}Vi^{0,14}$
Rai et al., 2000	Helical ribbon	–	$Nu = 0.55Re^{0.48}Pr^{0.33}Vi^{0.14}\left(\frac{H}{T}\right)^{-0.47}$
Petera et al., 2008	Six-blade turbine pitch angle 45°	Baffled	$Nu = 0.705Re^{0,681}Pr^{1/3}Vi^{0,14}$

[1] Unbaffled tank; [2] Baffled tank; [3] Standard configuration; [4] Non-Standard configuration; [5] Above the impeller plane; [6] Below the impeller plane

2.2 Applications of computational fluid dynamics in stirred tanks

Computational fluid dynamics has been applied as an effective tool for modeling, analysis, and verification of the detailed properties of the fluid motion on stirred tanks by solving Navier-Stokes equations. An appropriate CFD model of a stirred tank depends on several aspects such as impeller modeling approach, grid resolution, discretization schemes and turbulence models (DEGLON AND MEYER, 2006); these features will influence the accuracy of the CFD simulation and the computational cost.

The modeling of the impeller-baffle interaction requires particular treatment and has been classified into two categories: steady and unsteady state. The first one solves the model equations in a steady state mode. The most common approaches of this type are the steady-state impeller boundary condition (IBC) or black box approach, which uses the exact boundary conditions taken experimentally, therefore depending strictly on the experimental data and does not provide details of the flow within the impeller region. The inner-outer (IO) model uses two steady-state solutions: one for the impeller area and another for the whole tank flow (BRUCATO, *et al.* 1998). For last, the multiple reference frame technique (MRF) introduced by LUO *et al.* (1994) solves the inner region (related to the impeller), which does not actually move, using a rotating framework, and the outer region (associated to the baffles) with a stationary framework. The MRF-Frozen rotor can be considered a pseudo-steady state model because the position of the rotating and stationary domains remains fixed respect to each other (RAJ *et al.,* 2014).

The unsteady state approaches solve the time-dependent interaction of the impeller and the working fluid. This category includes the time-dependent sliding-mesh (SM) evaluating two regions: an inner rotating domain to represent the impeller and an outer stationary domain containing the baffles to model the impeller-baffle interaction. This approach can be applied to different tank/impeller configurations; however, it is computationally high-demanding (JOSHI *et al*., 2011).

The impeller interaction has been studied comparing steady and unsteady state approaches. The impeller boundary condition (IBC) have shown inaccurate solutions without experimental data of the impeller regions and big limitations to calculate parameters such as the power number. The inner-outer (IO) approach led to an adequate simulation of the flow and turbulence fields without experimental resources. The best agreement with experimental data for transient conditions was obtained with the sliding-mesh (SM) approach, but it requires larger computational effort (BRUCATO *et al*. 1998). According to MONTANTE *et al*. (2001), the IO model may substitute the SM model due to the slight differences found in both results that also were in agreement with the experimental data, as well as the lower computational effort required.

Several authors indicate that the most frequently approaches used are the multiple reference frame technique (MRF) and the unsteady state sliding mesh (SM) approach. However, the MFR model gives adequate results for the predicted flow field, power number, mean velocity components, turbulent kinetic energy and reduces the computational expenses compared to transient models (DEGLON AND MEYER, 2006; AUBIN *et al*., 2004; RAJ *et al*., 2014).

The discretization schemes, used to transfer the partial differential equations into numerical form, are considered an important choice to obtain accuracy in the solution of the equations. Some authors have studied it to determine their effect on the flux patterns. It has been observed that the first order upwind method tends to under predict the turbulence kinetic energy, while the higher-order methods show more accurate results compared to Laser Doppler Velocimetry (LDV) data. However, the higher order methods are less robust and need a longer time to reach convergence in the solution (AUBIN *et al*., 2004; BRUCATO *et al*., 1998; DEGLON AND MEYER, 2006).

The grid resolution and the discretization scheme have substantial effects over the turbulence kinetic energy and show less influence in the flow field and mean fluid velocity. However, a very refined grid showed no visible difference in the results using second or third-order scheme (DEGLON AND MEYER, 2006).

Turbulence models are employed to simulate the effects of turbulence in small-scale motion, but without solving all scales of the smallest turbulence fluctuations (SONDAK, 1992). The Large Eddy Simulations (LES) turbulence model can predict with accuracy all the flow variables. However, this model needs high computational effort with a fine grid.

The k- ε turbulence model is one the most used in turbulence flows. The predictions of the standard k- ε turbulence model by Launder and Spalding (1974) have been widely studied founding that it generally under or over-predicts turbulence quantities (MURTHY AND JOSHI, 2008; DEGLON AND MEYER, 2006; MONTANTE et al., 2001). Some modifications of this model have been made to improve the CFD predictions such as the Chen Kim k- ε and the Renormalization Group (RNG) k- ε models (CHEN AND KIM, 1987; YAKHOT AND ORSZAG, 1986).

Researchers have suggested that the turbulence models based on the *Reynolds Average Navier-Stokes* (RANS) equations (e.g. RSM, standard k-ε, SST k-ω model) might be the main CFD tool to produce accurate results with less computational resources (MURTHY AND JOSHI, 2008). The Reynolds Stress Model (RSM) and standard k-ε model usually under-predict the turbulent kinetic energy in the impeller region but can capture well all the mean flow characteristics when disc turbine impeller is used (MURTHY AND JOSHI, 2008).

The Shear Stress Transport SST k-w model has been used to develop the flow field near to the wall where the k-ε model is deficient and obtain the characteristics of the turbulent flow near the impeller. This model has been used extensively with the multiple reference frame (MRF) approach and the second order upwind scheme, the outcomes have shown a good correlation with experimental data and values of the non-dimensional distance (y^+) less than 10 (RAJ *et al*., 2014).

When compared meshes of different densities, the finer numerical grids of agitated jacketed vessels used along with the standard k- ε and optimized Chen-Kim models have shown closer values of both the local heat transfer coefficient and the kinetic turbulence energy values compared to experimental data (ZAKRZEWSKA AND JAWORSKI, 2004).

Different arrangements of internal and external heat transfer surfaces have been studied using computational fluid dynamics. It was observed that the mechanical configuration of the tank and agitation method significantly affects the temperature and flow problems. It can be optimized using both jackets and coils, which reduce the temperature difference inside the tank and result in a better distribution (NUNHEZ AND McGREAVY, 1994).

Some authors have proposed taking into account the non-dimensional distance (y +) as a parameter to control mesh size in CFD models with thermal calculations. The estimation of the heat transfer coefficient depends on the refinement of the heating surface in the tank and must be independent of the mesh. Values of y+ less than 0.1 are suggested to achieve independence of the heat-transfer predictions of the CFD model and obtain good agreement with the experimental data (JAIMES AND NUNHEZ, 2017).

2.3 Mathematical and CFD modeling

The mathematical modeling is used to analyze the fluid flow in stirred tanks and to understand the physical and chemical phenomena. The computational fluid dynamics is based on the continuity, momentum, and energy equations and provide solutions for chemical reactions, heat transfer, and different flow situations.

2.3.1 Dimensional analysis

The dimensional analysis is used to define the physical meaning of the expressions that determine the heat transfer within a system. The dimensionless Nusselt number is widely used to calculate the heat transfer in stirred tanks and it is a function of other dimensionless numbers such as the Reynolds number, the Prandtl number, and the geometric relationships (as presented in section 2.1.3)

2.3.1.1 Reynolds number (Re)

The Reynolds number denotes the relationship between the inertial and viscous forces acting on the system. For stirred tanks, the Reynolds number is defined as:

$$Re = \frac{D^2 N \rho}{\mu} \tag{2.6}$$

where D is the impeller diameter, in m and N is the impeller speed, in rev/s; ρ is the fluid density, in kg/m^3 and μ is the fluid dynamic viscosity, in kg/m·s. The flow in a mixing tank ranges continually from low Reynolds numbers (Re<10), where the viscous forces dominate, to high Reynolds numbers where inertial forces dominate (Re>10^4) (HEMRAJANI AND TATTERSON, 2004).

2.3.1.2 Prandtl number (Pr)

The Prandtl number is defined as the ratio of the momentum diffusivity to the thermal diffusivity (υ/α), which symbolizes the transport properties of the fluid regarding the momentum and the heat, respectively. Its definition can be writing as follows:

$$Pr = \frac{C_p \mu}{\kappa} = \frac{\upsilon}{\alpha} \tag{2.7}$$

where C_p is the specific heat, κ the thermal conductivity, υ the kinematic viscosity and α the thermal diffusivity. The Prandtl number is used as a measure of the rate at which the momentum and energy are transported, in the velocity and thermal boundary layers. Small values of Prandtl number means better heat transport compared with momentum transport (SCHLICHTING, 1979).

2.3.1.3 Nusselt number (Nu)

The Nusselt number represents the ratio of convection to pure conduction heat transfer. In a jacketed tank, the Nusselt number has the following form:

$$Nu = \frac{h_o T}{\kappa} \tag{2.8}$$

where h_o is the heat transfer coefficient, T is the diameter of the tank and κ is the thermal conductivity of the fluid. A large Nusselt number indicate that heat transfer by convection is dominant, which is characteristic of the turbulent flows.

2.3.1.4 Power number (Np)

Power number relates the resistance force to the inertial force. This parameter is a measure of the power consumption of the impeller and it is very commonly used in equipment design. For stirred tanks, the power consumed for the turbine can be determined by the power number correlation, as follows:

$$Np = \frac{P}{\rho N^3 D^5} \tag{2.9}$$

where P is the impeller power in Watts, ρ is the density of the liquid in Kg/m^3, N is the impeller speed in rev/s, and D is the impeller diameter in meters.

2.3.2 Transport equations

The conservation or transport equations describe the changes in the fluid movement in time and space due to the processes of convection, diffusion and other sources. The continuity equation represents the physical principle of the conservation of mass. For general cases, using the Einstein notation, the continuity equation has the form:

$$\frac{\partial \rho}{\partial t} + \frac{\partial \rho U_i}{\partial x_i} = 0 \tag{2.10}$$

Here ρ is the fluid density and U_i the ith component of the fluid velocity. The first term on the left-hand side describes the change in the fluid density and the second term describes the transport of the fluid.

The momentum equation results from the application of Newton's second law and indicates the conservation of momentum in the three component directions. Known as Navier-Stokes equations, the momentum equation involving additional sources besides the transport by convection and diffusion can be expressed as given below:

$$\frac{\partial(\rho U_i)}{\partial t} + \frac{\partial}{\partial x_j}(\rho U_i U_j) = -\frac{\partial \mathrm{p}}{\partial x_i} + \frac{\partial}{\partial x_j}\left[\mu\left(\frac{\partial U_i}{\partial x_i} + \frac{\partial U_j}{\partial x_j} - \frac{2}{3}\frac{\partial U_k}{\partial x_k}\delta_{ij}\right)\right] + \rho g_i + F_i \tag{2.11}$$

The left-hand side takes into account the temporal and convective transport effects, respectively. The right-hand side considers the effect of the pressure gradients, the divergence of the stress tensor that means the transport of momentum due to molecular viscosity, the gravity effects and the source term due to both centrifugal and Coriolis forces, respectively (MARSHALL AND BAKKER, 2004).

The energy equation satisfies the fundamental principle of the conservation of energy. Usually, the heat transfer in stirred tanks is represented by the energy equation, which concerning the total energy takes the following form:

$$\frac{\partial(\rho E)}{\partial t}+\frac{\partial}{\partial x_i}[U_i(\rho E+p)]=\frac{\partial}{\partial x_i}\left[k_{eff}\frac{\partial T}{\partial x_i}-\sum_{j'} h_{j'}J_{j',i}+U_j(\tau_{ij})_{eff}\right]+S_h \tag{2.12}$$

The first term on the left-hand side indicates the energy variation; the second term is the convective term of energy transport. On the right-hand side, the first term represents the diffusive heat transfer, including a correction for turbulent simulations in the effective conductivity term k_{eff}. The second term on the right-hand represents the heat transfer due to the chemical species diffusion, in there $J_{j',i}$ is the diffusion flux. The third term indicates the heat losses through viscous dissipation, and the fourth denotes the sources due to processes as reactions, radiation, or others (MARSHALL AND BAKKER, 2004).

The total energy E is the sum of both the internal and kinetic energy, and related to the enthalpy is written as:

$$\mathrm{E}=\mathrm{h}-\frac{p}{\rho}+\frac{\mathrm{U}^2}{2} \tag{2.13}$$

A mixture of fluids with different physical properties in an incompressible flow has a static enthalpy expressed in function of the mass fractions, $m_{j'}$, and enthalpies, $h_{j'}$, of the individual species, as follows

$$\mathrm{h}=\sum_{j'} m_{j'}h_{j'}+\frac{p}{\rho} \tag{2.14}$$

For each species j' there is an enthalpy $h_{j'}$ dependent on the temperature of the specific heat expressed as:

$$h_{j'} = \int_{T,ref}^{T} C_{p,j'} dT \tag{2.15}$$

Considering that the working fluid used in this work is incompressible fluid (constant ρ) and monophasic, then the transport equations in Cartesian coordinates take the form:

$$\frac{\partial \mathrm{U_i}}{\partial \mathrm{x_i}} = 0 \tag{2.16}$$

$$\left[\frac{\partial U_i}{\partial \mathrm{t}} + U_i \frac{\partial (U_j)}{\partial \mathrm{x_j}}\right] = -\frac{1}{\rho}\frac{\partial \mathrm{p}}{\partial \mathrm{x_i}} + \frac{\partial}{\partial x_j}\left[\mu\left(\frac{\partial U_i}{\partial x_i} + \frac{\partial U_j}{\partial x_j} - \frac{2}{3}\frac{\partial U_k}{\partial x_k}\delta_{ij}\right)\right] + g_i + \sum F_i \tag{2.17}$$

$$\frac{\partial(\rho E)}{\partial t} + \frac{\partial}{\partial x_i}[U_i(\rho E + p)] = \frac{\partial}{\partial x_i}\left[k_{ef}\frac{\partial T}{\partial x_i} + U_j(\tau_{ij})_{ef}\right] + S_h \tag{2.18}$$

2.3.3 Turbulence

The turbulence phenomenon was initially detected by Leonardo da Vinci in 1507 when he called “la turbolenza” to the whirling flow observed in the water (ECKE, 2005). Afterward, Osborne Reynolds (1984) did experiments to study the behavior of the water using a large pipe of glass and established two regimens of the fluid flow. The laminar regime represents a fluid flow stable without disruption between layers, and the turbulent regime that is characterized by perturbations and instabilities in the fluid flow. Reynolds also established a single dimensionless parameter to determine the transition phase between the laminar and turbulent regime and recognize which is the behavior of the fluid flow. This parameter was called the Reynolds number (Re) (Equation 2.6).

In stirred tanks, the turbulent flow is generated due to the continuous action of the impeller creating large eddies that deconstruct into smaller eddies which possess his kinetic energy; the baffles contribute producing greater turbulence. For these reasons, the flow turns into unsteady, with unpredictable moves in the form of cross currents and with randomly changes in the velocity and the flow properties. High values of Reynolds number, more than 10.000, characterized the turbulent flow.

An efficient mixing process is described by a highly turbulent fluid flow (Re>10.000). Considering turbulence as a time-varying phenomenon the best resolution of the physics should be transient or time-depending simulations (KRESTA AND BRODKEY, 2004). *Direct Numerical Simulation* (DNS) uses the continuity, momentum, and energy equations to solve the turbulent regime directly with small grid spaces and time-steps. However, it requires very fine computational grids and large computational resources, which is hard to achieve nowadays. One alternative to model the mechanism of the turbulent flow is using the Navier-Stokes equations along with methods that introduce average and fluctuating quantities. The transport quantity is expressed as the sum of an equilibrium component and a fluctuation due to turbulence ($U_i + u'_i$) to be introduced into the Navier-Stokes equations.

After an average of time over several fluctuation cycles, the sum of the fluctuations will be zero and only the terms containing the product of two fluctuating terms remain positive. The terms that remain constitute the called *Reynolds-average Navier-Stokes* (RANS) equation, which for momentum equation is:

$$\frac{\partial(\rho U_i)}{\partial t} + \frac{\partial}{\partial x_j}(\rho U_i U_j) = -\frac{\partial \mathrm{p}}{\partial x_i} + \frac{\partial}{\partial x_j}\left[\mu\left(\frac{\partial U_i}{\partial x_i} + \frac{\partial U_j}{\partial x_j} - \frac{2}{3}\frac{\partial U_k}{\partial x_k}\delta_{ij}\right)\right] + \frac{\partial}{\partial x_j}(-\rho\overline{u'_i u'_j}) + \rho g_i + F_i \quad (2.19)$$

The extra term on the right-hand side, $\overline{u'_i u'_j}$, is called the Reynolds stresses and represents the time-averaged values. Additional turbulence models have been developed to close the equations.

2.3.3.1 Boussinesq hypothesis

The hypothesis postulated by Boussinesq in 1877 assumes that the Reynolds stresses are proportional to the mean rate gradients and the constant of proportionality is the turbulent viscosity μ_t. For the general Reynolds stresses $\overline{u'_i u'_j}$ the Boussinesq hypothesis express:

$$-\rho\overline{u'_i u'_j} = \mu_t\left(\frac{\partial U_i}{\partial x_j} - \frac{\partial U_j}{\partial x_i}\right) - \frac{2}{3}\rho k \delta_{ij} \quad (2.20)$$

The turbulent or eddy viscosity is a property of the flow and is not homogenous. The turbulence kinetic energy is also introduced by the Boussinesq hypothesis and can be expressed, regarding the mean turbulence normal stresses, as follows:

$$k = \frac{1}{2}\left(\overline{u'^2} + \overline{v'^2} + \overline{w'^2}\right) \tag{2.21}$$

The conservation of momentum equation for the turbulent regime based on the turbulent viscosity can be written as given below:

$$\left[\frac{\partial U_i}{\partial t} + \frac{\partial(U_i U_j)}{\partial x_j}\right] = -\frac{1}{\rho}\frac{\partial \bar{p}}{\partial x_i} + \frac{\partial}{\partial x_j}\left[\mu_{ef}\left(\frac{\partial U_i}{\partial x_j} + \frac{\partial U_j}{\partial x_i}\right)\right] + g + Fi \tag{2.22}$$

Where, $\bar{p}$ is a modified pressure and μ_{ef} the effective viscosity defined as:

$$\mu_{ef} = \mu + \mu_t \tag{2.23}$$

2.3.3.2 Turbulence modeling

The techniques used in CFD to solve the equations of continuity and motion are classified in *Direct Numerical Simulation* (DNS), *Large Eddy Simulation* (LES) and *Reynolds Average Navier-Stokes* (RANS). DNS uses computational grids highly refined and minor time steps to solve exactly the Navier-Stokes equations and to obtain the full turbulence flow; however, demands enormous computational resources. LES is a transient formulation and have valuable advantages but also require for larger computational resources. Lastly, the RANS approach introduces the turbulence viscosity to solve the averaged Navier-Stokes equations with accuracy, simplicity and using less computational power (JOSHI *et al.*, 2011).

The turbulence models were developed to model the effect of viscous dissipation mechanism of the turbulence flows using the governing conservation laws and without the restriction of the fine mesh and direct numerical simulation. The turbulence models more widely used are the two-equation models (k-ε, k-ω, and SST k-ω).

2.3.3.3 Shear stress transport (SST) k-ω turbulence model

The Shear Stress Transport (SST) k-ω model created by MENTER (1994) combines the advantages of the k-ω model of WILCOX (1988) and the high Reynolds number k-ε model. The original formulation suggested a modification of the k-ε model in function of ω and the introduction of blending functions that are essentials for this method because it provides slow transition between the models, which can switch depending on the fluid flow conditions.

The SST model uses the equations of the k-ε in the region of high velocities (free-stream flow) and the k-ω equations in the area of low velocities (near the wall). This model was developed for Aeronautics application; however, due to the right predictions in fluid flow simulations that require an accurate solution of both the boundary layer and the free-stream flows, it is widely used for other industrial purposes (MENTER, 2003).

Menter (2003) made two modifications on the original formulation based on different experiences using the SST model, the first one replaced the vorticity for the strain rate, S, in the Equation 2.28 (vt) and the change of factor 20 in the production limiter for the value of 10.

In the complete formulation, the kinetic turbulence energy k and the turbulence frequency ω are defined by

$$\frac{\partial(\rho k)}{\partial t}+\frac{\partial(\rho U_i k)}{\partial x_i}= \tilde{P}_k-\beta^*\rho k\omega+\frac{\partial}{\partial x_i}\left[(\mu+\sigma_k\mu_t)\frac{\partial k}{\partial x_i}\right] \tag{2.24}$$

$$\frac{\partial(\rho\omega)}{\partial t}+\frac{\partial(\rho U_i\omega)}{\partial x_i}=\alpha\rho S^2-\beta\rho\omega^2+\frac{\partial}{\partial x_i}\left[(\mu+\sigma_\omega\mu_t)\frac{\partial\omega}{\partial x_i}\right]+2(1-F_1)\rho\sigma_{\omega^2}\frac{1}{\omega}\frac{\partial k}{\partial x_i}\frac{\partial\omega}{\partial x_i} \tag{2.25}$$

The first term on the left-hand side is the rate of change of ω and the second represent the transport by convection. In the right-hand side, the first and second terms are the rate of production and dissipation, respectively. The third term is the transport by turbulent diffusion, and the fourth is the cross-diffusion term, which results from the modification of the k-ε model equation (VERSTEEG AND MALALASEKERA, 2007).

The blending function F_1 is express as given below:

$$F_1 = \tanh\left(min\left[max\left(\frac{\sqrt{k}}{\beta^* \omega y}; \frac{500v}{y^2\omega}\right); \frac{4\rho\sigma_{\omega^2} k}{CD_{k\omega} y^2}\right]^4\right) \tag{2.26}$$

In this expression, y is the nearest distance to the wall, v is the kinematic viscosity or turbulent eddy viscosity, and the $CD_{k\omega}$ is the positive portion of the cross-diffusion term of Eq. 2.26 and is represented as follows:

$$CD_{k\omega} = \max\left(2\rho\sigma_{\omega^2} \frac{1}{\omega} \frac{\partial k}{\partial x_i} \frac{\partial \omega}{\partial x_i}, 1x10^{-10}\right) \tag{2.27}$$

Near to the wall, F1 takes the value of one allowing the use of the k-ω model. Away from the surface, F1 decreases to zero when it comes out of the boundary layer and the k-ε model is activated.

Due to the model over-predicts the eddy-viscosity in smooth surfaces and free shear, the definition was limited to the following formulation:

$$v_t = \frac{\alpha_1 k}{\max\,(\alpha_1 \omega; SF_2)} \tag{2.28}$$

where S is an invariant measure of the strain rate and F_2 is a blending function that restricts the limiter to the wall boundary layer as indicated below:

$$F_2 = tanh\left[\left[\max\left(\frac{2\sqrt{k}}{\beta^* \omega y}; \frac{500v}{y^2\omega}\right)\right]^2\right] \tag{2.29}$$

The SST model uses a production limiter (P_k) to prevent the build-up of turbulence in stagnation areas:

$$P_k = \mu_t \frac{\partial U_i}{\partial x_j}\left(\frac{\partial U_i}{\partial x_j} + \frac{\partial U_i}{\partial x_i}\right) \rightarrow \tilde{P}_k = (P_k, 10 \cdot \beta^* \rho k \omega) \tag{2.30}$$

The empiric constants are calculated merging the constants from the k-ε and the k-ω models as in the equation 2.31.

$$\alpha = \alpha_1 F + \alpha_2 (1 - F) \tag{2.31}$$

The values of the constant for the SST model are given in Table 2.3.

Table 2.3. Coefficients for the SST model

Constant	$\boldsymbol{\alpha_1}$ **(k-ω)**	$\boldsymbol{\alpha_2}$ **(k-ε)**
β	0.075	0.0828
β*	0.09	0.09
σ_ω	0.5	0.856
σ_k	0.85	1.0
α	5/9	0.44

Data from: MENTER, (2003)

2.3.4 Numerical methods

Numerical methods are used to obtain an approximate solution of the general transport equations by discretizing the equations in time and space. The numerical method solves the differential equations by replacing the existing derivatives with algebraic expressions that are applied to the fluid domain divided into a discrete number of points. This process is named discretization. With a greater number of points, the numerical solution will be closer to the exact solution. However, the computational cost increases due to the larger number of linear equations to be solved. Several approaches as finite element, finite difference, and finite volume methods are used to do the discretization process.

2.3.4.1 Finite volume method

The finite volume method is widely used in CFD codes and can be applied to both structured and unstructured mesh because the control volume has no shape constraints. The fluid domain (physical space occupied by the studied fluid) is divided into subdomains that represent the fluid dynamics and its properties through the domain. These subdomains are the mesh cells acting as control volumes. Each control volume has a centroid that store relevant quantities as the fluid properties and the solutions of the variables (velocity, temperature, concentration, etc.).

The element-based finite volume method (EbFVM), used by Ansys CFX, is based on control volumes formed by connecting the center of the elements to its mid-face around a certain node. The vertex of an element becomes the center of the control volume and portions (sub-control volumes) of the neighboring elements form the control volume; this method is also called cell-vertex (Figure 2.7) (MALISKA, 1995).

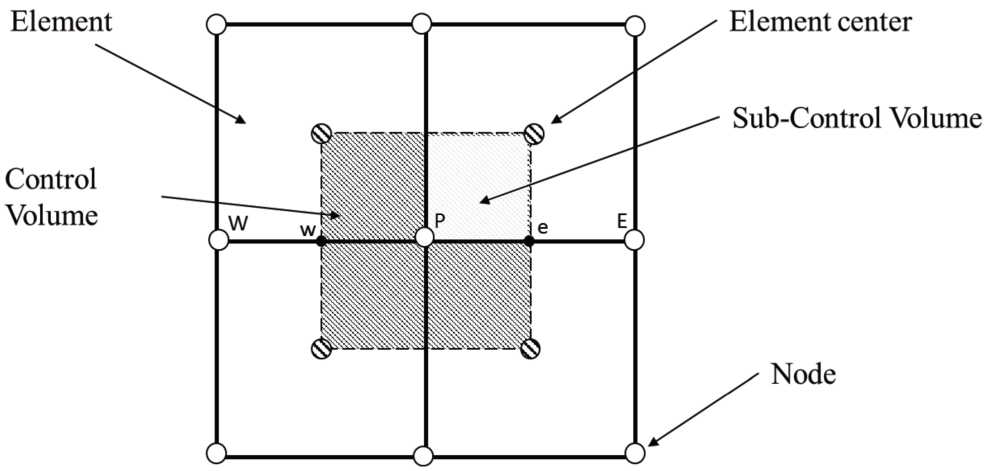

Figure 2.7 Elements and construction of the control volumes

2.3.4.2 Interpolation schemes

In a particular problem, all variables are calculated in the center of the control volumes. Therefore, the values of the variables on the control volume face have to be expressed in terms of the central values. Interpolation functions are used to facilitate the connections between the central points. There are numerous possibilities available in which; two of the most common are the first-order *upwind differencing scheme* (UDS) and the *high resolution* scheme that is a second-order upwind scheme. Both are implemented in ANSYS 16.0.

The one-dimensional problem of diffusion/advection of the property ϕ without the transient and source terms can be expressed as:

$$\frac{\partial}{\partial x}(\rho U \phi) = \frac{\partial}{\partial x}\left(\Gamma^{\phi}\frac{\partial \phi}{\partial x}\right) \qquad (2.32)$$

where ϕ is a scalar quantity and Γ^{ϕ} is the transport equation. The integration of Equation 2.32 in the control volume shown in Figure 2.7 have the form:

$$\rho U\phi|_e - \rho U\phi|_w = \Gamma^{\phi}\frac{\partial\phi}{\partial x}\bigg|_e - \Gamma^{\phi}\frac{\partial\phi}{\partial x}\bigg|_w \tag{2.33}$$

The *upwind differencing scheme* (UDS) approximate the value of ϕ_e to be identical to the value at the node upstream or upwind of "*e*" following the conditions:

$$\phi_e = \phi_P \;\; if \;\; U > 0$$
$$\phi_e = \phi_E \;\; if \;\; U < 0$$

This scheme is very robust in terms of convergence, but it softens the value of a variable in cases where the gradient is too large introducing diffusive discretization errors. Taylor series expansion around *P* can be used to modify this scheme into a *second-order upwind differencing*. It offers great accuracy, though requires more computational power. For $U > 0$:

$$\phi_e = \phi_P + (x_e - x_P)\left(\frac{\partial\phi}{\partial x}\right)_P + \frac{(x_e - x_P)^2}{2}\left(\frac{\partial^2\phi}{\partial x^2}\right) + H \tag{2.34}$$

where *H* describes the higher order terms. When the value at the face is approximated to the first term on the right-hand side, it is considered as a first-order method.

2.3.5 Boundary layer

In 1904, Ludwig Prandtl introduced the concept of the boundary layer as a thin region of fluid near a smooth solid wall with large velocity gradients and significant viscous stresses (SCHLICHTING, 1979). Within this layer, the value of the fluid velocity varies from zero at the wall to 99% of the free-stream velocity (U_∞), at the height of "δ" which is the boundary layer thickness.

In Figure 2.8 can be observed the transitions from the laminar to the turbulent boundary layer, that is influenced by the characteristics of the surface, the type of fluid, the surface temperature, among others parameters.

The turbulent boundary layer can be divided into four individual regions near the wall (Figure 2.6). The first layer called the *viscous laye*r has laminar characteristics where viscous forces are dominant over the Reynolds shear stresses. Immediately above is the *buffer layer,* in this region, the flow initiates the transition to turbulent, but the viscous stresses and heat conduction are still significant. The next area is known as *overlap layer,* where the turbulent flow is more present, but the viscous effects are still leading. Eventually, the turbulence effects dominate, and the flow is fully turbulent in the *free-stream region* (ÇENGEL AND CIMBALA, 2006).

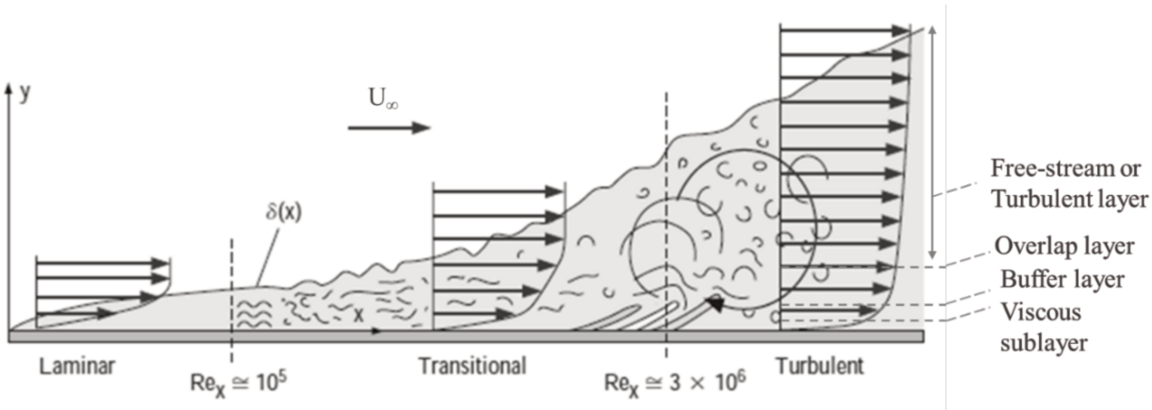

Figure 2.8. Transition of the laminar boundary layer to a fully turbulent boundary layer, and the different flow regions (Adapted from ÇENGEL AND CIMBALA, 2006)

The laminar sublayer has a nearly constant velocity profile at dv/dt = v/y and the shear stress at the wall can be defined as:

$$\tau_w = \mu \frac{u}{y} = \rho v \frac{u}{y} \quad or \quad \frac{\tau_w}{\rho} = \frac{vu}{y} \tag{2.35}$$

here, *y* is the distance from the wall. In the literature, the square root of the term τ_w/ρ tends to be used to refer to the *friction veloci*ty, denoted u_τ. Equation 2.35 can be rewritten as:

$$\frac{u}{u_\tau} = \frac{yu_\tau}{v} \tag{2.36}$$

This expression is called the *law of the wall* and using the dimensionless quantities of distance and velocity (y^+, u^+). Equation 2.36 takes the following form:

$$u^+ = y^+ \tag{2.37}$$

where

$$u^+ = \frac{u}{u_\tau} \tag{2.38}$$

$$y^+ = \frac{yu_\tau}{v} \tag{2.39}$$

In the overlap region, the velocity is related to the logarithm of the non-dimensional distance to the wall y^+. The *logarithmic law* is expressed as:

$$u^+ = \frac{1}{k} lny^+ + A \tag{2.40}$$

where k and A are universal constants, the experimental values are k=0.41 and A=5.2.

Substituting experimental data in the previous equations the following limits are obtained for each region (Figure 2.9):

- Laminar sublayer: $y^+ \leq 5 \;\; u^+ = y^+$
- Buffer layer: $5 < y^+ < 30$
- Logarithmic layer: $30 < y^+$

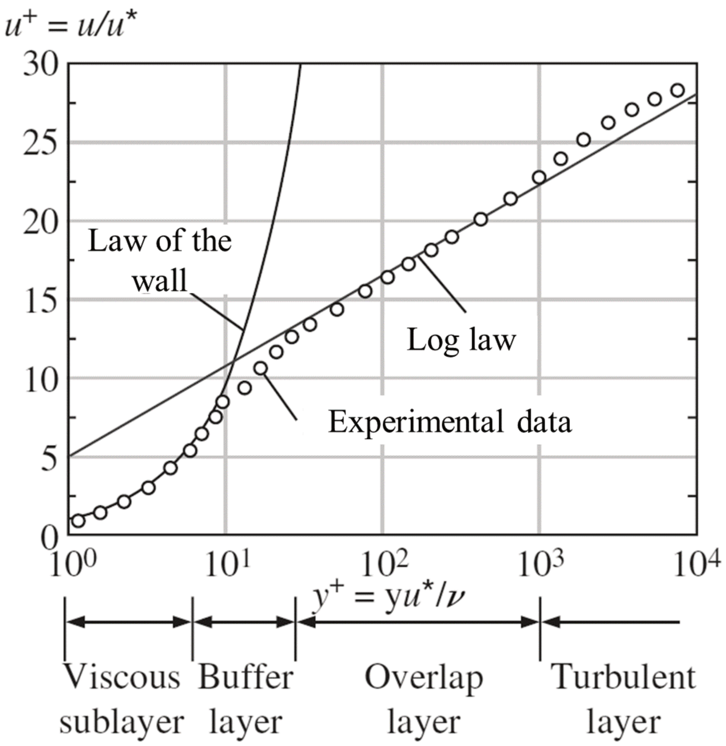

Figure 2.9. Experimental data compared with results of the law of the wall and logarithmic law. (Adapted from ÇENGEL AND CIMBALA, 2006)

To capture the details of the boundary layer flow, it is usual in the simulations to use a wall function in the near-wall regions.

2.3.5.1 Near-wall modeling

The near-wall modeling, commonly known as Low-Reynolds-number modeling, is as important as the turbulence models in CFD simulations. This approach solves the boundary layer numerically using the integration through the viscous sublayer. However, an accurate solution for the viscous region requires some modifications on the turbulence models and a grid fine enough near to the wall. A non-dimensional distance value approximate to one ($y^+ \sim 1$) is recommended to use the low-Re approach (MENTER, 2009). Figure 2.10 shows a scheme of the desired mesh for this method.

Turbulence models based on the turbulence frequency ω -as the Shear Stress Transport (SST- k-ω) and the k-ω models- have proven to be adequate for use the low Re-number method, despite the disadvantages such as a large number of nodes in the near-wall zone that require both high computational power and run time.

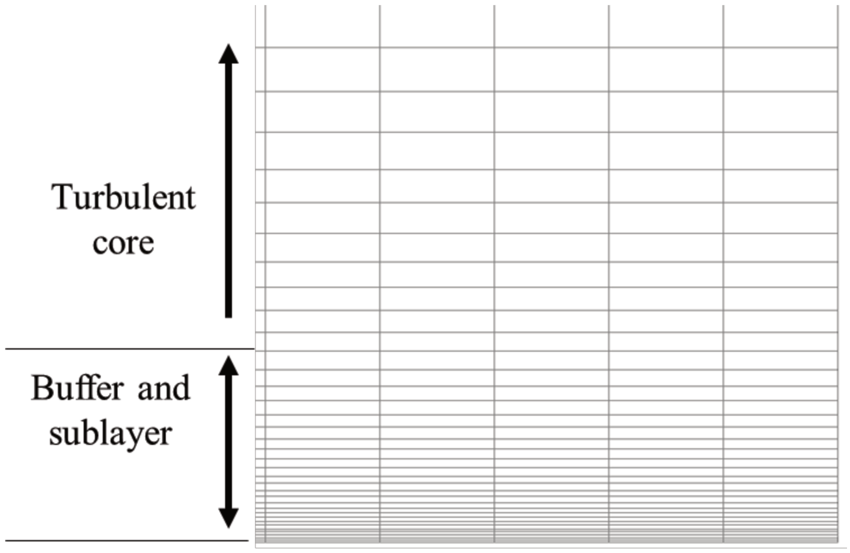

Figure 2.10. Near-wall modeling approach

ANSYS CFX uses an automatic wall treatment based on switching gradually between the wall function and the low Re-number model keeping the accuracy and decreasing the resolution requirements. This boundary condition is settled by default for all the turbulence models based on the ω-equation (SST, k-ω).

Chapter 3

Methodology

The section below discusses the data and methodology commonly used in CFD simulations to create the geometry and to generate the mesh, the assumed initial and boundary conditions, and the mathematical models used in the solution. The procedure is developed following the stages that are shown in Figure 3.1.

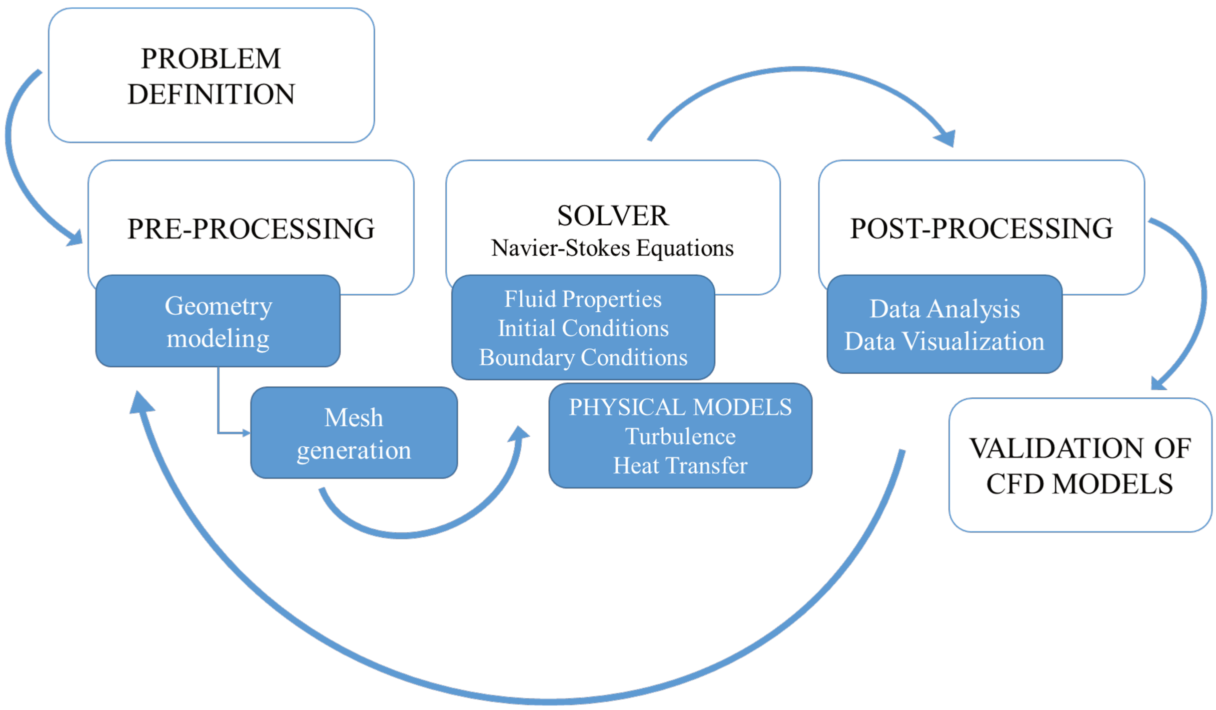

Figure 3.1 Flow chart of the CFD methodology

The methodology begins defining the problem and the mathematical model, followed by the creation of the geometry and mesh generation. The solver applies numerical methods (discretization) to solve equations for the fluid field variables at every cell of the mesh. At last, the solution is post-processed to obtain the quantities of interest, and validate the results with experimental data to prove the accuracy of the model. Finally, a review of the model is recommended to determine if it is appropriate and represents the physical phenomenon. If the model does not accurately predict the response, it must be updated by returning to the pre-processing stage until satisfactory results are obtained.

3.1 Problem identification

As indicated previously, the current investigation aims to obtain a Nusselt number correlation to calculate the heat transfer coefficient in a conventional jacketed stirred tank to facilitate the equipment design and the scale-up of tanks with integrated mixing and heat exchange.

The tank consists of a cylindrical vessel with a flat bottom and four baffles attached to the wall, equipped with a turbine impeller with six flat blades, type Rushton turbine. A three-dimensional model is developed to characterize the tank, and computational fluid dynamics is used to solve the conservation equations for mass, momentum, and energy in the fluid flow of interest. This geometric configuration is identical to that used in the experimental work of Strek (1963) in order to validate the results of the CFD model.

3.1.1 Tank configuration

The geometry of the tank (Figure 3.2) had a diameter (T) of 0.3 m; containing four baffles with a width (B) of 0.03 m (1/10T) equally spaced. The fluid height (Z) was maintained constant at 0.3 m in a relation of 1:1 with the tank diameter. The impeller was varied in height (C) using the ratio C/T of 0.10, 0.25 and 0.45.

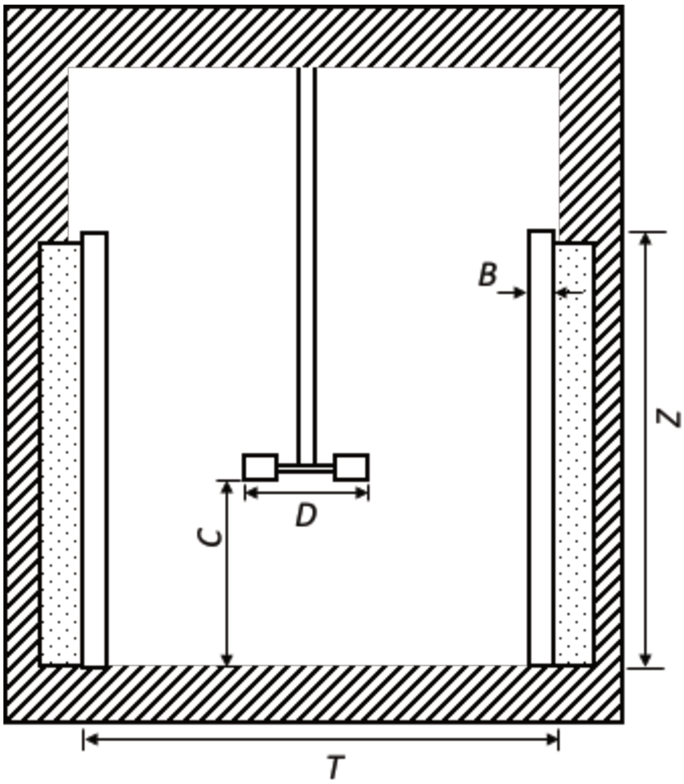

Figure 3.2. Schematic diagram used experimentally

3.1.2 Impeller configuration

The impeller used was a Rushton turbine with six blades (Figure 3.3) with the same dimensions of the impellers used in the experimental work of Strek (1963). Six different sizes of impellers were utilized with diameters of 0.05, 0.10, 0.12, 0.15, 0.18 and 0.220 m. The thickness of the blades, shaft, and the disc was taken from standards sizes of Rushton turbines because these parameters were not reported in the referenced study. The geometrical relationships of the Rushton impeller are given in Table 3.1.

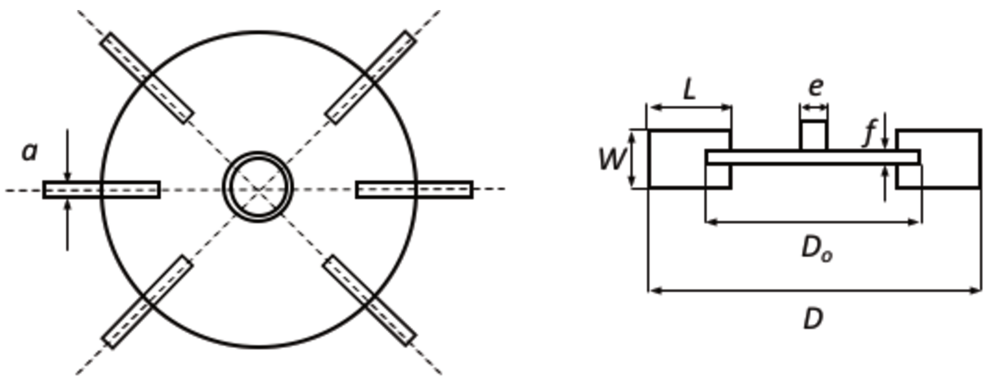

Figure 3.3. Sketch of a Rushton turbine impeller

Table 3.1. Impeller main dimensions

Parameter	***Symbol***	***Dimensions***
Diameter	D	1/6T; 2/5T; 1/2T; 3/5T; 3/4T
Disk diameter	Do	3/4 D
Blade width	W	1/4 D
Blade Height	L	1/5 D
Blade thickness (mm)	a	2
Shaft diameter (mm)	e	10
Disc thickness (mm)	f	3

3.1.3 Flow regime

A turbulent flow regime condition was studied in the fluid domain. The Reynolds number values were between $6.6x10^4$ and $4.8x10^5$.

3.1.4 Heat transfer surface

The heat exchange between the fluid and the tank walls was investigated experimentally by STREK (1963) using a conventional jacket without internal components covering only the cylindrical part of the tank. The tank was insulated on the top and on the bottom. The heating agent was steam with a mass flow rate of 50 kg/h and a pressure range of 0 – 0.5 atm. Under these conditions, the tank walls reached an average temperature of 98ºC for the experimental tests. Fixed temperature was adopted in the CFD model as a boundary condition to represent the heating jacket. This condition was assumed taking into account that the experimental heating agent was steam with a constant saturation temperature.

3.2 Pre-processing

The following stage of the CFD methodology consists of creating the geometry, the discretized domain (meshing) and set the initial and boundary conditions and the mathematical models. A three-dimensional solid model was created using Computer-Aided Design (CAD) software to represent the design of the stirred tank and the impeller. The working fluid and the initial conditions were the same as those used in the experimental study of Strek (1963) (Section 3.2.3).

3.2.1 Geometry creation

The geometry of the tank and the Rushton impeller were created with ANSYS ICEM CFD 16.0. This software allows users to create or edit points, curves, and surfaces, which will shape the boundaries of the desired design. The designed geometry is a 3D model that reproduces only half of the tank considering the symmetry of the configuration (Figure 3.4). The symmetry application causes some benefits such as the reduction of design difficulty, resolution increase for a fixed number of cells and shorter execution time.

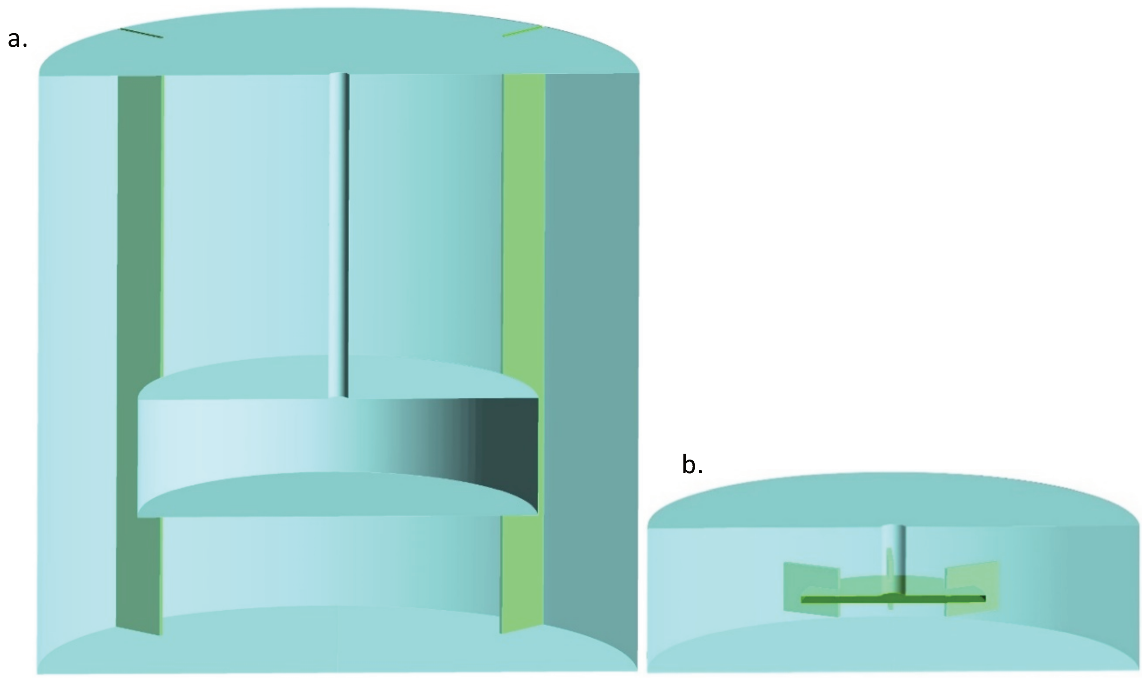

Figure 3.4 Geometry of a. Stationary domain (Half tank) b. Rotating domain (Half impeller)

The simulation domain in stirred tanks with CFD models is composed of two main regions: a rotating volume containing the impeller and a stationary volume enclosing the baffles and the walls of the tank. These zones are called rotating and stationary domain, respectively, and are connected by an interface (Figure 3.5).

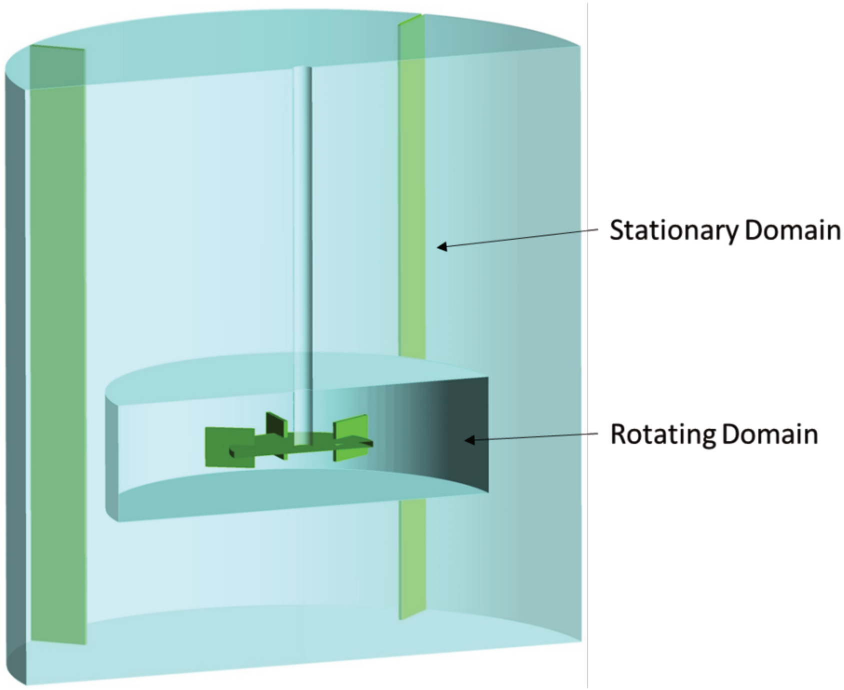

Figure 3.5. Stationary and rotating domains of the model

The interface location between the rotating and stationary domain cannot be arbitrary since it must be in regions where the flow of variables does not change considerably with the angular location or over time. In this work, the interface was located at a radial distance from the center of the impeller of ± 0.7T and an axial distance of ± 0.25T, as suggested in previous researches (GHADI AND SINKAKARIMI, 2014; LANE *et al*., 2000). For the bigger impeller (0.22 m), the interface diameter was 0.26 m localized at the midpoint between the impeller blades and the baffles.

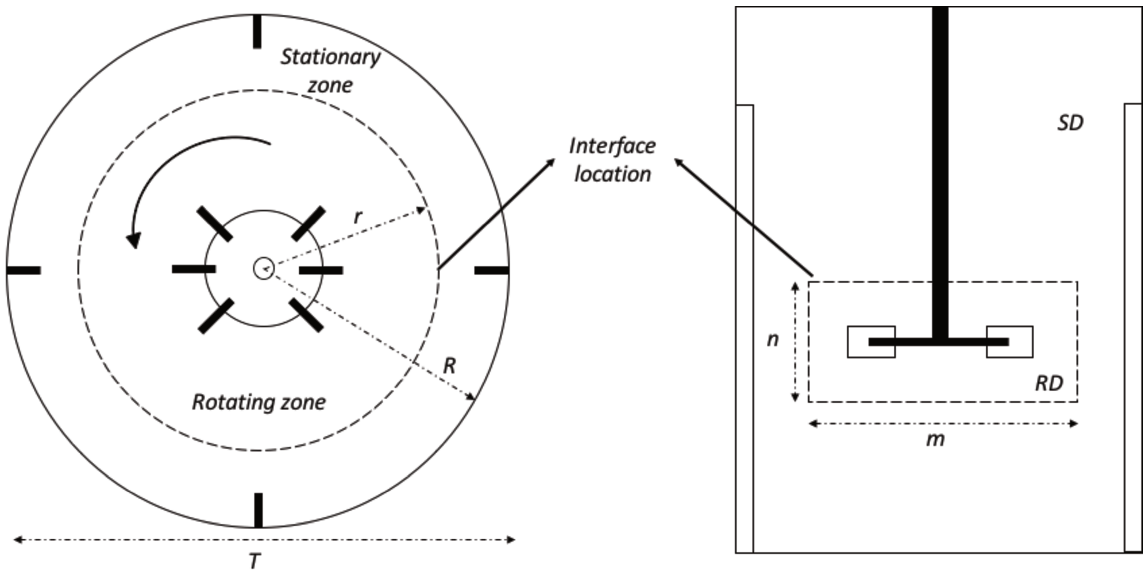

Figure 3.6. Scheme of the interface location bounding the rotating domain

3.2.2 Mesh generation and grid independence test

The generation of the mesh is the subsequent stage in the CFD methodology. A well–constructed mesh is of extreme importance for successful results. It is vital to generate a refined enough grid that represents well the fluid flow. However, a huge number of cells is not desirable due to the higher computational cost.

An hexahedral mesh was chosen to ensure precise modeling of the boundary layer and also because it offers several benefits such as reduced discretization error, small number of cells and high reliability (RAJ et al., 2014). ANSYS ICEM CFD 16.0 was used to produce the structured hexahedral mesh based on a block topology model, which consists in dividing the domain into sub-regions that are occupied by a structured grid. Subsequently, the nodes on the blocks are merged and the full mesh is generated (Figure 3.7).

Local refinement was implemented in the areas where viscous forces predominate such as walls, baffles and impeller regions. Different levels of refinement were used depending on whether it is a surface with heat exchange or not, as the impeller blades.

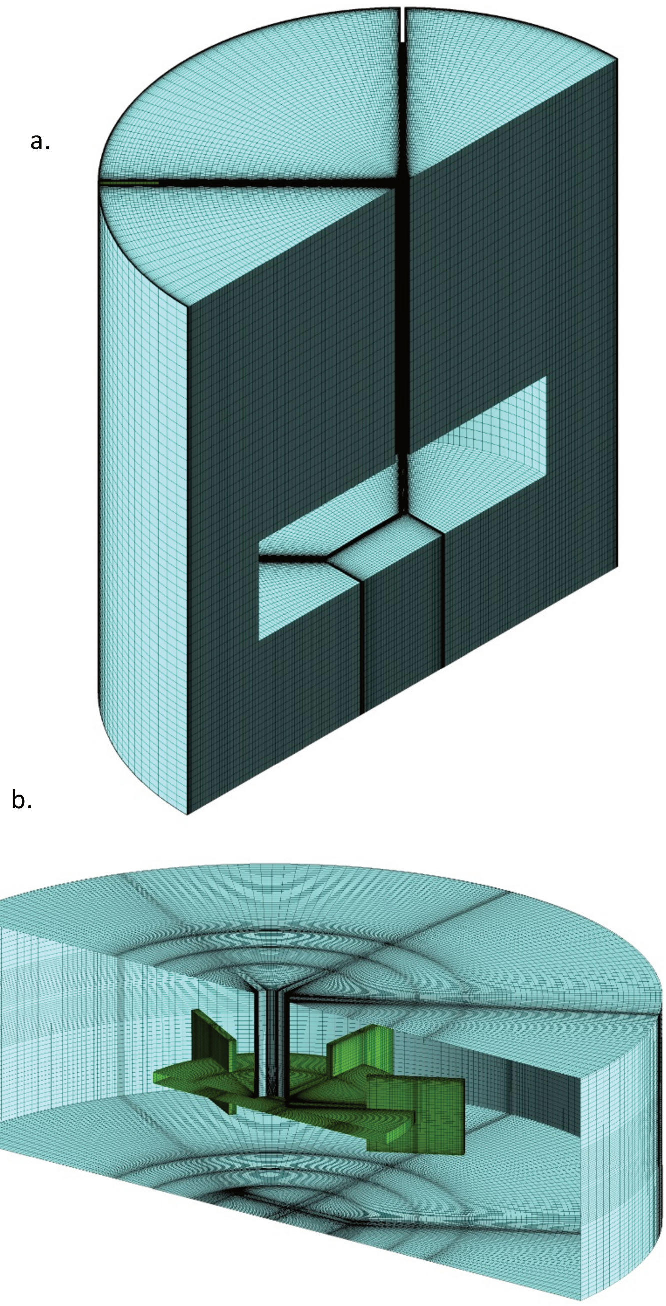

Figure 3.7. Hexahedral meshes. a. Stationary domain b. Rotating domain.

An automatic blocking strategy called O-grid was used to adjust the outer boundary of the geometry on an “O-type” or semicircle to avoid the highly skewed and deformed cells at the perimeter of the geometry. This strategy, commonly employed on cylindrical type geometries, improves the quality of the mesh by reducing the angle between two adjacent faces of a block. The same procedure was developed to create the mesh of both rotating and stationary domains (Figure 3.8).

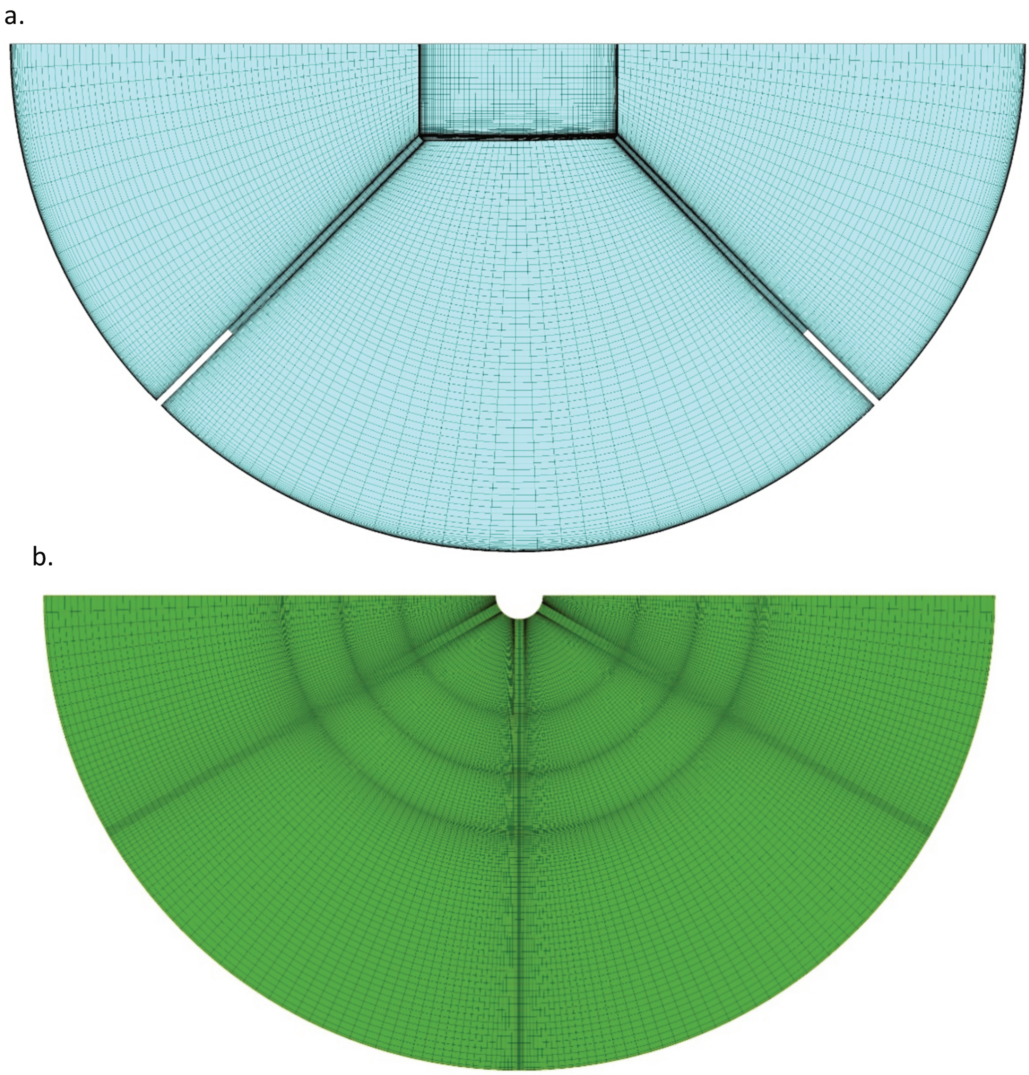

Figure 3.8. O-grid a. the bottom of the stationary domain b. top of the rotating domain.

3.2.2.1 Grid independence study

Grid independence studies are performed to ensure numerical accuracy and a solution independent of the mesh. Additionally, they are used to identify the influence of the mesh density on an established variable. Typical mesh independence tests are made starting with a coarse mesh, which is gradually refined until the value of the response variable is stable or until the percentage of the variation between two mesh levels is small enough (KARCZ AND KACPERSKI, 2012).

Usually the meshes are not fine enough near to the wall and cannot solve precisely the velocity and temperature profiles in the boundary layers. In this work, the mesh was refined in the regions with high gradients such as the tank wall, baffles, and impeller blades. The non-dimensional distance y^+ (Eq. 2.39) was used to evaluate the mesh quality in the viscous layer near to the walls as well as to corroborate that the refinement was appropriate for the turbulence model. CFD packages suggest the verification of the average values of the y^+ to confirm if the mesh size is appropriate for the model.

In order to be able to use the variable y^+ (related to the fluid dynamic boundary layer) in thermal calculations, the relationship between the thermal and fluid dynamic boundary layers should be considered. This relationship is represented as follows (INCROPERA AND DEWITT, 2007):

$$\frac{\delta}{\delta_T} = Pr^n = \left(\frac{C_p \mu}{k_f}\right)^n \tag{3.1}$$

where Pr is the Prandtl number; δ is the thickness of the hydrodynamic boundary layer; δ_T is the thickness of the thermal boundary layer; C_p is the specific heat; μ is the dynamic viscosity; and k_f is the thermal conductivity of the fluid. Equation 3.1 shows that the size of the boundary layers depends on the properties of the fluids involved. As the fluid used in this works is water, then $\delta_T \ll \delta$.

As the size of the thermal boundary layer is smaller than the fluid dynamic boundary layer, the y^+ value should be lowered to obtain correct thermal results. Several authors have recommended values of y^+ less than five in the heating surfaces to guarantee that the first cell next to the wall is within the viscous sublayer (JAIMES AND NUNHEZ, 2017; KARIMI *et al.*, 2012; SONDAK, 1992).

The mesh independence test used in this work follows the procedure of JAIMES AND NUNHEZ, 2017. The test consisted of generating five meshes with different levels of refinement variating the first layer height and the growth rate. These parameters were calculated to ensure a y+ in the range of 0.06 to 25 in the tank wall and approximately 1 in the impeller surfaces (See details in the Appendix A). A quantity of 20 cells was used in the boundary layer for both the tank wall and the surfaces of the impeller.

The grid independence test was conducted at an impeller speed of 945 rpm for a 0.1m diameter impeller, yielding a Reynolds number of $4.1\text{x}10^5$. The working fluid was water and the temperature at the surface of the tank wall was set as 98ºC. The testing data are provided in Table 3.2. It should be highlighted that no independence test was required for the number of mesh elements because the coarser mesh was already sufficiently refined ($2.95\text{x}10^6$ elements) for a mixing tank, as compared to the values found in the literature (KARCZ AND KACPERSKI, 2012; ZAKRZEWSKA AND JAWORSKI, 2004). However, it was necessary to ensure the adequate amount of elements close to the wall.

Table 3.2 Mesh parameters used in the tank wall surface

Parameter	***Mesh Levels***				
	1	*2*	*3*	*4*	*5*
Number of nodes in the tank	$2.95\text{x}10^6$	$3.0\text{x}10^6$	$3.02\text{x}10^6$	$3.5\text{x}10^6$	$3.52\text{x}10^6$
Spacing of the first cell	$1.16\text{x}10^{-4}$	$5.78\text{x}10^{-5}$	$1.15\text{x}10^{-5}$	$1.16\text{x}10^{-6}$	$5.78\text{x}10^{-7}$
Growth rate	1.0878	1.1262	1.2206	1.3695	1.4178
Average value of y^+	10	5	1	0.1	0.05

3.2.3 Models and methods

Once the mesh was created, boundary and initial conditions, material properties, and physical models were specified.

3.2.3.1 Physical properties of the fluid

The initial conditions were maintained as in the experimental work of STREK (1963) to reproduce the model with fidelity. The fluid flow was monophasic, using water as working fluid with constant initial temperature and pressure of 25ºC and 1 atm, respectively. The physicochemical properties of the water are presented in Table 3.3.

Table 3.3 Physicochemical properties of the water

Property	***Units***	***Value***
Density	Kg/m3	998.2
Dynamic viscosity	Pa/s	0.001026
Molar mass	Kg/Kmol	18.02
Thermal conductivity	W/m K	0.5984
Specific heat	J/kg K	4181.7

3.2.3.2 Boundary conditions

An appropriate definition of the boundary and initial conditions is a crucial part of the simulation that leads to solving with accuracy the governing equations to obtain the most realistic solution for the physical process evaluated. The boundary conditions and additional considerations were adopted based on the results of previous research that found the most accurate models to describe the physical phenomenon in stirred tanks with heat transfer (JAIMES AND NUNHEZ 2017; MENTER, 2009; ZAKRZEWSKA AND JAWORSKI, 2005)

➢ *Wall Boundary Conditions*

- At the solid walls of the fluid domain, it is frequently applied a *no-slip* boundary condition, which means that the fluid velocity at the stationary wall point is zero ($u = \upsilon = 0$) due to the viscous effects. The influence of the wall on the flow causes velocity gradients affecting the velocity profile. This condition was utilized in the impeller blades, disc, baffles and tank bottom along with an adiabatic condition.

- The surfaces of the shaft in both rotating and stationary domains were considered rotating walls that have the same rotational speed as the impeller.

- The *no-slip* condition was also applied to the cylindrical wall of the tank. The thermal boundary condition was defined as a fixed temperature of heating Tw = 98ºC. This value is taken as the average temperature reached by the wall in the experimental study of STREK (1963) with the steam supplied in the jacket (as explained in Section 3.1.4). A subdomain was created in the stationary domain to apply a volumetric source of energy (W/m^3). This source is specified as a constant negative heat flux condition to model the system heat flux losses, which contributes to achieve a faster steady state. In the energy equation (Eq. 2.12), the negative heat flux appears in the Sh term.

- The upper wall of the fluid domain was considered flat and the shear stresses and axial velocities were set to zero to model it as a free surface. For this case, the *free slip* condition was used considering that there is not mass flux and the central vortex is reduced due to the presence of the baffles.

The heat transfer coefficient was determined using Equation 3.2 taking into account only the fluid and not the solid surface in the calculations. As the condition of no-slip was applied on the cylindrical surface of the tank, it could be considered that there is no fluid movement, and the heat is transferred only by conduction. Therefore, the heat transfer rate across the boundary layer is defined by the conditions of the thermal boundary layer that has a high impact on the temperature gradient of the wall $\left(\frac{\partial T}{\partial y}\right)_{y=0}$ (INCROPERA AND DEWITT, 2007):

$$h_o = \frac{-k_f\left(\frac{\partial T}{\partial y}\right)_{y=0}}{\left(T_w - T_f\right)} \tag{3.2}$$

where h_o is the heat transfer coefficient between the wall and the fluid, T_w is the wall temperature at 98ºC, T_f is the average fluid temperature, and k_f is the thermal conductivity of the fluid.

➢ *Domain interfaces*

- Grid interfaces have to be used to connect both the stationary and rotating meshes. The *General Grid Interface (GGI)* interpolation method was applied to solve the interfaces between the domains (Figure 3.9). This method uses an intersection algorithm to allow the change of the grid topology and physical distribution across the interface. GGI connections are conservative and implicit and can be selected even if the cells on the two sides have different type and location as shown in Figure 3.10. The interfaces were considered as non-coincident surfaces as well as fluid-fluid type.

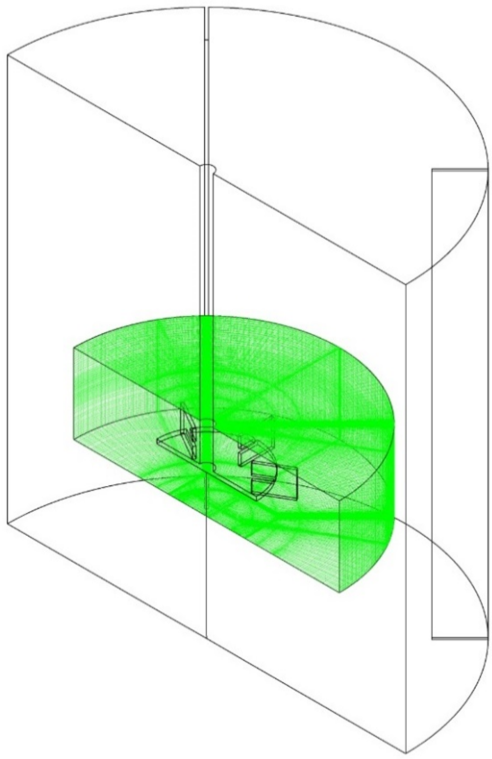

Figure 3.9 Rotating zones around the impeller and surfaces connected with GGI.

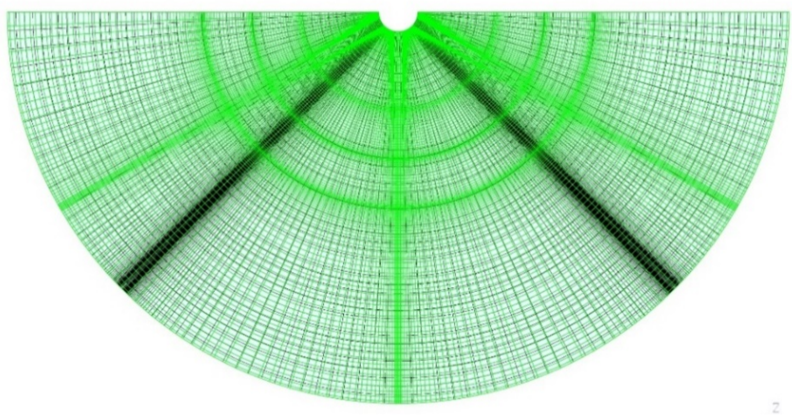

Figure 3.10 Interface between the top of the rotating domain (green) and the surface of the stationary domain (black).

- Since only half of the full geometry was modeled, the rotational periodic condition was applied on the surfaces 1 and 2 of both domains (Figure 3.11), taking advantage of the geometrical symmetry. This setting creates a link between two identical surfaces, which means that the flow entering through a periodic plane is the same flow that leaves on the opposed plane.

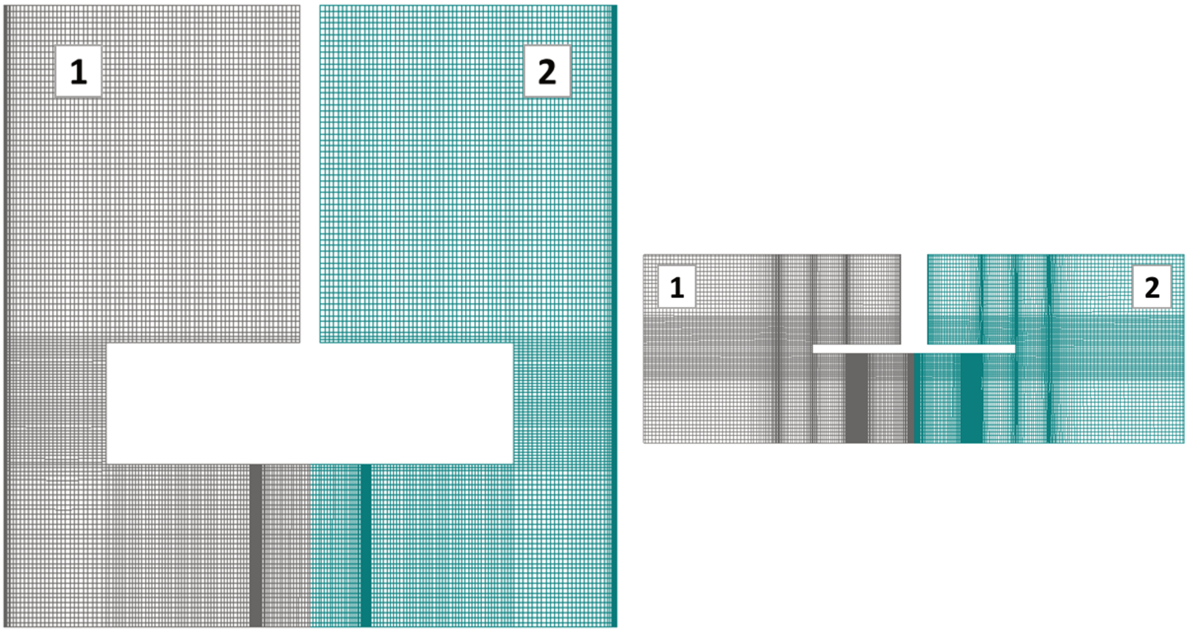

Figure 3.11. System surfaces on the periodic condition

The initial and boundary conditions and assumptions applied in the simulations cases are summarized in Table 3.4. All the cases were simulated starting at the initial state until the flow profile was fully developed, and the convective heat transfer coefficient achieved a steady state.

Table 3.4 Summary of Initial and boundary conditions

Variable	***Initial condition***
Velocity components	0 m/s
Temperature	25 ºC
Pressure	1 atm
Location	***Boundary Conditions***
Tank cylindrical wall	No-slip, constant temperature 98ºC
Bottom, baffles	No-slip, adiabatic
Impeller, Shaft	Rotating wall, adiabatic
Tank top	Free-slip, adiabatic
Domain interfaces	Fluid-Fluid interface
Inlet-Outlet Surfaces	Rotational periodicity

3.2.3.3 Physical and numerical models

The numerical simulations were conducted employing the Multiple Reference Frame approach (MRF - Frozen rotor) to deal with the impeller motion. The Shear Stress Transport (SST) k-ω was used to model the turbulence flow and the first-order Upwind Difference Scheme (UDS) was applied to discretize the transport equations.

The MRF - Frozen rotor approach was chosen due to the stability and the reduced computational power without losses in accuracy. The rotating domain was defined by a rotation axis and a rotation speed of the impeller. The SST k-ω was selected because it can capture with accuracy both the boundary layer at the tank wall and the flow field at the free stream region (MENTER, 2003). This model was used together with the automatic near-wall treatment of ANSYS CFX 16.0.

The first-order *upwind difference* scheme (UDS) was used to solve the advection terms in all simulations of the current work. Previous studies consider that the UDS scheme is appropriate when the convection is dominant and the flow is aligned with the grid as is the case of the hexahedral mesh used in this work (MARSHALL & BAKKER, 2004; JAIMES & NUNHEZ, 2017). It was also expressed by previous researchers that the *upwind* scheme when used in a very refined mesh on the tank wall (where the heat transfer coefficient is calculated) provides accurate solution (BRUCATO et al., 1998; DEGLON AND MEYER, 2006).

The First Order Backward Euler scheme was utilized to solve the transient term. This scheme is a robust first-order formulation that conducts to numeric stability. A time step size of 0.01 s and residual values (RMS) less than $1x10^{-5}$ was implemented to ensure convergence.

3.2.3.4 Model validation

An identical geometry of the experimental configuration used by STREK (1963) was simulated to validate the proposed computational model. The geometric parameters and the operational conditions (impeller speed, diameters and the impeller height from the bottom of the tank) were taken from the experimental work. Fifteen cases were simulated in order to determine a Nusselt number correlation (Table 3.5). The working fluid was water and the tank diameter was 0.3m. Additional parameters are also presented in the table below.

Table 3.5 Simulated cases for obtaining the Nusselt number correlation

Case	***Impeller Speed (rpm)***	***Impeller Diameter (m)***	***Impeller height (m)***
1	130	0.1	0.1
2	220	0.1	0.1
3	418	0.1	0.1
4	540	0.1	0.1
5	790	0.1	0.1
6	850	0.1	0.1
7	945	0.1	0.1
8	360	0.1	0.03
9	360	0.1	0.75
10	360	0.1	0.135
11	220	0.05	0.1
12	220	0.12	0.1
13	220	0.15	0.1
14	220	0.18	0.1
15	220	0.22	0.1

3.3 Solver

The next step in the CFD methodology is the solution of the computational model. Numerical simulations were performed using the commercial ANSYS CFX-Solver 16.0 for CFD, which is based on the element-based Finite Volume Method (EbFVM), as described in Section 2.1.4.

This software starts the solution from the initial values given by the user. Then it determines the error in the mass and momentum balances into each cell of the domain and make adjustments to improve the balances until the error is smaller than the tolerance value previously defined in the pre-processing step. In this work, once the error achieved values less than $1x10^{-5}$ and the convective heat transfer coefficient in the tank wall was settled, the solution was considered converged and concluded.

3.4 Post-processing

The post-processing is the final stage of the CFD methodology. The ANSYS CFD-Post 16.0 was used to make a detailed analysis of the results generated by the solver. The outcomes and analysis are presented in the following chapter.

Chapter 4

Results and discussion

In this chapter, the computational results and the analysis of the simulation of a jacketed stirred tank with Rushton impeller are presented. The simulations were carried out following the methodology presented in Chapter 3.

4.1 Convergence monitoring

The convergence criteria are used to guarantee that the simulation has reached satisfactory results. In this work, three conditions had to be met: the residual RMS error values, the stability of the variable of interest (convective heat transfer coefficient) and the domain imbalances.

For all the simulation cases, numerical convergence with RMS values below $1\mathrm{x}10^{-5}$ was accepted. The RMS values are based on the residual errors of the numerical solution of mass, momentum and energy equations. Once the simulations were time-dependent, it was necessary to run for a time long enough to ensure that the variable of interest and velocity fields achieved stability. From Figure 4.1, it can be seen that the RMS values decreased below the established criteria and after 10s approximately (1000 accumulated time steps) the values were nearly constant. Since all the simulated cases achieved the convergence criteria, Case Nº 2 was chosen as an example to discuss the monitoring of the convergence criteria.

A monitor point was set at the solver to supervise the convective heat transfer coefficient and to verify when the value has reached a constant state. Figure 4.2 shows the monitoring of the heat transfer coefficient at the tank wall for Case Nº2.

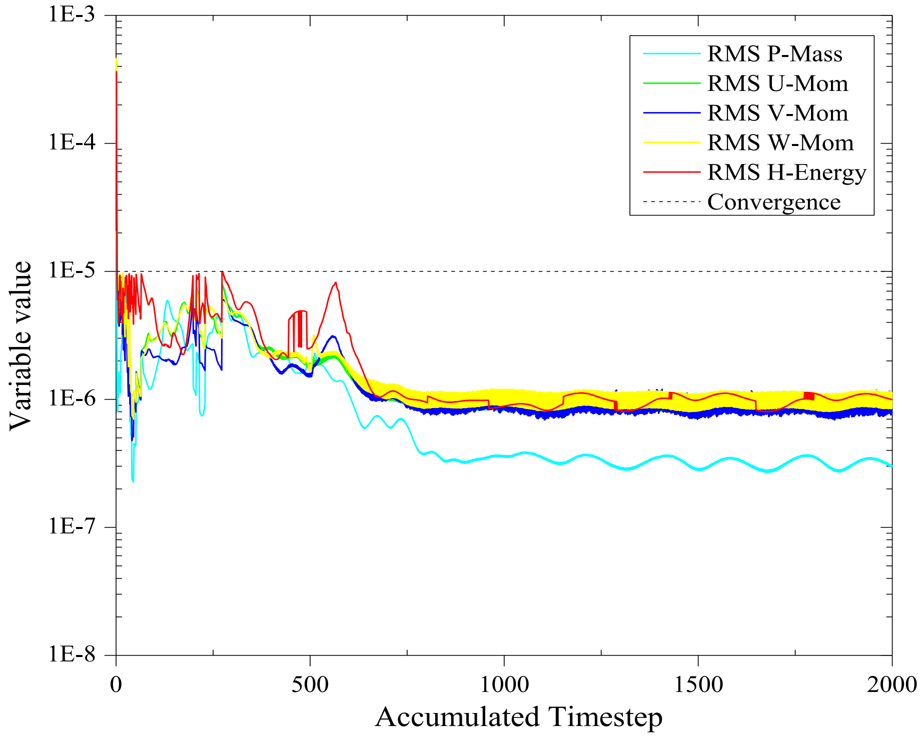

Figure 4.1 Residual error value (RMS) in case Nº 2

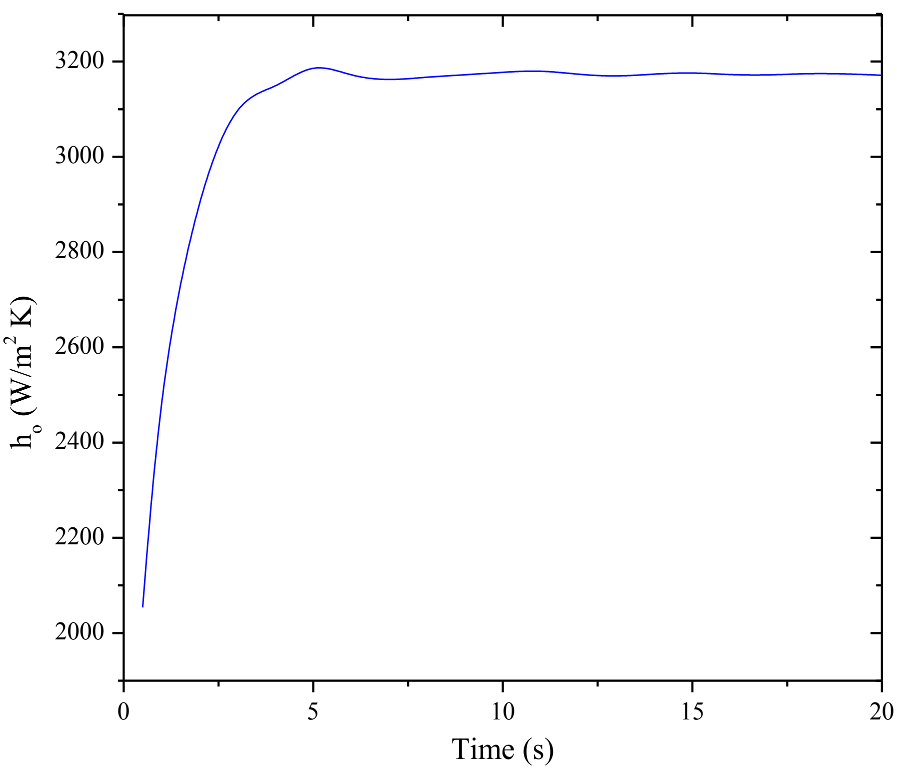

Figure 4.2. Monitoring of the convective heat transfer coefficient at the tank wall in case Nº 2

The heat transfer coefficient initiates an almost constant behavior at 8 s. However, it was assumed the steady state only after 12s when the RMS values also became constant.

The last condition to be satisfied is related to the imbalances of the conservation equations, which should be below of 1% for all the equations. Figure 4.3 shows the monitoring of the imbalances in the stationary domain for Case Nº 2.

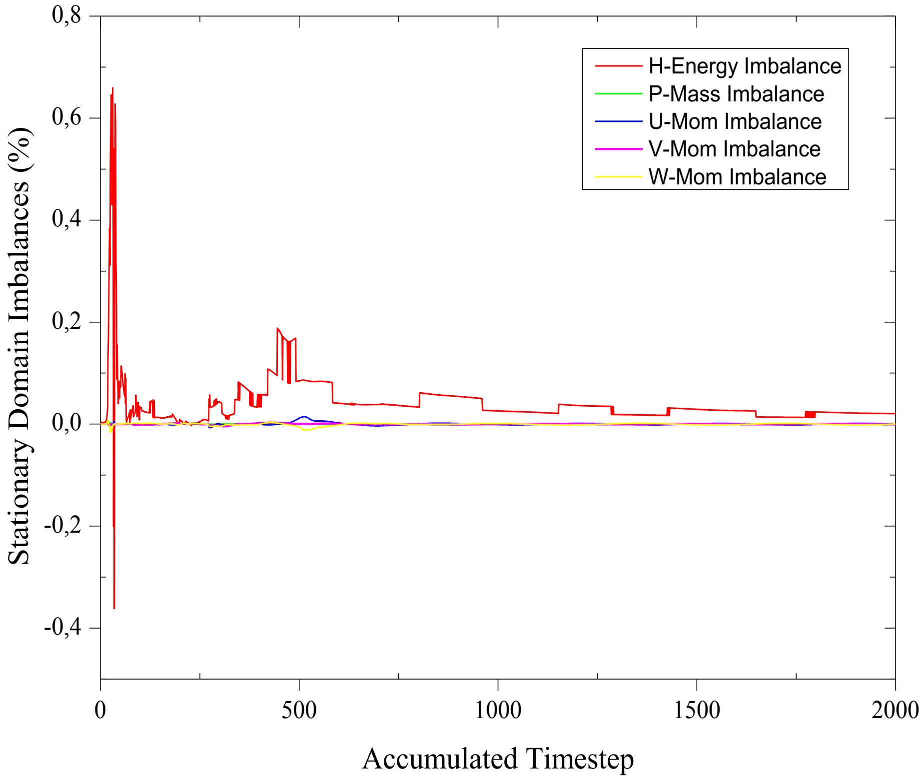

Figure 4.3. Imbalances of the conservation equations in the stationary domain for Case 2

Due to the different geometric configurations and operating conditions, it was necessary to run all simulations during 20s to ensure that the velocity field, flow profile and other quantities of interest were fully developed.

4.2 Grid independence study – effect of the wall y+ on heat transfer coefficient

The grid independence study was done to observe the effect of the non-dimensional distance (y+) at the tank wall on the convective heat transfer coefficient (h_o) and to find the value of the y+ where h_o is independent of the mesh refinement. The different levels of the wall refinement related to the y+ value are shown in Figure 4.4.

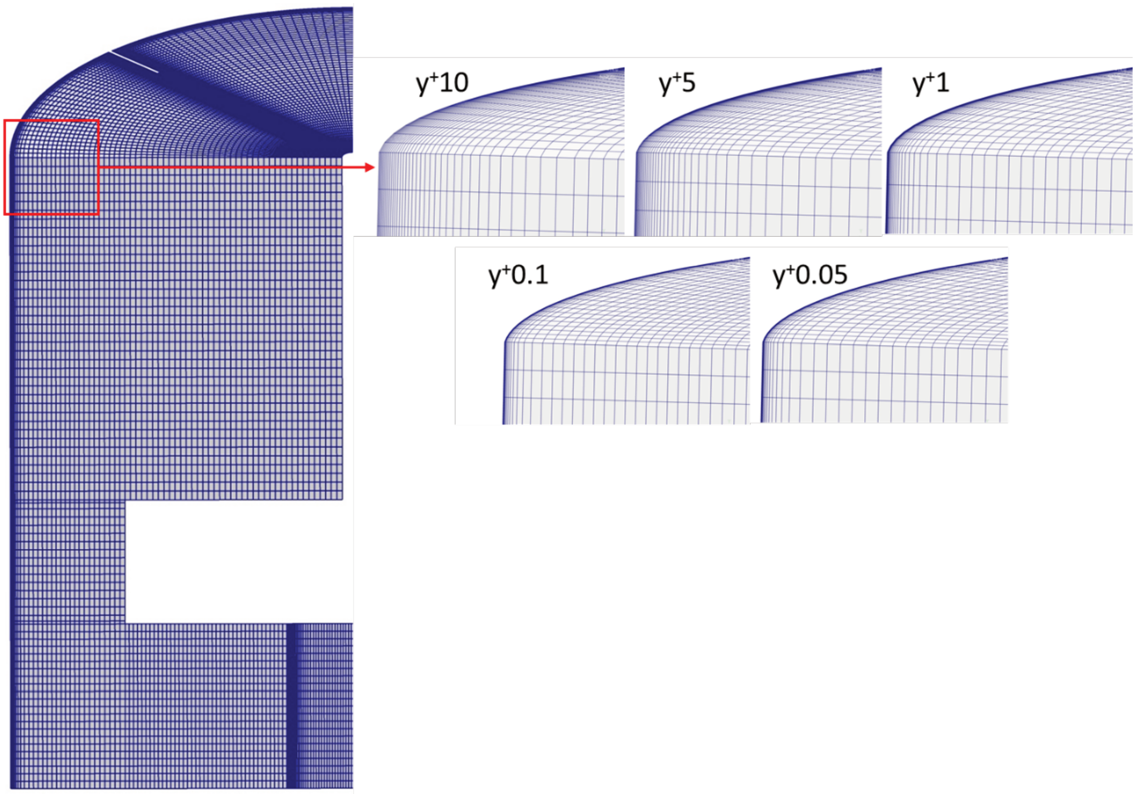

Figure 4.4. Wall refinement on the hexahedral meshes with different y+

Table 4.1 summarizes the results of the heat flux (q) and the heat transfer coefficient (h_o) for the five levels of mesh. It can be observed that the mesh levels 4 and 5 have equal values of h_o demonstrating that a minor y^+ would not change the calculated heat transfer coefficient in the tank walls. Because no further refinement is required, the mesh Nº 4 with $3.5x10^6$ numbers of elements and y^+= 0.1 was selected to be employed in the simulations. Also, the heat flux calculated for both meshes has very similar values confirming the accuracy of the mesh Nº 4.

Table 4.1. Results of the grid independence test

PARAMETERS	***MESH LEVELS***				
	1	***2***	***3***	***4***	***5***
Average value y+	10	5	1	0.1	0.05
h_o (W/m^2 K)	9401.19	9961.72	10190.9	10425.24	10425.11
% Variation of h_o	--	5.96	2.30	2.30	0.00
Heat flux q (W/m^2)	372165	380468	382811	387819	387835
% Variation of q	--	2.23	0.62	1.31	0.00

Figure 4.5 shows the effect of the wall y+ on the heat transfer predictions. The simulations reflect an increase in the values of h_o and q until they reached a constant value in the refined meshes with $y^+ < 0.1$. The mesh with $y^+ = 0.1$ was chosen because provides independence in the results and an acceptable computational cost since it is not the most refined mesh. The parameters of the mesh N° 4 (growth rate and the spacing of the first cell) showed in Table 3.2 were used to generate all the meshes needed in this work. This finding is agree with results found in the literature recommending the use of $y^+ < 0.1$ for surfaces with heat exchange (JAIMES AND NUNHEZ, 2017).

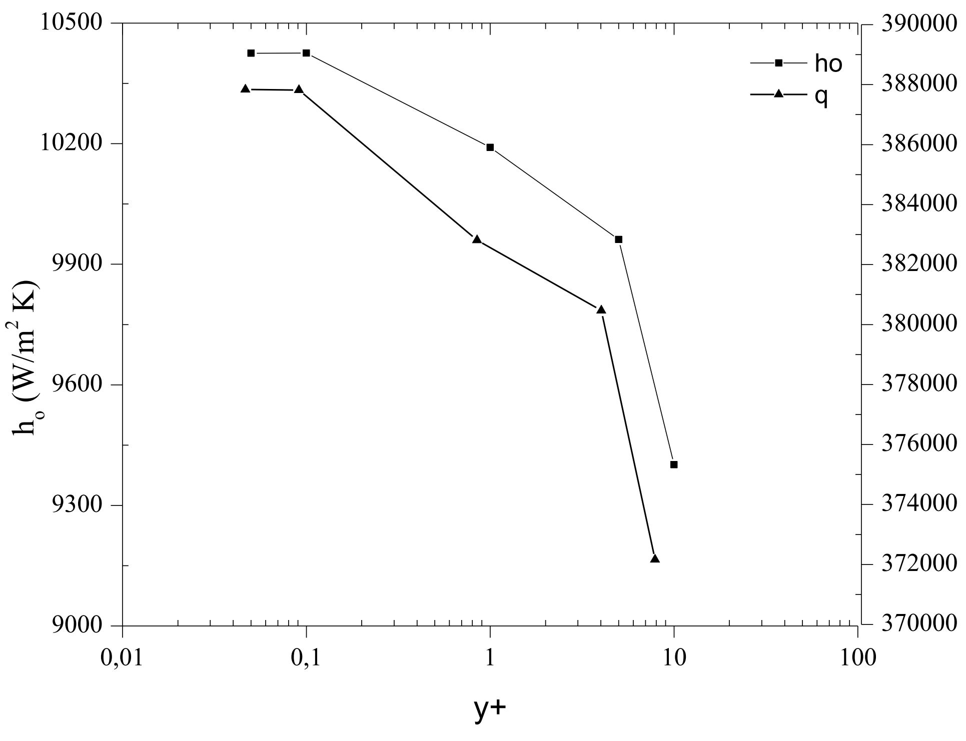

Figure 4.5 Effect of the reduction of the y^+ in tank wall on the value of the heat transfer coefficient and the wall heat flux

4.3 Flow characteristics

4.3.1 Flow patterns

A vector and contour plot of the flow produced by the Rushton impeller inside the studied baffled tank are presented in Figure 4.6 and Figure 4.7. Near the impeller blades, it can be seen the habitual radial discharge stream produced for this type of devices. The strong radial component in the blades directs the flows towards the vessel walls and are divided into two circulation loops, one in the upper and one in the lower zones of the impeller (Figure 4.7). These results present a satisfactory agreement with previous experimental and numerical studies confirming that the computational model correctly predicted the typical fluid flow pattern (BRUCATO *et al*., 1998; DRISS *et al*., 2014; HUANG AND LI, 2013).

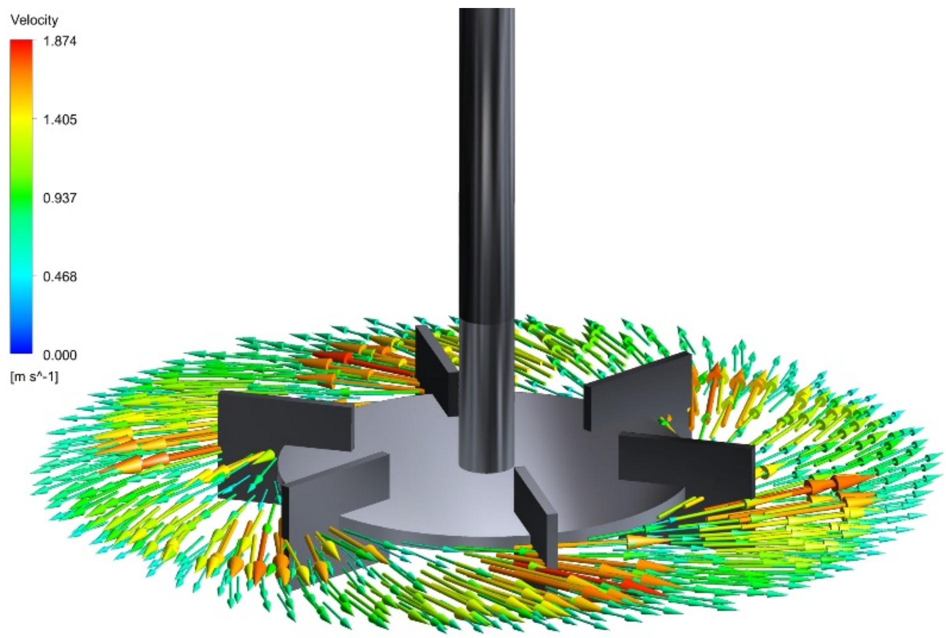

Figure 4.6. Velocity vectors of the radial flow pattern near to the Rushton impeller blades

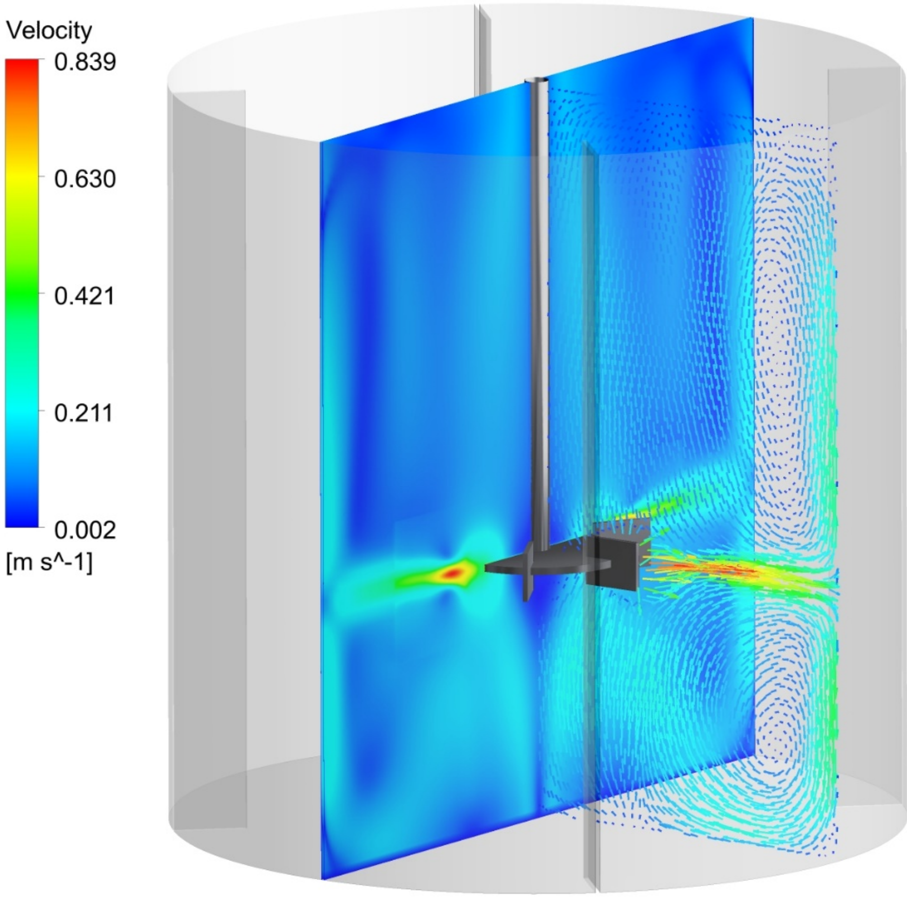

Figure 4.7 Velocity vectors and contours of the general flow pattern created by the Rushton impeller

The flow field throughout the tank was analyzed for the five meshes with different refinement; it was observed that the coarsest mesh ($y^+ = 10$) presented a flow pattern very similar in shape to the finest mesh ($y^+ = 0.05$) as can be seen in Figure 4.8. Therefore, it can be noted that values of the non-dimensional distance in the tank wall less than 10 did not have significant effect on the prediction of the primary flow pattern generated by the Rushton impeller.

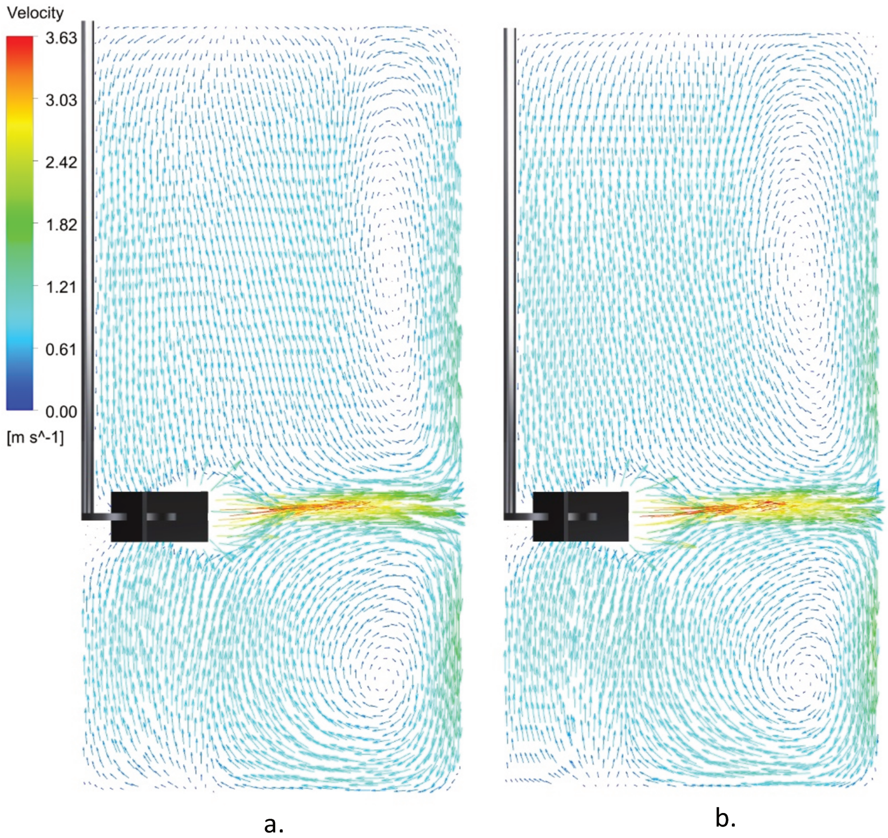

Figure 4.8. Flow patterns. a. Mesh level 1, $y^+ = 10$. b. Mesh level 4, $y^+ = 0.1$

4.3.2 Power number

The power number was calculated to assure the correct behavior of the Rushton impeller and check the validity of the CFD simulation. Equation 2.13 was used to quantify the power number in a Rushton impeller with 0.1m diameter and rotating speed of 220 rpm. The torque value on the impeller blades was taken from the CFD-Post processing and then the impeller power was calculated.

The type of discretization scheme employed in the simulations seems to have a significant effect on the calculation of the power number of the impeller, as can be seen in Table 4.2. The power number calculated with the *upwind* scheme was 9.7% lower than that calculated with *high-resolution*. According to DEGLON AND MEYER (2006), the power number is improved as the order of the discretization scheme increases.

However, it should be noted that the experimental values found in previous works for Rushton turbine impeller at similar Reynolds number are between 4.5 to 5.5 (Brucato et al., 1998). The mostly constant behavior of the power number in turbulent flows was confirmed by calculating the value for Cases 1 to 9 (Table 3.5), a value close to 4.5 was obtained in all cases using the *upwind* scheme.

Table 4.2 Comparison of predicted power number with both discretization schemes

Method	***Torque (N m)***	***Power (W)***	***Power Number***
Upwind Scheme	0.09	2.14	4.55
High Resolution Scheme	0.11	2.47	5.02
Experimental values [a]	-	-	4.5 - 5.5

[a] Brucato *et al*., 1998

In the industry it is commonly adopted a power number value of five (5.0), because of that it is recommended to use second-order discretization schemes when power calculation is fundamental to the research.

4.4 Nusselt number correlation – Model validation

The detailed methodology described in Chapter 3 were developed with the aim of obtaining a Nusselt number correlation combining the Reynolds (Re) and Prandtl (Pr) numbers and the geometric relationships in the form of Equation 2.5. This correlation was developed to facilitate the calculations of heat transfer coefficients in stirred tanks with different geometries and fluids.

Equation 3.2 (page 65) was used to calculate the average heat transfer coefficient (h_o) using the average data of the wall heat flux (q) and the average bulk temperature (T_f). It was considered the thermal conductivity of the fluid and not that of the material of the tank, also it was used the average bulk temperature and not the temperature of the neighboring cell as it is the standard option in the CFX/ANSYS software. Therefore, the calculation was carried out at the very laminar portion of the boundary layer.

Figure 4.9 and 4.10 shows the local behavior of the heat flux and the heat transfer coefficient along the tank wall, respectively. It can be observed that the heat transfer coefficient is higher in the zone where the jet produced by the impeller hits the wall, as is expected.

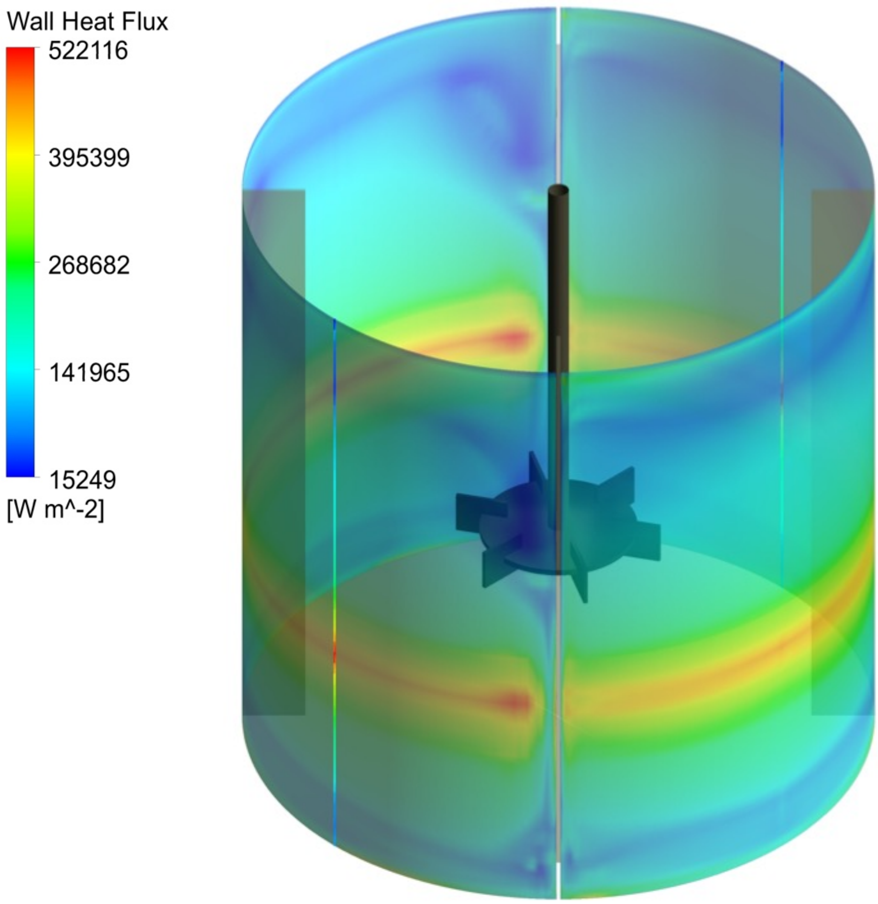

Figure 4.9 Heat flux profile along the tank wall for Case 2

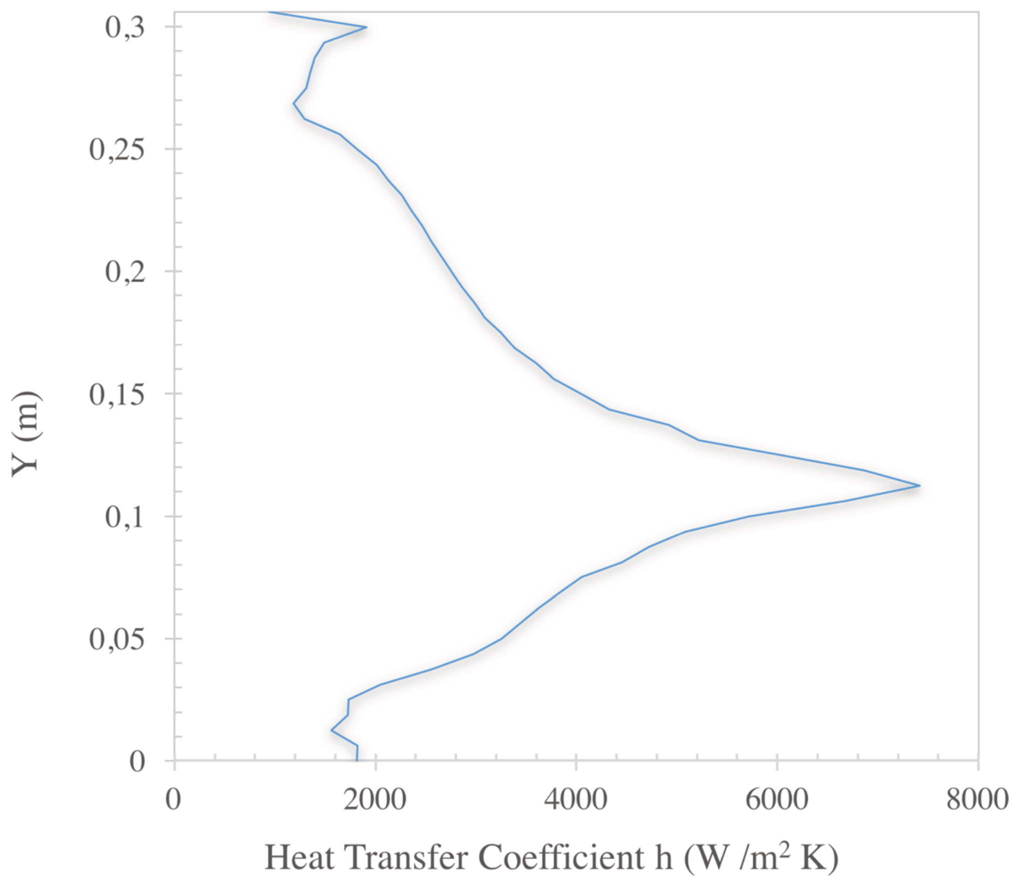

Figure 4.10 Heat transfer coefficient profile for Case 2 (height of the impeller 0.1m)

The Nusselt (Nu), Reynolds (Re) and Prandtl (Pr) numbers were also calculated for each simulated case. The results shown in Table 4.3 and the geometric relations (D/T and C/T) were employed to estimate the parameters and adjust the correlation. Since the working fluid (water) was not varied, the Prandtl number calculated at the average temperature of the fluid remained constant at 3.14 for all the simulation cases.

Table 4.3 Results of dimensionless groups from the CFD model

Nº Simulated Case	Nu	Re	(D/T)	(C/T)
1	969	29269	0.33	0.33
2	1462	53528	0.33	0.33
3	2447	117440	0.33	0,333
4	3015	162222	0.33	0.33
5	4134	252966	0.33	0.33
6	4531	293648	0.33	0.33
7	4780	331296	0.33	0.33
8	1594	89251	0.33	0.10
9	2169	95990	0.33	0.25
10	2257	97699	0.33	0.45
11	846	12139	0.167	0.33
12	1926	82976	0.40	0.33
13	2768	143862	0.50	0.33
14	3499	221153	0.60	0.33
15	4241	357028	0.73	0.33

The parameters (K, a, b, c, d) of the Nusselt number correlation were acquired using the Matlab function *fminsearch*. This function widely used for parameter estimation is based on the derivative-free method and was employed to find the minimum of the sum of absolute relative error (Equation 4.1) between the Nusselt number obtained by the simulations and the Nusselt number predicted by the correlation.

$$min: f_{obj} = \sum_{i=1}^{15} \left| \left(\left\{ \frac{\left(Nu_{simulated} - \left(K(Re)^a (Pr)^b (d/D)^c (h/D)^d\right)\right)}{Nu_{simulated}} \right\} \right) \right| \tag{4.1}$$

Once the parameters were estimated, the general Nusselt number correlation adjusted with CFD simulations was formed as follows:

$$Nu = \frac{h_o T}{\kappa} = 1.22 \left(\frac{D^2 N}{\mu}\right)^{0.651} \left(\frac{C_p \mu}{\kappa}\right)^{0.333} \left(\frac{D}{T}\right)^{0.116} \left(\frac{C}{T}\right)^{0.157} \tag{4.2}$$

Equation 4.2 is quite similar to the experimental correlation estimated graphically by STREK (1963) that has the following form:

$$Nu = \frac{h_o T}{\kappa} = 1.02 \left(\frac{D^2 N}{\mu}\right)^{2/3} \left(\frac{C_p \mu}{\kappa}\right)^{1/3} \left(\frac{D}{T}\right)^{0.13} \left(\frac{C}{T}\right)^{0.12} \tag{4.3}$$

To evaluate the agreement of the results provided by the numerical correlation in relation to the experimental data, the mean and standard deviation were calculated according to Equation 4.4 and 4.5, respectively.

$$Mean\ deviation = \frac{100}{n} \sum_{i=1}^{n} \left(\frac{Nu_{calculated} - Nu_{measured}}{Nu_{calculated}}\right) \tag{4.4}$$

$$Standard\ deviation = 100 \left[\frac{1}{n-1} \sum_{i=1}^{n} \left(\frac{Nu_{calculated} - Nu_{measured}}{Nu_{calculated}}\right)^2\right]^{1/2} \tag{4.5}$$

Where n is the number of case studies.

The CFD correlation (Equation 4.2) described the data of 85 experimental cases with an average deviation of 7.5% and standard deviation of 11.8%. The Nusselt number predicted by the CFD correlation obtained in this work was related to the experimental results reported by Strek (1963) in a deviation graph for each of the given cases as shown in Figure 4.11. It can be seen that the CFD correlation present a little dispersion with a slight underestimation for Nusselt numbers higher than 7000. The coefficient of determination (R^2) for this correlation was found as 0.9247.

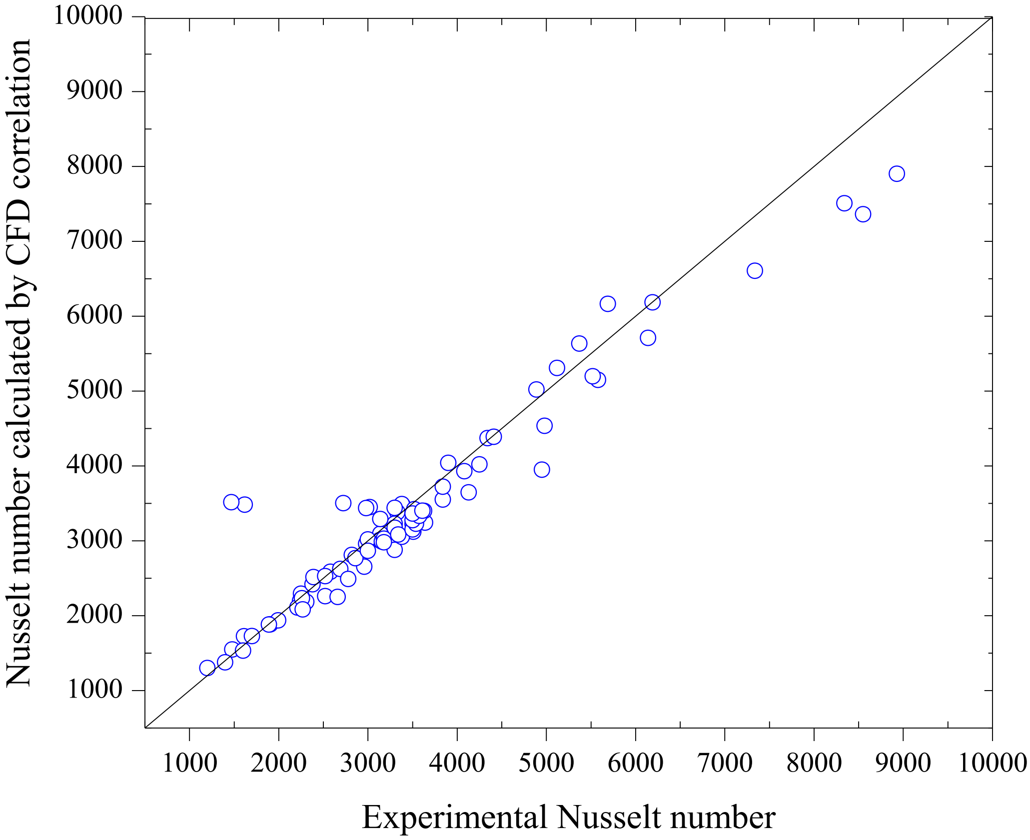

Figure 4.11 Comparison between experimental data and CFD Nusselt number correlation.

The experimental correlation (Equation 4.3) was also applied to describe the 85 experimental data. The comparison of the experimental data and the experimental correlation are plotted in Figure 4.12. The values of the average and standard deviations were 6.2% and 10.8%, respectively. It can be observed a similar behavior to the CFD correlation, however with a better approximation and less dispersion in comparison to the numerical correlation. The coefficient of determination (R^2) for this correlation is 0.932.

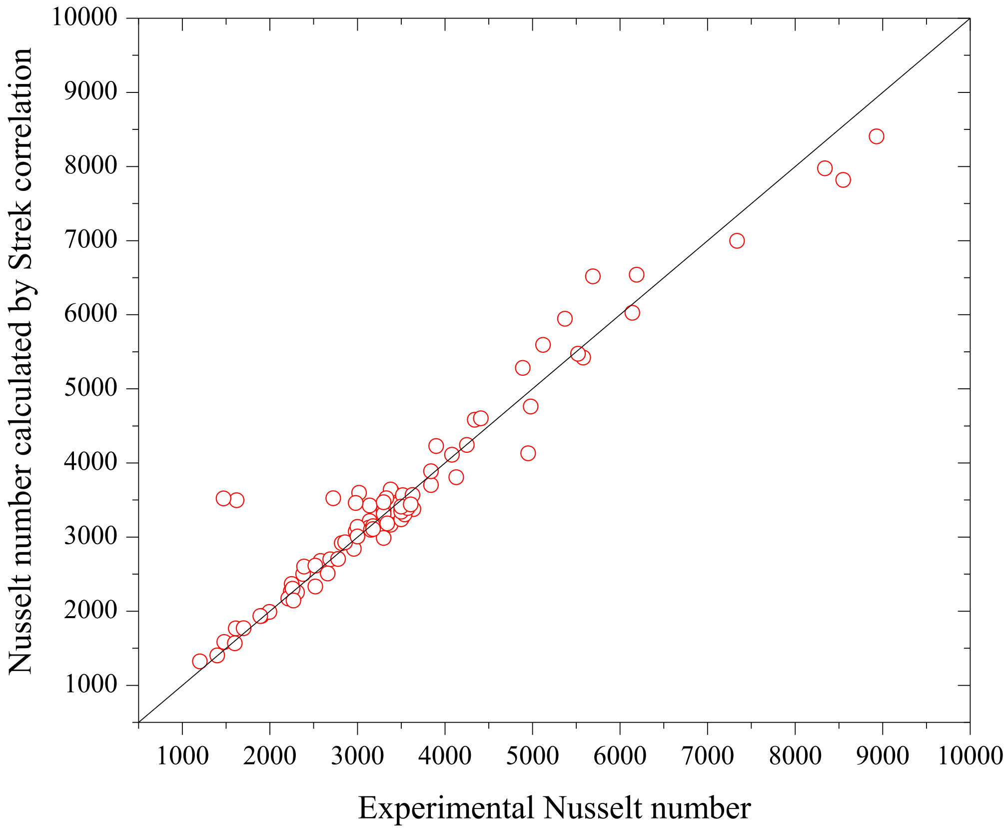

Figure 4.12 Comparison between the experimental data and correlation by STREK (1963).

The CFD correlation results compared with the experimental results are summarized in a graph showing the relation of the Reynolds number with $Nu/Pr^{0.333}(D/T)^{0.116}(C/T)^{0.157}$, as shown in Figure 4.13. The continuous line representing the CFD correlation (Equation 4.2) describe a linear trend with a slope of 0.651, which corresponds to the exponent of the Reynolds number in the correlation; the points represent the experimental data (STREK, 1963), confirming a satisfactory agreement between them.

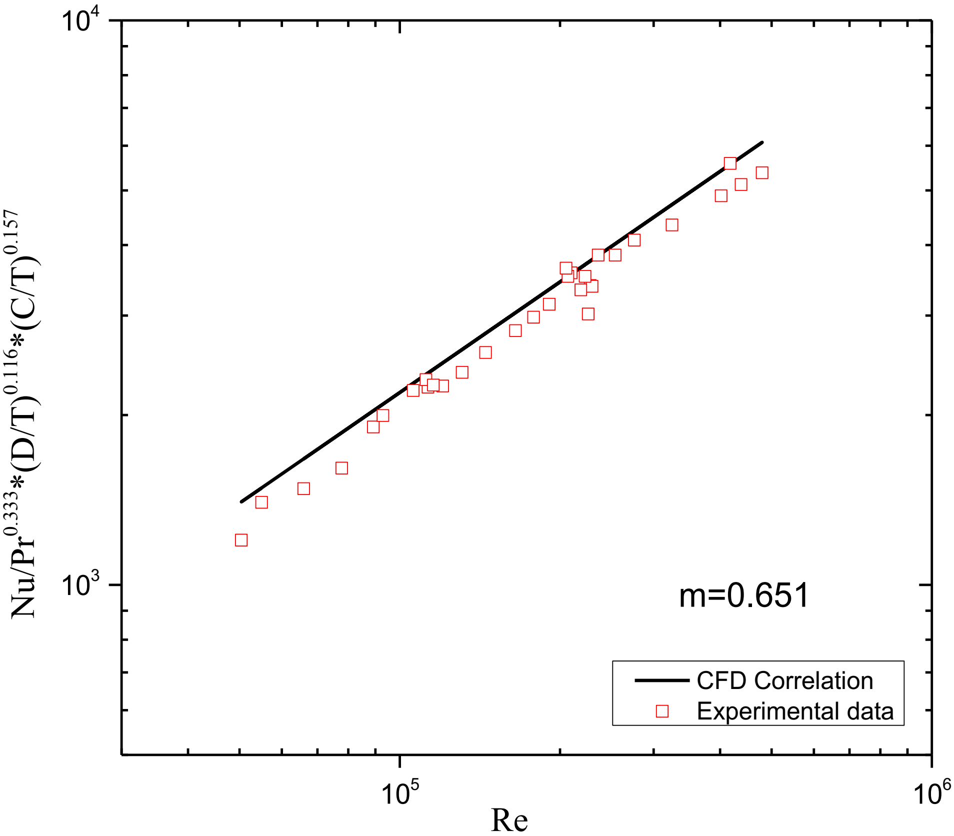

Figure 4.13 Overall correlation of h_o

Figure 4.14 illustrates the CFD correlation results compared with the experimental and the Strek correlation data for the variation of the Nusselt number against the Reynolds number. It can be observed that the heat transfer coefficient, and hence the Nusselt number, is influenced by the impeller speed in a directly proportional relationship, this can be explained due to the increase in the intensity of the mixing and turbulence, which contributes to better heat transfer. From Figure 4.12 it can also be seen that the CFD correlation tends to slightly underestimate the heat transfer coefficient compared with the Strek correlation mainly in the cases of larger Re numbers.

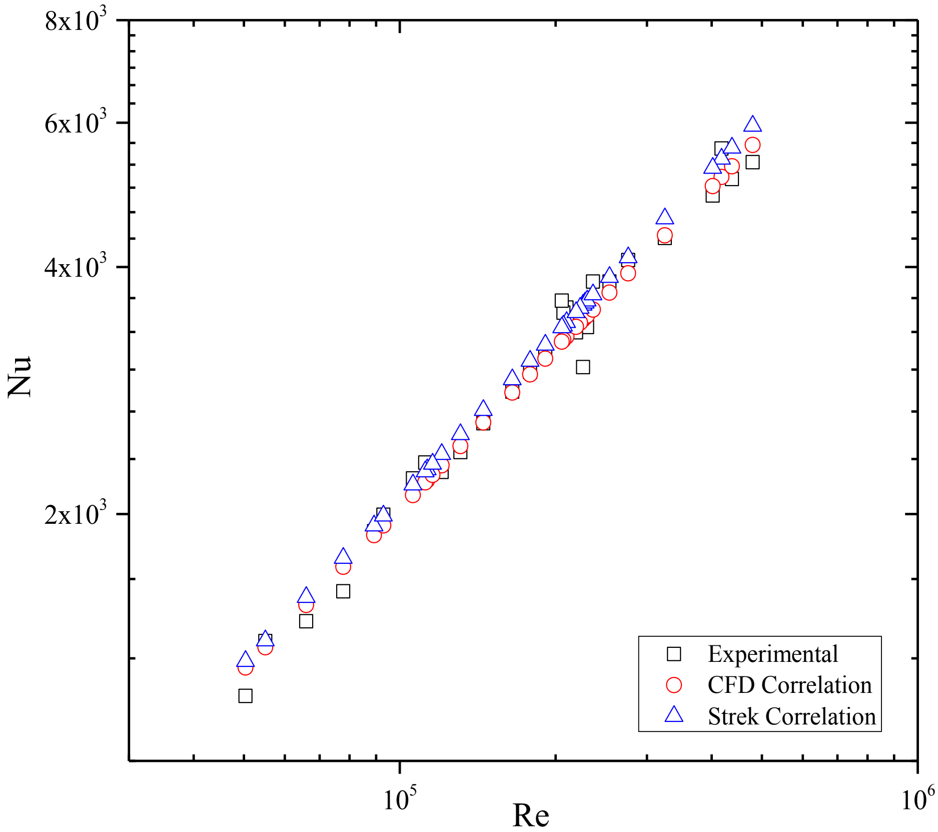

Figure 4.14 Variation of the Nusselt number against the Reynolds number

It follows from the results and deviations obtained by the numerical correlation that the CFD model predicts satisfactorily the heat transfer coefficient in a jacketed stirred tank with Rushton impeller therefore it can describe with accuracy the physical phenomena. The Nusselt number correlation proposed in this work can be used to determine heat transfer coefficient for jacketed stirred tanks with geometric similarity. However, this correlation should be employed only in the range of Reynolds number studied, since the heat transfer coefficient strongly depends on the geometry and speed of the impeller.

It should be highlighted that the methodology applied in this work can be used to model any desired system by varying geometry, fluids and boundary conditions. Following this methodology, accurate results could be quickly achieved.

4.5 Effect of impeller speed

A qualitative analysis was made to observe the influence of the rotational speed of the impeller in the flow pattern and the heat transfer coefficient. Velocity vectors were plotted in an axial plane located between two impeller blades and two baffles, as shown in Figure 4.15.

It can be observed that the flow pattern describes the characteristic flow of radial impellers in mixing tanks. In this way, the consistency of the numerical solution with the physical phenomena involved can be confirmed. It is also noticed that for all velocities, the flow pattern is very similar since the circulation loops formed above and below the impeller maintain the same size and shape. However, at higher speeds the flow leaving the impeller blades in the radial direction exhibits a stronger jet, which hits with more intensity in the wall producing greater turbulence and hence efficient heat transfer in the tank.

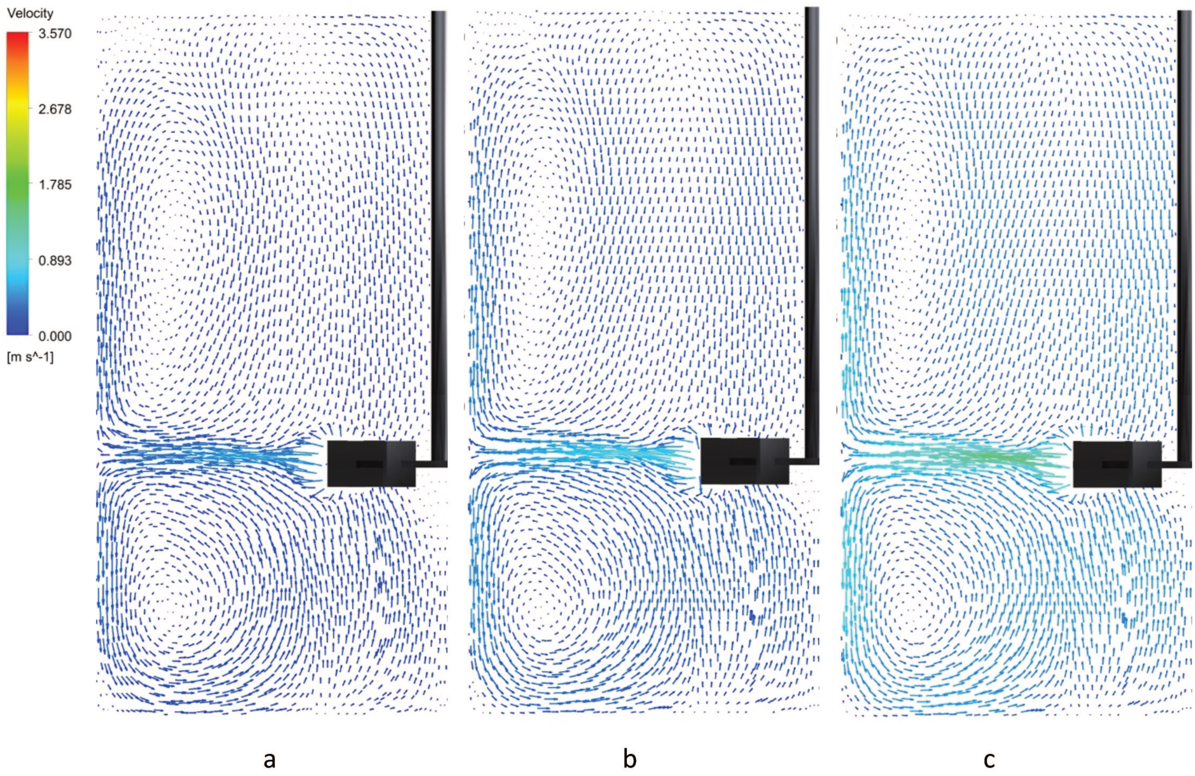

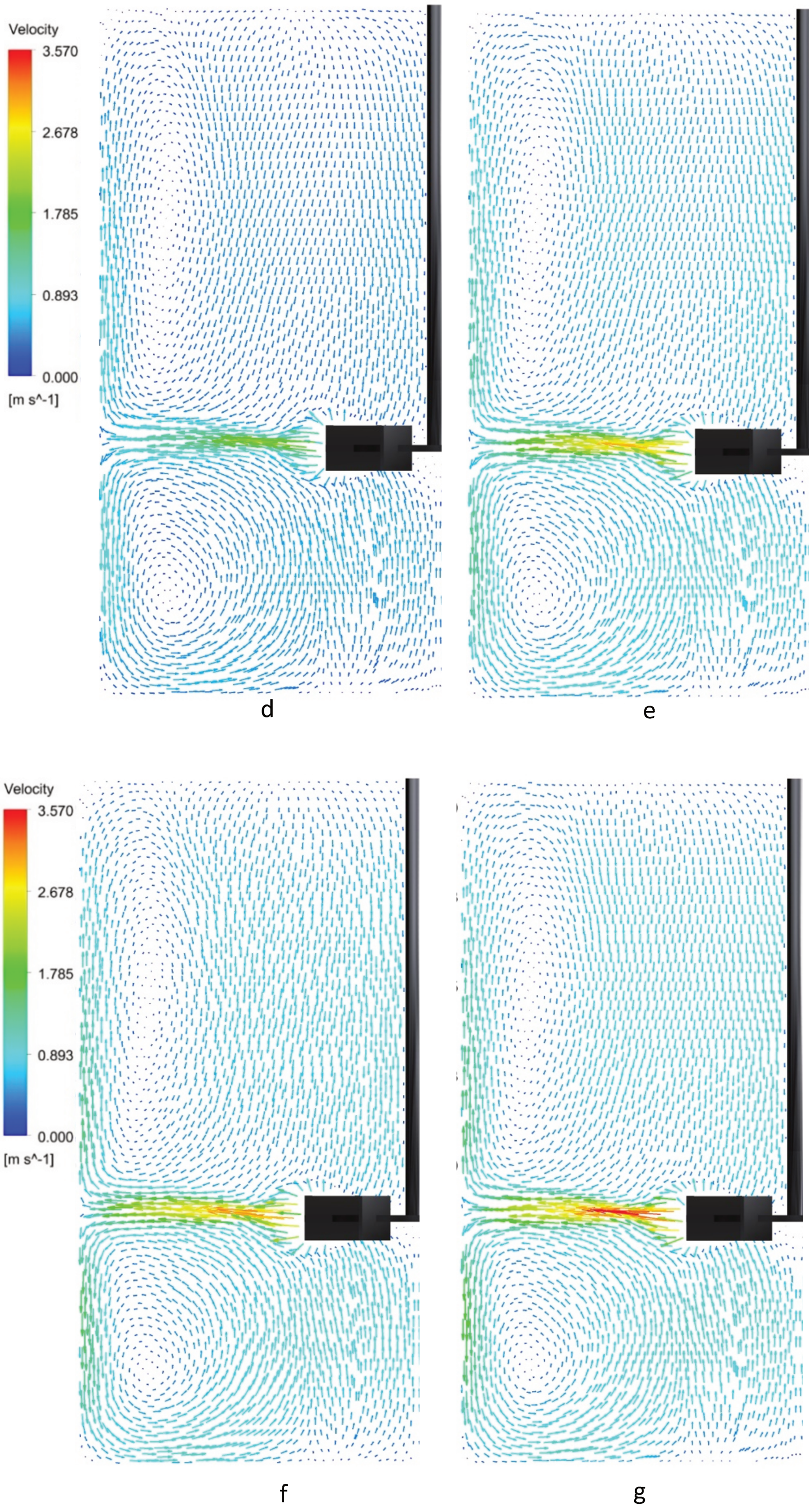

Figure 4.15 Flow patterns produced by Rushton impeller at different speeds. a. 130 rpm b. 220 rpm c. 418 rpm d. 540 rpm e. 790 rpm f. 850 rpm g. 945 rpm

4.6 Effect of D/T ratio

Simulation cases were made varying the impeller diameter taking into account the smaller and the bigger ones used in the experimental work of STREK (1963). The blades size was changed according to the geometric relationships with the impeller diameter. The height and speed of the impeller remain unchanged as C/T = 1/3 and 220 rpm, respectively.

The heat transfer coefficient can be increased by increasing the impeller size as can be observed in Figure 4.16. The log-log plot of $Nu/Re^{0.651}Pr^{0.333}$ versus D/T ratio, showed a linear behavior with a slope of 0.116, corresponding to the exponent of the D/T ratio in the CFD correlation (Equation 4.2).

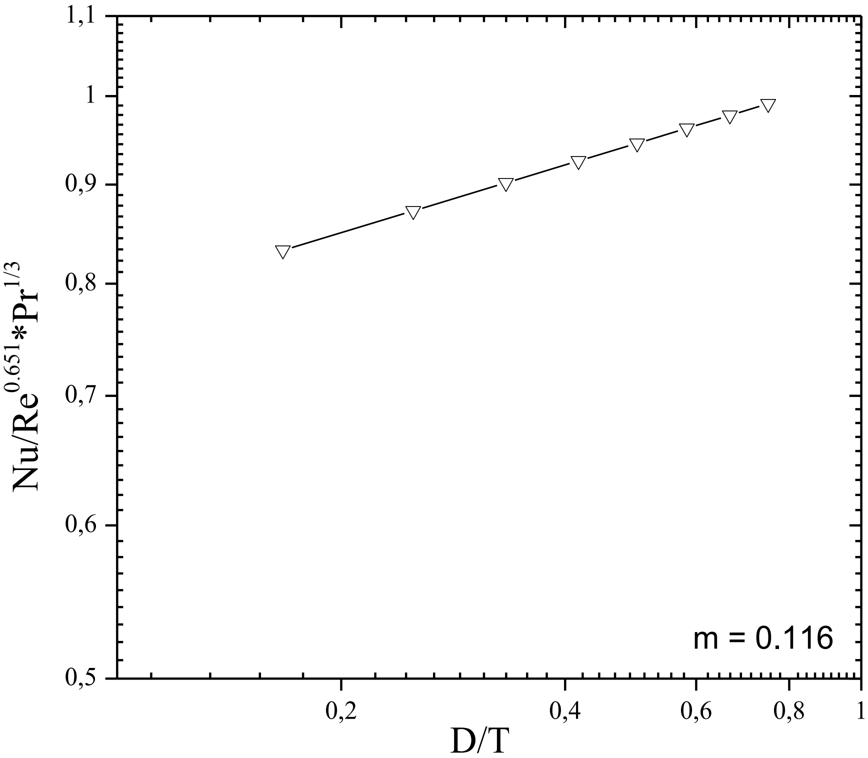

Figure 4.16 Effect of the D/T ratio on the heat transfer coefficient

Figure 4.17 shows the velocity vectors produced by a Rushton impeller with different sizes. It can be observed that the larger impellers (D/T ≥ 0.5) are more efficient than the smaller ones (D/T < 0.3), because they generate a very strong radial flow towards the tank wall and can move a greater amount of fluid mass. However, the larger impeller analyzed in this work (0.22

m in diameter) appears to concentrate the turbulence near the impeller blades generating dead zones in the bottom and the tank top (Figure 4.17f).

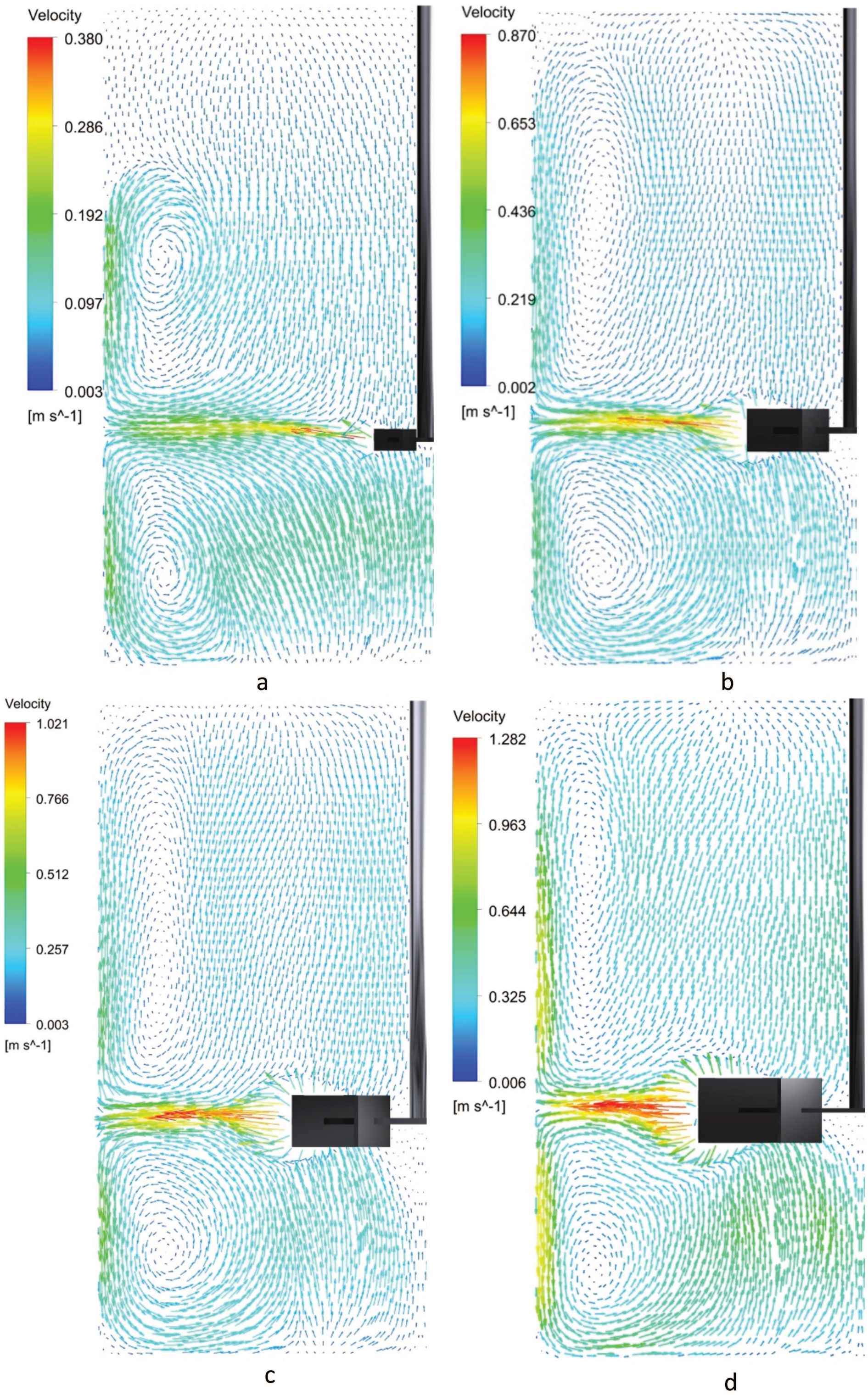

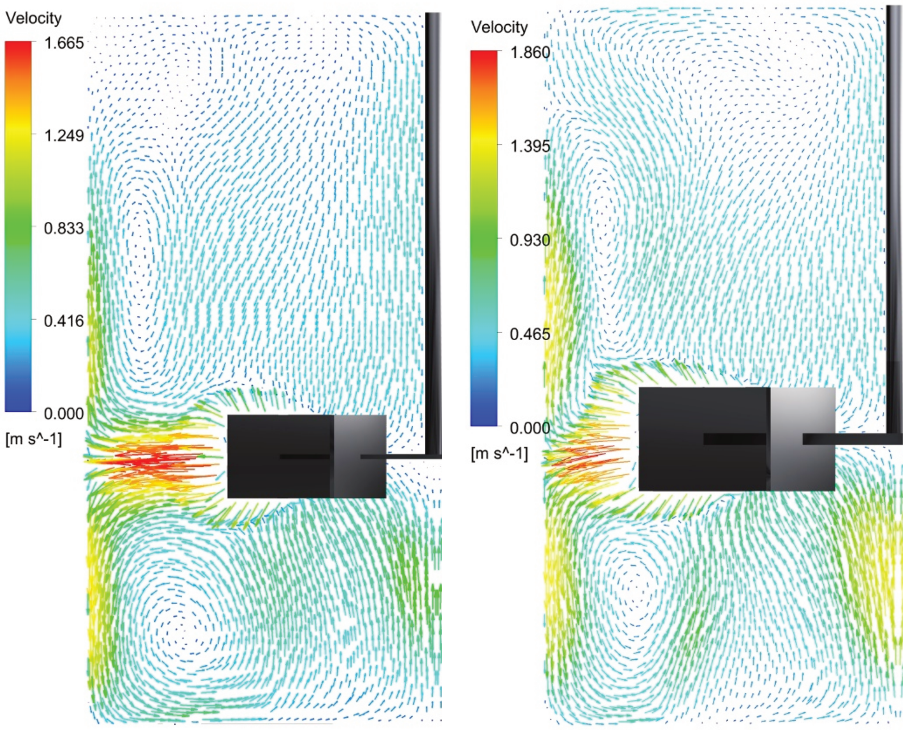

e   f

Figure 4.17. Flow pattern in the form of velocity vector predicted by a Rushton impeller with a different diameter. a. 0.05m b. 0.1m c. 0.12m d. 0.15m e. 0.18 m f. 0.22 m

An increase of 20% or 50% in the impeller diameter increases the heat transfer coefficient by 31% and 91%, respectively. This increment can be explained because the size and speed of the jets produced by the larger impeller blades are bigger, covering a larger area when encountering the heating wall. Consequently, the boundary layer is reduced and temperature gradients in the area closest to the wall are increased, improving the heat transfer inside of the tank. Nevertheless, according to Dorian (1995) there is a high dependence on the power consumption with the diameter and the speed of the impeller. A 10% increase in the diameter of the impeller will increase the power required by approximately 60%. This dependence presents a less extent with the impeller speed, showing that an increment of 10% will increase the power by more than 30%.

By comparing the power consumption for the impellers with 0.1 m and 0.12m diameter, it could be confirmed that a 20% increase in the impeller diameter increased the heat transfer coefficient by 31.5% and the power of the impeller by 170%. On the other hand, an increment of 30% in the impeller speed increased the heat transfer coefficient by 24% and the agitation power by 117%. Nevertheless, it is necessary a more detailed study to choose the correct improvement on the configurations depending on each specific case and the desired results.

4.7 Effect of C/T ratio

The height of suspension of the impeller (C) is considered as the distance from the bottom of the tank to the lower edge of the impeller blades. The ratio C/T was changed to determine its influence on the heat transfer coefficient. Figure 4.18 shows a log-log plot of $Nu/Re^{0.652}Pr^{0.333}$ versus C/T; it reflects a low Nusselt number when the C/T is small, that is, when the impeller is placed close to the bottom. The Nusselt number present and increment as the height of the impeller is increased. The value of $Nu/Re^{0.652}Pr^{0.333}$ increases with increase in C/T ratio with a slope of 0.1567. Nevertheless, previous studies found in the literature (STREK, 1963; RAI, *et al.*, 2000) have shown that for C/T ≥ 0.6 the Nusselt number begins to decrease, so the slope should not be considered valid for C/T higher than that value.

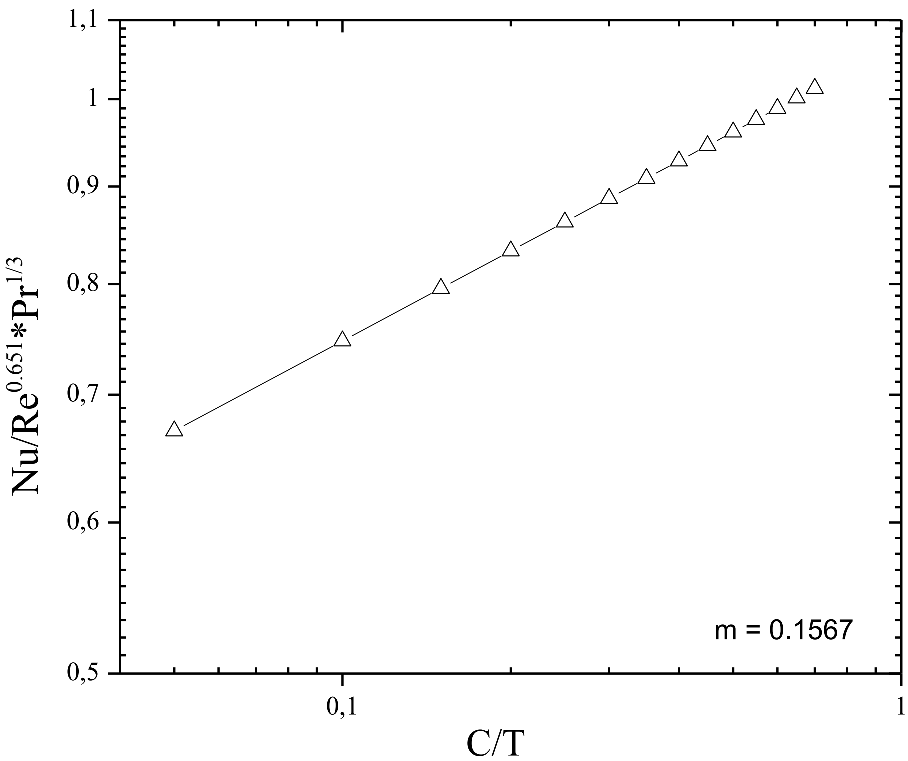

Figure 4.18 C/T ratio influence on the Nusselt number

Figure 4.19 shows the flow pattern for three cases where the impeller height of suspension was varied. For the first case where C/T = 1/10, the flow pattern produced by the impeller develop only one large vortex in the tank and the lower recirculation flow is absent. The size of the loop is not large enough to cover the entire tank and reduced velocity in the top is observed. This profile yields to dead zones that cause weak agitation and lower heat transfer coefficient in the top of the tank.

When the impeller was located at C/T ratios of 1/4 and 4/9, the typical flow pattern with the two circulation loops dividing the flow above and below the impeller can be noted. The size of the circulation loop below the impeller depends on the height of suspension. Therefore, for the impeller with C/T =1/4 large recirculation flows above and below the impeller are present (Figure 4.19b).

For the impeller closer to the middle of the tank (Figure 4.19c), the loops had similar size, which is commonly called 'double-eight' flow regime; this form improves mixing and avoids dead zones in the top and bottom of the tank. It can be inferred that placing the impeller near to the middle of the tank could improve the heat transfer coefficient since it covers a larger area of the heating surface and produces a more homogeneous flow. This assumption can be supported quantitatively from the numerical results that showed an increment of 5% in the heat transfer coefficient for the larger height (C/T = 4/9).

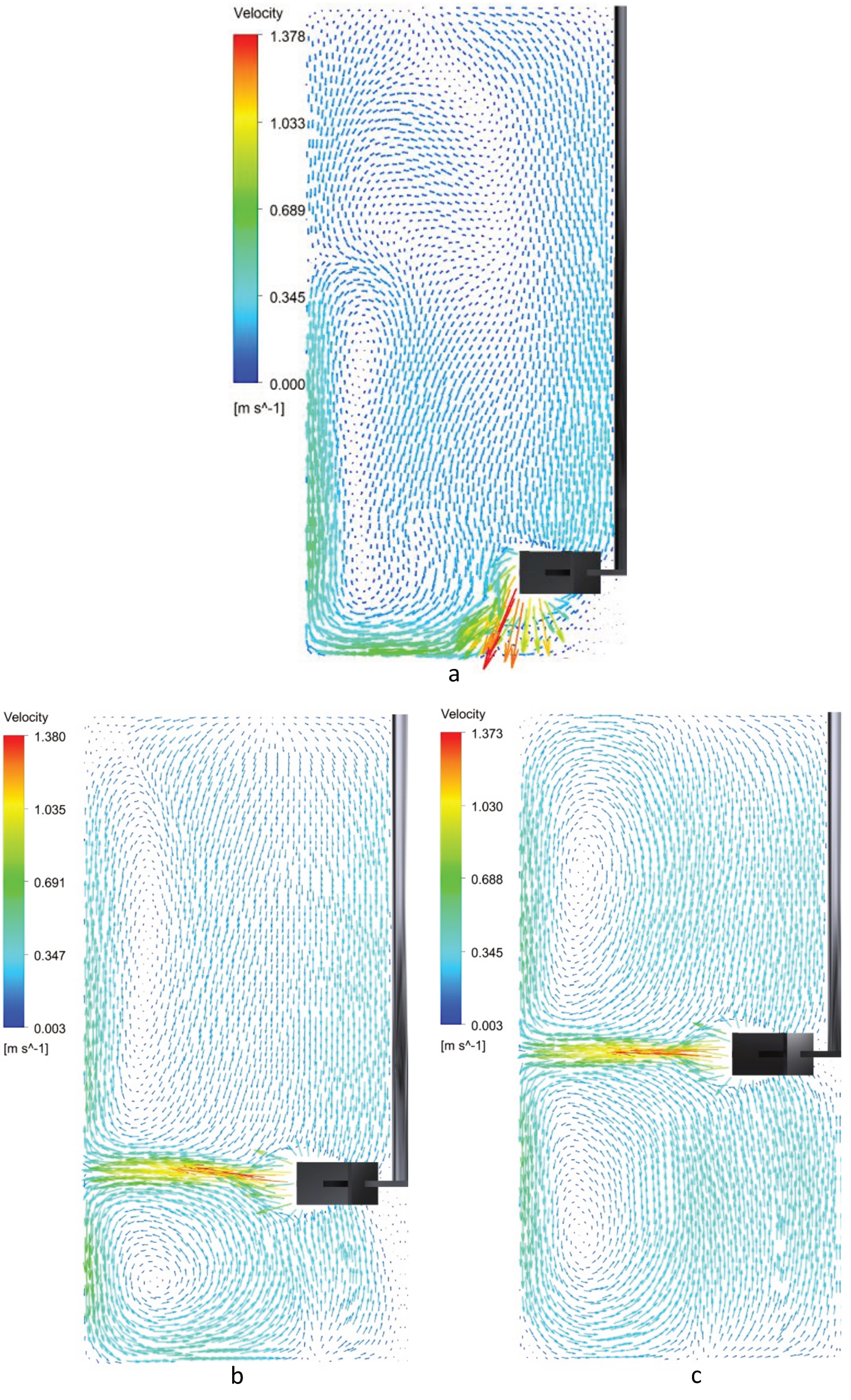

Figure 4.19 Impeller height suspension at a. 0.03 m (C/T =1/10) b. 0.075m (C/T =1/4) c. 0.135m (C/T = 4/9)

Chapter 5

Conclusions and suggestions for future works

The present chapter presents the major findings of the analysis conducted in this research. The suggestions for future works are also presented.

5.1 Conclusions

The main goal of the current study was to determine a Nusselt number correlation of a jacketed stirred tank equipped with a Rushton turbine impeller through CFD modeling. The outcomes presented in this dissertation demonstrated that the three-dimensional model with refined hexahedral mesh satisfactorily predicts the Nusselt number equation and the typical flow pattern of the stirred tank.

The numerical results of the CFD correlation were compared to specific Nusselt numbers obtained experimentally by STREK (1963) showing a slight dispersion with an average deviation of 7.8% and a standard deviation of 11.5%. These findings suggest that the CFD modeling is a capable and functional tool for predicting the fluid flow and the heat transfer in stirred tanks.

The results of the grid independence test indicated that there is a significant influence of the non-dimensional distance y^+ on the heat transfer coefficient. The accuracy of the numerical results depends significantly on the refinement of the mesh close to the heating surface, which in this case is the wall of the tank representing the jacket. Results of this work suggest that values of y^+ less than 0.1 should be used to ensure a proper performance of the Near-wall treatment along with the Shear Stress Turbulence model. Meanwhile, the refinement of the heating wall made no significant difference to the general flow produced by the Rushton turbine impeller. These results are in accord with those obtained by JAIMES AND NUNHEZ, 2017.

Variations in the impeller size and speed showed that there is an influence on the average heat transfer coefficient because larger faster impellers produce more turbulence and more effective heat transfer. However, the agitation power also increases in both cases. The choice of the better improvement on the configuration will depend of the specifications of the case and the desired results.

Regarding to the height suspension of the impeller, the results of this work suggest a placement of the impeller between C/T ratios of 1/4 and 4/9, as homogeneous agitation is achieved. These conditions involve more heating area and avoid dead zones by improving the heat transfer coefficient.

5.2 Suggestions for future works

Experimental measurements on stirred tanks with different heating surfaces (e.g. external half-pipe coils) are suggested to be carried out by expanding the conventional geometric configurations usually found in the literature. In conjunction with the use of CFD, a better understanding of flow fields and heat transfer in stirred tanks can be obtained. In this way, the numerical data can be easily validated with the experimental measurements.

The effect of the discretization scheme is of vital importance in the CFD predictions of the mixing in stirred tank. In this work, it was seen that the first order *upwind* scheme could predict with accuracy the heat transfer coefficient using a hexahedral mesh. However, more research is needed to better understand when and under what circumstances the implementation of the first order *upwind* scheme can provide good results compared to the *high resolution* scheme.

The influence of the size, speed, and height of a Rushton turbine impeller on the heat transfer coefficient have been investigated in this work. A detailed study of the influence of another type of impellers such as axial flow or unconventional impellers is worth being investigated.

By means of the implementation of the proposed CFD methodology, parameters, boundary conditions and optimum geometric configurations can be determined to find correlations that improve the heat transfer in stirred tanks used at industrial level.

References

Akse H., Beek W.J., Van Berkel F. C. A. A.The local heat transfer at the wall of a large vessel agitated by turbine impellers. *Chemical Engineering Science*. 1967;22: 135–146.

Ansys CFX User's Guide 16.0. *ANSYS CFX Release*

Askew W. S., Beckmann R. Heat and mass transfer in agitated vessel. *I&EC Process Design and Development*. 1965;4.

Aubin J., Fletcher D. F., Xuereb C. Modeling turbulent flow in stirred tanks with CFD: The influence of the modeling approach, turbulence model and numerical scheme. *Experimental, Thermal and Fluid Science*. 2004;28:431–445.

Balakrishna M., Murthy M. Heat transfer studies in agitated vessels. *Chemical Engineering Science*. 1979;*35*:1486–1494.

Brooks G., Su GJ. Heat transfer in agitated kettles. *Chem. Eng. Prog*. 1959;*55*(10):54–57.

Brucato A., Ciofalo M., Grisafi F., Micale G. Numerical prediction of flow fields in baffled stirred vessels: A comparison of alternative modelling approaches. *Chemical Engineering Science*. 1998;*53*(21):3653–3684.

Çengel Y. A., Cimbala J. M. Mecánica de fluidos fundamentos y aplicaciones. *McGraw-Hill*. 2006;1.

Chapman F.S, Dallenbach H., Holland F.A, Heat trasnfer in baffled, jacketed agitated vessels. Trans. Instn. Chem. Engrs, 1964;42:398-406

Chilton TH, Drew TB., Jebens RH. Heat transfer coefficeints in agitated vessels. *Industrial and Engineering Chemistry*, 1944;*36*(6):510–516.

Coker K.A. *Modeling of Chemical Kinetics and Reactor Design*. Houston, Texas: Gulf Publishing Company. 2001

Couper J.R., Penney RW., Fair J.R., Walas S.M. *Chemical Process Equipment: selection and desing*. 2nd Edition Elsevier Inc. 2005

Cummings GH., West AS. Heat transfer data for kettles with jackets and coils. *Industrial & Engineering Chemistry Research*. 1950;42.

Debab A., Chergui N., Bekrentchir K., Bertrand J. An investigation of heat transfer in a mechanically agitated vessel. *Journal of Applied Fluid Mechanics*, 2011;4(3):43–50.

Deglon DA., Meyer CJ. CFD modelling of stirred tanks: Numerical considerations. *Minerals Engineering*, 2006;*19*(10): 1059–1068.

Dorian, P. *Bioprocess Engineering Principles*. Elsevier Science & Technology Books, 1995:151-152

Driss Z., Kaffel A., Ben Amira B., Bouzgarrou G., Salah Abid M. PIV Measurements to study the effect of the Reynolds number on the hydrodynamic structure in a baffled vessel stirred by a Rushton turbine. *American Journal of Energy Research*, 2014;2(3): 67–73.

Ecke R. The Turbulence Problem. *Los Alamos Science*, 2005;(29):124–141.

Ferziger J.H., Perić M. Computational methods for fluid dynamics. Third edition. Springer, 2002.

Ghadi A., Sinkakarimi A. Investigation of interface location in Rushton turbine stirred tanks. *International Journal of Chemical*. 2014;2(1):1–5.

Hemrajani R.R, Tatterson G.B. Mechanically stirred vessels. In *Handbook of industrial mixing: science and practice*. John Wiley & Sons, 2004:345–390.

Huang W., Li K. CFD Simulation of flows in stirred tank reactors through prediction of momentum source. *Nuclear Reactor Thermal Hydraulics and Other Applications*. 2013

Incropera FP, DeWitt DP, Bergman TL, Lavine AS. Fundamentals of heat and mass transfer. John Wiley & Sons Inc., 6th Edition, 2007:350.

Jaimes R., Nunhez J R. Numerical prediction of a Nusselt number equation for stirred tanks with helical coils. *AIChE Journal*. 2017;63(9):3912-3924

Joshi JB., Nere NK., Rane CV., Murthy B. N., Mathpati CS., Patwardhan AW., Ranade V.V. CFD simulation of stirred tanks: Comparison of turbulence models. Part I: Radial flow impellers. *Canadian Journal of Chemical Engineering*. 2011;89(1):23–82.

Joaquim Junior C.F., Cekinski E., Nunhez J. R., Urenha L. *Agitação e mistura na industria*. Rio de Janeiro: Livros Técnicos e Científicos Editora S.A. 2007.

Karcz J., Kacperski L. An effect of grid quality on the results of numerical simulations of the fluid flow field in an agitated vessel. *14th European Conference on Mixing Warszawa*. 2012.

Karcz J., Strek F. Heat transfer in jacketed agitated vessels equipped with non-standard baffles. *The Chemical Engineering Journal*, 1995;58:135–143.

Karimi M., Akdogan G., Bradshaw SM. Effects of different mesh schemes and turbulence models in CFD modelling of stirred tanks. *Physicochemical Problems of Mineral Processing*. 2012;*48*(2):513–532.

Kresta S.M, Brodkey R.S. Turbulence in mixing applications. In *Handbook of industrial mixing: science and practice*. John Wiley & Sons, 2004:345–390.

Lane G.L., Schwarz M.P., Evans G.M. Comparison of CFD methods for modelling of stirred tanks. *10th European Conference on Mixing*, (eds.) Akker, H.E.A.V.D & Derksen, J.J., Elsevier Science, Amsterdam, 2000.

Launder B.E., Spalding D.B. The numerical computation of turbulent flow. *Computer methods in applied mechanics and engineering*. 1974;3:269-289.

Maliska C.R. *Transferência de calor e mecânica dos fluidos computacional*. Segunda Edição. Rio de Janeiro, Livros Técnicos e Científicos Editora S.A. 2004.

Man K. L., Edwards M. F., Polley G. T. A Study of local heat transfer coefficients in agitated vessels. *The Institution of Chemical Engineers Symposium Series*, 1984;*89*:193–207.

Marshal E.M, Bakker A. Computational fluid mixing. In *Handbook of industrial mixing: science and practice*. John Wiley & Sons, 2004:257–343.

Menter F. R. Two-equation eddy-viscosity turbulence models for engineering applications. *AIAA Journal*, 1994;32(8):1598–1605.

Menter F. R. Review of the shear-stress transport turbulence model experience from an industrial perspective. *International Journal of Computational Fluid Dynamics*. 2009;23(4):305–316.

Menter F. R., Kuntz M., Langtry R. Ten years of industrial experience with the SST turbulence model. *Turbulence, Heat and Mass Transfer 4*. 2003.

Mohan P., Emery A.N., Al-Hassan T. Review heat transfer to newtonian fluids in mechanically agitated vessels. *Experimental Thermal and Fluid Science* 1992;5:861883

Montante G., Lee K. C., Brucato A., Yianneskis M. Numerical simulations of the dependency of flow pattern on impeller clearance in stirred vessels. *Chemical Engineering Science*. 2001;56(12):3751–3770.

Murthy B. N., Joshi J. B. Assessment of standard k - ε, RSM and LES turbulence models in a baffled stirred vessel agitated by various impeller designs. *Chemical Engineering Science*. 2008;63(22):5468–5495.

Nunhez, J.R. and McGreavy, C. A comparison of the heat transfer in helical coils and jacketed stirred tank reactors. In 10th Internacional Heat Transfer Conference, Brighton -England. IChme, 1994:345-350

Nagata S., Nishikawa M., Kayama T., Nakajima M. Heat transfer to cooling coil acting as rotating impeller in highly viscous liquids. *Journal of Chemical Engineering of Japan*. 1972;*5*(2):187–192.

Ochieng A., Onyango M., Kiriamiti K. Experimental measurement and computational fluid dynamics simulation of mixing in a stirred tank: A review. *South African Journal of Science*, 2009;105: 421–426.

Oldshue J. Y. *Fluid Mixing Technology*. Chemical Engineering McGraw-Hill. 1983.

Pedrosa S.M.C.P., Nunhez J.R. Improving heat transfer in stirred tanks cooled by helical coils. *Brazilian Journal of Chemical Engineering*. 2003;20(2):111-120

Petera K., Dostál M., Rieger F. Transient measurement of heat transfer coefficient in agitated vessel. *Czech Technical University in Prague*. 2008;9.

Rai C.L, Devotta I., Rao P.G. Heat transfer to viscous Newtonian and non-Newtonian fluids using helical ribbon agitator. *Chemical Engineering Journal*. 2000;79:73-77.

Raj T. K. R., Singh A. D., Tare S., Varma S. Study of fluid flow around impeller blades in rushton turbine in a baffled vessel using computational fluid dynamics. *ARPN Journal of Engineering and Applied Sciences*. 2014;9(5):659–666.

Schlichting H. (1979). *Boundary-Layer Theory*. Seventh Ed, Vol. 20. McGraw Hill.

Sieder E. N., Tate G. E. Heat transfer and pressure drop of liquids in tubes. *Ind. Eng. Chem.* 1936;*28*(12):1429–1435.

Sondak DL. Wall functions for the k - [epsilon] turbulence model in generalized nonorthogonal curvilinear coordinates (1992). Retrospective Theses and Dissertations. Paper 9954.

Starikovičius V, Čiegis R, Jakušev A. Analysis of upwind and high-resolution schemes for solving convection dominated problems in porous media. Mathematical Modeling and Analysis. 2006;11(4):451-474

Strek F. Heat transfer in liquid mixers: study of a turbine agitator with six flat blades. *International Chemical Engineering* 1963;3.

Uhl V. W. (1955). Heat trasnfer to viscous materials in jacketed agitated kettles. *Chem. Eng. Prog. Symp.* 1955;*51*(17):93–108.

Versteeg H. K., Malalasekera W. *An Introduction to Computational Fluid Dynamics* (Second edition). Pearson Education Limited, 2007.

Wilcox D. C. Reassessment of the scale-determining equation for advanced turbulence models. *AIAA Journal*, 1988;*26*(11):1299–1310.

Yang C., Mao Z.S. *Numerical simulation of multiphase reactors with continuous liquid phase*. First Edition. Academic Press, 2014.

Zakrzewska B., Jaworski Z. CFD modelling of turbulent jacket heat transfer in a Rushton turbine stirred vessel. *Chemical Engineering and Technology*. 2004;*27*(3):237–242.

Zakrzewska B., Jaworski Z. Turbulent heat transfer modelling in a vessel stirred by a pitched blade turbine impeller. In *3rd IASME/WSEAS Int. Conf. on Heat transfer, thermal engineering and environment*. 2005:311–315.

Appendix A

Minimum node spacing

The proper resolution of the boundary layer guarantees the accuracy of the results in thermal calculations. Two criteria should be accomplishing to judge the quality of a mesh, a minimum number of nodes and the minimum spacing between them within the boundary layer.

The near wall mesh spacing (Δy) is determined in terms of Reynolds number and a $\Delta y+$ target value, which depends on the near wall treatment that will be used. Using correlations for a flat plate with Reynolds number expressed as:

$$Re_L = \frac{L\ U\ \rho}{\mu} \tag{A.1}$$

where U is the characteristic velocity and L the length of the plate.

The correlation for the wall shear stress coefficient (c_f) is written as follows:

$$c_f = 0.027\ Re_x^{-1/7} \tag{A.2}$$

where x is the distance take it from the leading edge.

The definition of $\Delta y+$ can be expressed as:

$$\Delta y^+ = \frac{\Delta y \mu_\tau}{\nu} \tag{A.3}$$

with Δy as the spacing between the wall and the first node of the mesh near to the wall.

Using the definition

$$c_f = 2\frac{\rho {\mu_\tau}^2}{\rho U^2} = 2\left(\frac{\mu_\tau}{U}\right)^2 \tag{A.4}$$

Replacing μ_τ in equation A.3 leads to:

$$\Delta y = \Delta y^+ \sqrt{\frac{2}{c_f}}\frac{\nu}{U} \tag{A.5}$$

In addition, c_f is eliminated using equation A.2 to yield:

$$\Delta y = L\Delta y^+ \sqrt{74} Re_x^{-1/4}\frac{1}{Re_L} \tag{A.6}$$

Assuming that $Re_x = CRe_L$ and C is some fraction that can be expressed as $C^{-1/4} \approx 1$, then Equation A.6 can be written as:

$$\Delta y = L\Delta y^+ \sqrt{74} Re_L^{-13/14} \tag{A.7}$$

Equation A.7 allows to set a desired Δy+ value at a given x location and determine the first layer height on the boundary layer.

Another requirement to have a good mesh resolution is a minimum number of nodes in the boundary layer for the chosen turbulence model and the near wall treatment. As a general rule, the boundary layer should have at least 10 nodes for the wall function and 15 for the low-Reynolds model.

The thickness of the boundary layer δ can be obtained from:

$$Re_\delta = 0.14 Re_x^{6/7} \tag{A.8}$$

$$\delta = 0.14 L Re_x^{6/7}\frac{1}{Re_L} \tag{A.9}$$

Assuming that Re_δ is 25 % of Re_L, then the thickness of the boundary layer take the form:

$$\delta = 0.035 L Re_L^{-1/7} \tag{A.10}$$

The growth rate of the boundary layer can be calculated from:

$$Growth\ rate = \left(\frac{\delta}{\Delta y}\right)^{1/n} \tag{A.11}$$

where n is the number of nodes placed in the boundary layer.

For stirred tanks, Re_L is defined as:

$$Re_L = \frac{d^2 N \rho}{\mu} \tag{A.12}$$

where the speed of the impeller (N) is the characteristic velocity, and the impeller diameter (d) is the length.